UNIVERSITY OF SOUTHAMPTON

# The Use of Raman Spectroscopy in Pharmaceutical Analysis

A thesis submitted to the University of Southampton in support of candidature for the degree of Doctor of Philosophy

by Anne TG De Paepe Drs. M.Res.

Department of Chemistry, July 2001

UNIVERSITY OF SOUTHAMPTON

ABSTRACT

FACULTY OF SCIENCE

DEPARTMENT OF CHEMISTRY

Doctor of Philosophy

# THE USE OF RAMAN SPECTROSCOPY IN PHARMACEUTICAL ANALYSIS

by Anne Thérèse Gustaaf De Paepe

In this thesis, the use of Raman spectroscopy in pharmaceutical analysis is evaluated. Sample rotation in FT-Raman spectroscopy is studied. Sample rotation is particularly important when analysing heat sensitive samples such as polymorphs. By rotating the sample, laser heating by the near infrared laser is reduced. However modulation and double modulation in the FT-instrument might induce spurious lines into the Raman spectrum. Therefore it is essential that rotational speeds are kept reasonably low. Another important reason to rotate samples is to avoid sub sampling. Especially when performing quantitative analysis, this is of major concern.

An attempt is made to further develop FT-Raman spectroscopy into a quantitative technique with the aim to make it applicable for analysis of pharmaceutical tablets. A study into FT-Raman intensity reproducibility of both liquids and solids is performed. Subsequently different sets of tablets were prepared and the correlation between concentration and Raman intensity evaluated. In addition, a comparison between internal and external standardisation is made.

In another chapter, a study into a local anaesthetic system is performed. Vibrational spectroscopy is used to assess the extent of interactions between the two active ingredients in the formulation. In addition, interactions between the two actives and an aqueous solution of two block copolymers, in which they are present, are evaluated. On increasing the temperature, this aqueous solution of block copolymers goes into the gel state. Therefore the conformation changes of an aqueous solution of block copolymers with and without the two active components were studied.

A last chapter deals with the polymorphism of sulfathiazole. Sulfathiazole, an antibacterial agent, can exist in five different polymorphic forms. Polymorph I is thought to display unusual large anisotropic lattice expansion. This phenomenon is studied by vibrational spectroscopy and an attempt is made to correlate the NH stretching frequencies with the available X-ray data.

# ACKNOWLEDGEMENTS

I would like to express my gratitude to the following people for all their help and support while completing this research:

First of all my thanks goes out to my supervisors Prof. Patrick Hendra and Dr. Andrea Russell for making it possible for me to study for this degree and for all their help and support throughout the years. Also many thanks goes out to my advisor Dr. Bill Maddams.

I also want to thank my external supervisors at AstraZeneca, Sweden. Firstly I am greatly indebted to Dr. Astrid Arbin who has given me such wonderful support. My gratitude also goes out to Dr. Lynne Taylor, Prof. Frans Langkilde and Ulrika Eriksson for all their help and support.

Also a special thanks to Dr. Terry Threlfall, Prof. Mike Hursthouse, Dave Hughes and Ann Bingham for all their help with the polymorphism work. Thank you Ed Blayden for your help and wonderful support.

A warm thank you to George Tame at Perkin Elmer Ltd. for his invaluable help. Also thanks to everyone at Renishaw plc.

To the past and present members of the Hendra/Russell group: Fabrice, Jun, Stephanie, Chris, Abbe, Fabrizio, Linda, Becky, Colm and Andy. Thank you Gurjit and Juergen for the extra help in the last stages of finalising this thesis. To the present members of the Russell group, I wish them good luck.

I should not forget to thank 'min fantastiska chef ' Ulf Appelgren and all my new collegues at AstraZeneca Sweden for giving me so much support in writing this thesis. A special thanks to Anita, Viveka, Helena and Jan.

I want to thank my parents and Wim, Leen and Birte for being there when I needed them.

A very special thank you goes out to you, Ron. Thank you for always helping me out. Thank you for always being there for me.

Lastly, I am greatly indebted to AstraZeneca, Sweden for their generous financial support.

# CONTENTS

# Chapter 1 Introduction

## 1.1 Background and Aims of the thesis

Before the launch of a new drug, many years go into the research of potential drug candidates. Important factors that are studied are potency, bioavailabilty, stability and toxicity of the drug. Excipients are usually mixed with the drug to produce the final dosage form, hence research into possible interactions between the active component and excipients is required.

The present work focuses on two different dosage forms of a drug. One chapter is dedicated to the development of Fourier Transform (FT) Raman spectroscopy as an analytical tool for the analysis of tablets. The use of sample rotation in combination with FT-Raman analysis is discussed. In another chapter the emphasis lies on the composition and stability of a local anaesthetic system. In a last chapter the implications of polymorphism (the existence of more than one crystal modification of a compound) are studied.

In **Chapter 2**, the effect of sample movement in FT-Raman spectrometers is discussed. As sample rotation proved to be essential in the experimental work of all of the following chapters, a study into the advantages and disadvantages of sample rotation was performed. Important topics that were discussed include:

- reducing sample heating by the laser
- avoiding subsampling
- avoiding spurious lines in the spectra due to sample rotation

**Chapter 3** deals with the characterisation and temperature dependent structural changes of a local anaesthetic system. This system consists of two active components, lidocaine and prilocaine, that form a eutectic mixture [1]. In addition, two polymers in aqueous solution are added as excipients so that an easily applicable thermogelling system is formed.

The aims for this subsection are to use vibrational spectroscopy

- in the characterisation of the local anaesthetic system and its components
- to study the possibility of interactions between the active substances

- to study the possibility of interactions between the actives and excipients
- to study the influence of temperature changes on the structure of the different components in the formulation

Furthermore, the pharmaceutical industry is interested in reproducible, accurate and rapid quantitative analyses of their active compounds. It has been usual to apply HPLC[1], but this technique suffers from the disadvantage that a time consuming sample preparation is necessary. Raman spectroscopy, on the other hand, has the advantage that little or no sample preparation is necessary. Near-infrared spectroscopy [2] also avoids the problem of lengthy sample preparation, but the spectra are often difficult to interpret.

**Chapter 4** is dedicated to the development of quantitative FT-Raman analysis on tablets, a study critics have always regarded as difficult due to the 'uncontrollable nature' of the recording of Raman scattering.

The aims for this subsection were to determine:

- the reproducibility of FT-Raman spectra
- the feasibility of the use of an internal/external reference
- the quantitative analysis of tablets
- the quantitative analysis of actives in a local anaesthetic system

Another important topic in the pharmaceutical industry is polymorphism. Polymorphism can cause major problems because the different forms of the same molecule display different physico-chemical properties like rate of dissolution, melting point, hardness, etc. Since polymorphs have different conformations in their unit cells hence different intermolecular interactions, their vibrational spectra will differ and this makes infrared and Raman spectroscopy good techniques for studying polymorphs.

In **Chapter 5**, the antibacterial agent sulfathiazole was studied. Sulfathiazole is known to have five polymorphs.

The aims for this subsection were:

- to characterise all polymorphs with vibrational spectroscopy
- a study of the anisotropic lattice expansion of sulfathiazole polymorph I
- to correlate the hydrogen bonded NH stretching frequencies with the various bond lengths, obtained from X-ray crystallography

[1] HPLC: High Pressure Liquid Chromatography

**Chapter 6** contains the overall conclusion of the work and sets out some suggestions for future work.

## 1.2 Solid State Reactions

An important aim for the formulator in the pharmaceutical industry is to find a drug formulation with the best bioavailabilty. Nowadays, the vast majority of medication is in solid dosage forms, therefore it is important to know the common types of solid state reactions. The most important ones are solid-solid interactions, solid-gas interactions and solid transformations. Examples of solid-solid interactions are interactions between the excipient and active component or between active components. For example Carstensen has reported aspirin-codeine and aspirin-phenylephrine interactions [5].

Oxidation is a typical example of solid-gas interactions. Oxidation is the prime cause of product instability. In addition to the oxidation product, often a whole chain of other degradation products is formed. The interaction of solids with water is also very common. Whether this reaction should be classified as solid-gas reactions or as solution reactions, is not clear.

The solid transformations include polymorphic transitions, phase changes and decomposition.

The present study was focussed on the last type of solid state reactions, the solid transformations, more specific the polymorphic transitions and phase changes.

### Polymorphism

The term polymorphism is used when a molecule can exist in several different crystal forms. The problem lies in the fact that these different crystal forms display different physical properties like melting and sublimation temperatures, rate of dissolution, volume, density and many more. As a consequence the bioavailabilty of the compound is variable, depending on what crystal form is present [6,7].

The term pseudo polymorphism is used when a molecule can exist as a solvate, with the most common being the hydrates. One example is the change in hydration state of theophylline in tablets. As water is adsorbed and desorbed with changes in temperature and humidity, theophylline is present in either the crystalline anhydrate or monohydrate [8].

A wide range of techniques is available to study polymorphism. DSC[2] and TGA[3] allow a quick interpretation of thermodynamic and kinetic transformations [9-11]. However, quantitation with these techniques is difficult and not recommended. X-ray diffraction (XRD) [11-14] , vibrational spectroscopy [15-17] and solid state Nuclear Magnetic Resonance (NMR) spectroscopy [18-19] are the other techniques commonly used and are preferred for quantitative analysis.

### Phase changes

The main properties of the substance and of the final product are derived from the thermodynamic phase diagrams under influence of temperature and pressure. But not all systems show ideal phase change behaviour. Super-cooling or –heating and crystalline to amorphous transformations or vice versa also fall under this subsection. Detailed knowledge of these equilibration curves enables one to predict best storage conditions, stability and compatibility of certain products.
Thermal analysis, for example DSC measurements, is frequently used to study such processes. Vibrational spectroscopy as a function of temperature is another technique that can identify these phase changes.

## *1.3 A Local Anaesthetic Block Copolymer System*

The local anaesthetic system studied was made up of two active components lidocaine and prilocaine and an aqueous solution of two block copolymers as excipients.
The two actives are present in the thermogelling system as a eutectic mixture. The word eutectic comes from the Greek words for 'easily melted'. When two liquids are mixed, their freezing point usually lies below the freezing points of the pure components. That composition which has the lowest melting point is called the eutectic. A eutectic liquid made up of A and B will therefore freeze at a single temperature, at that composition, without previously depositing solid A or B. The eutectic mixture of lidocaine and prilocaine therefore has its melting point at 18°C, a lower temperature than both melting points of the pure substances.
The two polyethyleneoxide-polypropyleneoxide-polyethyleneoxide triblock copolymers as the excipients are well known non-ionic surfactants, hence their

[2] DSC : differential scanning calorimetry
[3] TGA : thermogravimetric analysis

applicability in detergency, dispersion, stabilization, foaming and emulsification. The required characteristics can be monitored by the architecture of the triblock, i.e. molecular weight and relative size of the copolymer blocks.

## 1.4 Vibrational Spectroscopy in Pharmaceutical Analysis

Spectroscopy is an important tool for the characterisation of both drug substances and final products. The characterisation techniques most commonly used in the pharmaceutical industry include XRD, NMR, infrared (IR) and also increasingly Raman spectroscopy. In the present study the emphasis was placed on the use of vibrational spectroscopy.

The infrared part of the electromagnetic spectrum can be divided into three major areas. The most commonly used area is the mid-infrared (MIR) area, which expands from 4000 $cm^{-1}$ to 400 $cm^{-1}$. Here we find the fundamental molecular vibrations and vibration-rotations. The region between 4000 and 14000 $cm^{-1}$ is known as the near-infrared (NIR) region. In this region we find the overtones and combination bands of the hydrogenic vibrations in the MIR. The lattice vibrations can be found in the region extending from 400 $cm^{-1}$ to 100 $cm^{-1}$. One of the advantages of vibrational spectroscopy over other techniques is that it is possible to study compounds in any state of matter: crystalline, amorphous, liquid, gas or plasma. MIR spectroscopy is the most widely used, but both Raman and NIR spectroscopies are rapidly expanding. They both offer advantages over MIR analysis in that they are non-destructive and virtually no sample preparation is required. However, the recent sample handling techniques based upon ATR[4] infrared spectroscopy are closing this gap.

Minimal sample preparation is an important advantage in the study of polymorphism where grinding a compound might induce a polymorphic transformation.

Both NIR and Raman spectroscopy allow the collection of spectra through blister packs and glass, which is advantageous when studying samples that are moisture sensitive. Aqueous solutions can be studied as well. One of the advantages of Raman spectra over the NIR equivalents is that Raman is essentially a fingerprint technique. Interpretation of the NIR spectra can be very difficult due to the broad and featureless bands due to overlapped overtones and combination bands.

[4] ATR: attenuated total reflection

## 1.5 *Infrared Spectroscopy*

Both infrared and Raman spectroscopy measure the molecular vibrations (and vibrational-rotational transitions). Whereas infrared spectroscopy is concerned with the absorption of the radiation, the latter relies on scattering.
Infrared spectroscopy can be used as a transmission as well as a reflection technique.

### Transmission Infrared

Transmission infrared spectra can be recorded of most types of samples, but some samples need careful sample preparation. Most gases and liquids can be measured directly whereas solids often need preparation into mulls, alkali halide discs or films. The reflection techniques, like DRIFT[5] and ATR minimize this sample preparation. In these techniques, the infrared beam is directed at the sample at an angle different from the normal. The attenuated radiation, reflected back from the surface, is then detected.

### Attenuated Total Reflection

ATR is a so-called Internal Reflection technique. When radiation strikes a surface it may be reflected, transmitted or absorbed. Whether the incident beam gets transmitted or reflected is dependent on the refractive indices of the two media and the angle of incidence.
As the infrared radiation hits the interface of two materials at an angle greater than the critical angle, reflection will take place, provided that the material through which the radiation has passed has a higher refractive index than that of the material at the other side of the interface (the sample). This concept is shown in Figure 1.1.

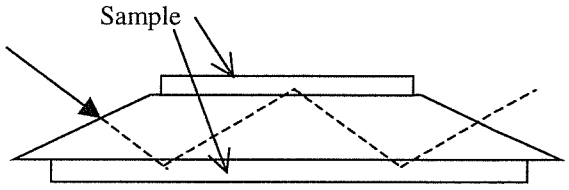


**Figure 1.1** As the infrared beam hits the sample/crystal interface at an angle greater than the critical angle, reflection occurs. In addition, the beam will penetrate the sample over a small distance, hence collecting absorption characteristics as well.

[5] DRIFT : diffuse reflectance infrared Fourier Transform

The critical angle can be written as $\alpha_c = n_2/n_1$ with $n_1$ and $n_2$ being the refractive indices of material 1 and 2, where material 1 is the high refractive index medium. When a sample is placed in contact with a higher refractive index material and the infrared beam is directed at the sample at an angle higher than the critical angle, internal reflection will occur at the boundary of the two materials.
In addition, the infrared beam penetrates the sample over a short distance before returning back through the higher refractive medium. Hence, some absorption characteristics from the sample are also collected. The penetration depth is given by

the following formula : $$d_p = \frac{\lambda}{2\pi(\sin^2\alpha - n_{21}^2)^2}$$

Where $\lambda$ is the wavelength of the radiation, $\alpha$ is the angle of incidence and $n_{21}$ is $n_2/n_1$.
The most commonly used materials are KRS-5, Ge and ZnSe, but diamond crystals are becoming more and more popular. The high refractive index of diamond ensures that for incidence angles of 45 degrees, a typical infrared penetration of around 2 microns is achieved. Also, the inertness and hardness of the material makes it a popular choice.

## 1.6 The Raman Effect

The Raman effect was predicted in the early 1920s [20,21] and subsequently demonstrated in India in 1928 by C.V. Raman [22], and almost simultaneously, by G. Landsberg and L. Mandelstam in the Soviet Union [23].
When a sample is exposed to a light source, radiation may be absorbed, reflected, refracted and scattered. Most of the incident radiation that is scattered will do so elastically, so-called Rayleigh scattering. In addition, some of the radiation will be inelastically scattered, which is called the Raman scatter. Scatter which has lower energy than the incident radiation gives rise to Stokes scatter and that with higher energy is known as anti-Stokes scatter. The various types of scattering processes are shown in Figure 1.2

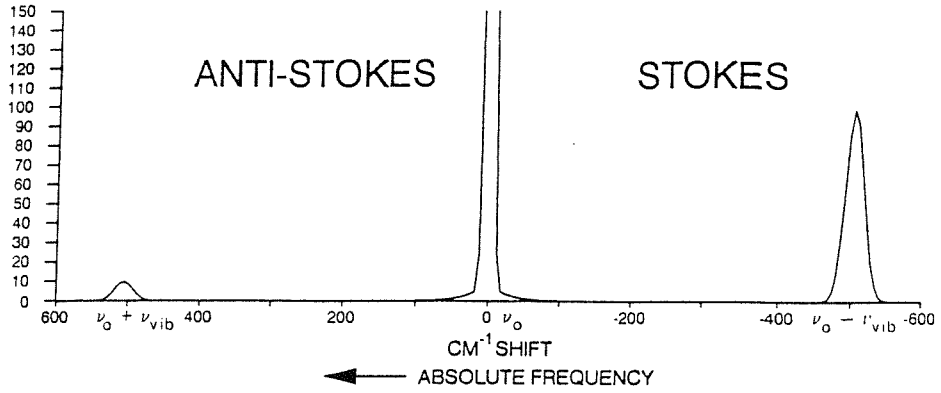


**Figure 1.2** The various types of scattering are displayed. The central band is the elastic (Rayleigh scatter) and the bands left and right are inelastic scattering (Stokes and anti-Stokes scatter). Reproduced with permission from *Fourier Transform Raman Spectroscopy* by *Hendra, Jones & Warnes.*

The frequency of the incident radiation is modified by its interaction with the inter-atomic motion of the sample. Analysis of the Raman scattering provides us with information about molecular vibrations and vibration-rotations and is therefore as a technique complementary to infrared spectroscopy. The shifts in frequency observed in Raman spectroscopy do not always correspond to observable IR absorption bands, because the two processes obey different selection rules relating to the interaction of the normal vibration of the molecule with the oscillating electric field of the electromagnetic radiation. Infrared absorption occurs when the radiation interacts with a normal mode of vibration in which the dipole moment of the molecule varies with time. Raman scattering occurs when the molecular motion produces a change in the polarizability of the molecule. Hence we can say that symmetric vibrations give rise to intense Raman lines, where non-symmetric ones are usually weak and sometimes unobservable. In infrared spectroscopy, the opposite effect is observed. If a molecule has a centre of symmetry, the rule of mutual exclusion becomes important. It states that if a molecule has a centre of symmetry, then Raman active vibrations are infrared inactive and vice versa. If there is no centre of symmetry then some, but not necessarily all, vibrations may be both Raman and infrared active.

## Classical Description of Raman scattering

According to the classical theory, the Raman scattering can be described as follows. The electric field $E$ associated with an incident beam of frequency $\nu_0$ fluctuates with time t as shown by Equation. (1-1):

$$E = E_0 \cos 2\pi \nu_0 t \qquad (1\text{-}1)$$

Where $E_0$ is the amplitude of the wave.

When this oscillating field interacts with the polarizable electric field, an electric dipole P is induced:

$$P = \alpha E = \alpha E_0 \cos 2\pi \nu_0 t \qquad (1\text{-}2)$$

Where $\alpha$ is the polarizability of the material. If the molecule is vibrating (or rotating) with a frequency $\nu_{vib}$, the nuclear displacement from the equilibrium position $q$ is given by:

$$q = q_0 \cos 2\pi \nu_{vib} t \qquad (1\text{-}3)$$

where $q_0$ is the vibrational amplitude. If the distortion is likely to cause a change in the polarizability, where for a small amplitude of vibration, $\alpha$ is a linear function of $q$, we can write:

$$\alpha = \alpha_0 + \left(\frac{\partial \alpha}{\partial q}\right)_0 q + \ldots \qquad (1\text{-}4)$$

Where $\alpha_0$ is the polarizability at the equilibrium position and $(\delta\alpha/\delta q)_0$ is the rate of change of the polarizability with distortion from the equilibrium position. Combining (1-2) with (1-3) and (1-4), we obtain:

$$\begin{aligned} P &= \alpha E_0 \cos 2\pi \nu_0 t \\ &= \alpha_0 E_0 \cos 2\pi \nu_0 t + \left(\frac{\partial \alpha}{\partial q}\right)_0 q E_0 \cos 2\pi \nu_0 t \\ &= \alpha_0 E_0 \cos 2\pi \nu_0 t + \left(\frac{\partial \alpha}{\partial q}\right)_0 q_0 E_0 \cos(2\pi \nu_{vib} t) \cos(2\pi \nu_0 t) \end{aligned}$$

By using the Simpson rules, we can rewrite this equation as follows:

$$P = \alpha_0 E_0 \cos 2\pi \nu_0 t + \frac{1}{2}\left(\frac{\partial \alpha}{\partial q}\right)_0 q_0 E_0 [\cos\{2\pi(\nu_0 + \nu_{vib})t\} + \cos\{2\pi(\nu_0 - \nu_{vib})t\}]$$

The first term represents an oscillation dipole that radiates light of frequency $\nu_0$ (Rayleigh scattering), while the second term gives the Stokes and anti-Stokes Raman frequencies of $\nu_0 - \nu_{vib}$ and $\nu_0 + \nu_{vib}$ respectively.

### The Quantum Mechanical Theory of the Raman Effect

The difference in intensities between the Stokes and anti-Stokes lines cannot be explained by the classical theory of Raman scattering. A simple quantum mechanical approach is used to clarify this. When a photon of energy $h\nu_0$ collides with a molecule, either elastic (Rayleigh scatter) or inelastic (Raman) scatter will occur. In the latter case, the molecule will undergo a transition to a virtual excited vibrational state and after relaxation will either have gained energy (Stokes scatter) or lost energy (anti-Stokes scatter). Therefore, the intensity of Raman scatter is related to the population of the initial state of the molecule. The ratio of Stokes to anti-Stokes lines is governed by the temperature. At thermal equilibrium this ratio can be determined by the Boltzmann distribution.

$$\frac{N_j}{N_i} = \frac{g_j}{g_i} e^{\frac{-\Delta E}{kT}}$$

Where $N_i$ and $N_j$ are the number of molecules in the lower and upper vibrational levels, $g_i$ and $g_j$ are the degeneracies of these states, $\Delta E$ is the energy difference between these levels, k is the Boltzmann constant and T is the temperature.
Figure 1.3 shows in detail the origin of Stokes and anti-Stokes scatter.

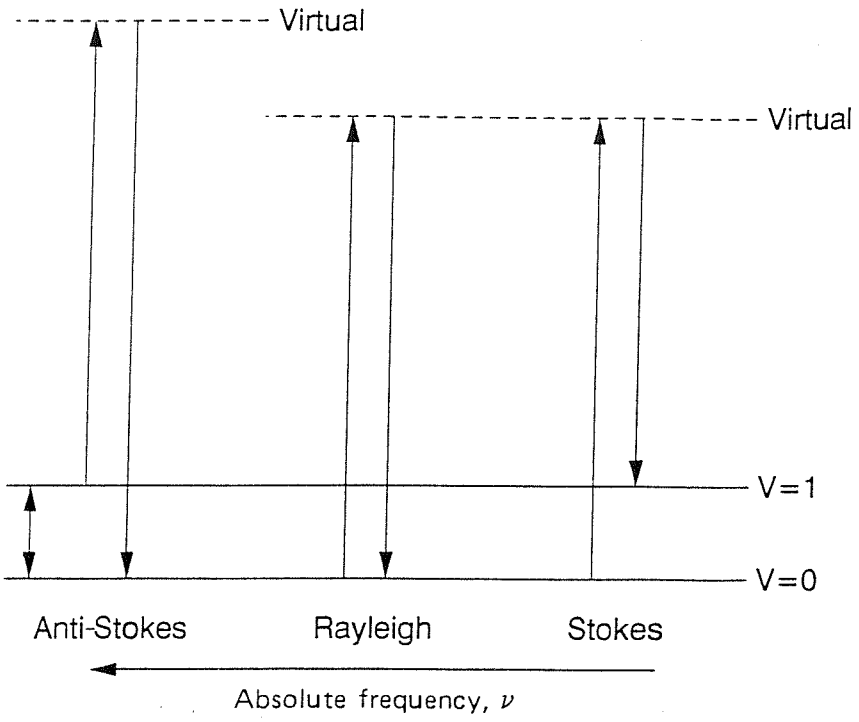


**Figure 1.3** An energy level diagram displaying the origin of Rayleigh, Stokes and anti-Stokes scatter. Reproduced with permission from *Fourier Transform Raman Spectroscopy* by *Hendra, Jones & Warnes.*

Thus, the Stokes lines are stronger than the anti-Stokes lines because the population of the ground state is higher than that of the first vibrational level. Although the intensity of the anti-Stokes scatter is lower compared to the Stokes scatter due to the population difference in the ground-state, the frequency of the light being scattered is higher and thus the scattering occurs more efficiently. It is known that the Raman scattering intensity depends on the fourth power of the frequency of the light being scattered.

## 1.7 Conventional Raman Spectroscopy

The sun was used as a source in C.V. Raman's first experiments [22], whereas Mandelstam and Landsberg used the mercury lamp as a source [23] and thus established the technique used through the 1930s and '40s.

Nowadays, lasers are used as the excitation source. The Argon, Krypton and Helium-Neon lasers offer a variety of excitation frequencies and tuneable dye lasers can be used to cover a considerable spectral range.

For the analysis of the Raman scattering a monochromator system is used, either in a scanning mode or as a spectrograph.

Until the mid '70s photomultiplier tubes (PMT) were the most practical electronic detectors available for the Raman detection. Various types of multichannel detectors have been developed over the years. A multichannel detector can be seen as the electronic equivalent of a photographic plate, but with a finite number of spectral elements. These multichannel detectors have advantages over the older PMT in that they can analyze many optical frequencies simultaneously, the so-called multiplex advantage. In recent years the CCD[6] detector has become very popular [24]. The CCD detector consists of a two-dimensional array of semiconductors the so-called pixels. When these pixels are hit by photons, a charge is developed by the photoelectric effect. These charges are then transferred to a charge sensitive amplifier by changing the potential over the CCD device.

## 1.8 Fourier Transform Raman Spectroscopy

Chantry et al [25] in 1964 were the first to suggest the idea of performing Raman spectroscopy by using a near-infrared excitation source and an interferometer. They demonstrated the feasibility by performing measurements on solutions of iodine in carbon tetrachloride and a carbocyanine dye in methanol. The use of near-infrared excitation as a means of minimising fluorescence was also discussed. Unfortunately spectroscopists did not take notice of this new method of Raman spectroscopy. It was not until commercial FT-IR instruments became available, when the multiplex and throughput advantages of a Michelson interferometer over a standard dispersive instrument had become established, that the possibility of performing FT-Raman measurements was reconsidered [26]. But it was not until the next decade (1974 – 1984) after new technological developments, like the CW[7] Nd:YAG laser and high sensitivity detectors for the visible and near-infrared, that FT-Raman spectroscopy began to take off.

### The source

The Nd:YAG laser is commonly used in near-infrared-FT Raman spectroscopy. It is a solid state device consisting of a crystal of yttrium aluminium garnet, doped with about 3% $Nd^{3+}$ ions. The pump is either a broadband source like a high pressure

[6] CCD: Charge Coupled Device
[7] CW : Continuous Wave

xenon arc lamp or a tungsten quartz lamp, or a near-infrared power source provided by a set of optically coupled arsenide injection lasers.
Nd:YAG lasers emit at 1.064 μm (9398 $cm^{-1}$) with a line-width of about 0.6 $cm^{-1}$ at powers up to several Watts. A great advantage of near-infrared excitation is the reduction in fluorescence compared with excitation in the visible [27-29].
Tuneable lasers (dye or Ti Sapphire) have been used mainly in the study of resonance Raman.

## The interferometer

FT-IR and FT-Raman spectrometers are usually built around a Michelson interferometer. The Michelson interferometer consists of a beamsplitter and a fixed and a moving mirror. The scattered light enters the interferometer through a circular entrance, the J-stop. It then hits the beamsplitter which reflects half of the beam to one mirror and transmits the other half to the other mirror. As stated above, one of the mirrors is fixed whilst the other moves. Both the fixed and moving mirrors reflect the radiation back to the beamsplitter. But since one mirror is moving, a path difference between the two beams is created. There will be a phase difference when they recombine at the beamsplitter.
When both mirrors are at an equal distance from the beam splitter, the so-called Zero Path Difference (ZPD), there is no path difference between the two beams and the maximum possible of the input light exits from the interferometer. This is the so-called centreburst, the most intense signal in the interferogram.
After passing the interferometer again, half of the light will go to the detector and the other half returns to the source. Thus, the theoretical maximum efficiency of an interferometer is 50%. As the mirror moves, the two beams recombine with different path difference and we get constructive interference or destructive interference, depending on the value of n in the following equation :

$$d = n\lambda/4$$

Where n is an integer, $\lambda$ is the wavelength of the light and d is the distance the moving mirror has translated. If n is odd, destructive interference will result. At all other distances the two rays are not completely out of phase and a signal will be observed at the detector.

The concept of the Michelson interferometer is shown in Figure 1.4.

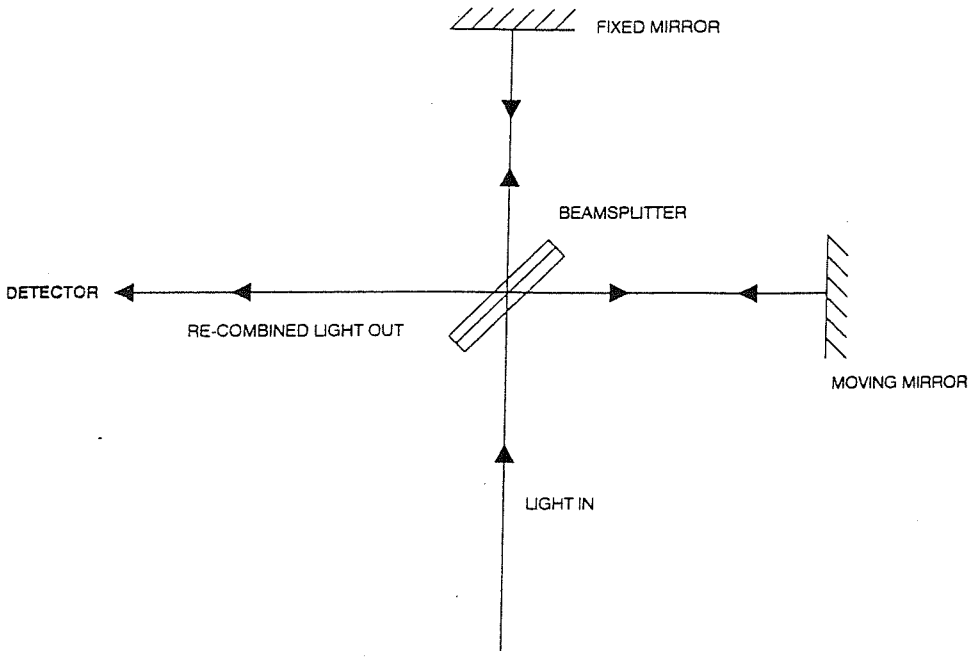


**Figure 1.4** Schematic diagram of a Michelson interferometer. Reproduced with permission from *Fourier Transform Raman Spectroscopy* by *Hendra, Jones & Warnes.*

Hence we get a signal as a function of optical delay (mirror distance), known as the interferogram. When an ideal monochromatic source passes through the interferometer and the optical delay is varied, the signal detected is a cosine wave. If two ideally monochromatic sources of different wavelength should pass through the interferometer, we would obtain the sum of two cosines. As the source becomes more polychromatic, the beat frequency becomes longer and longer. This is shown in Figure 1.5.

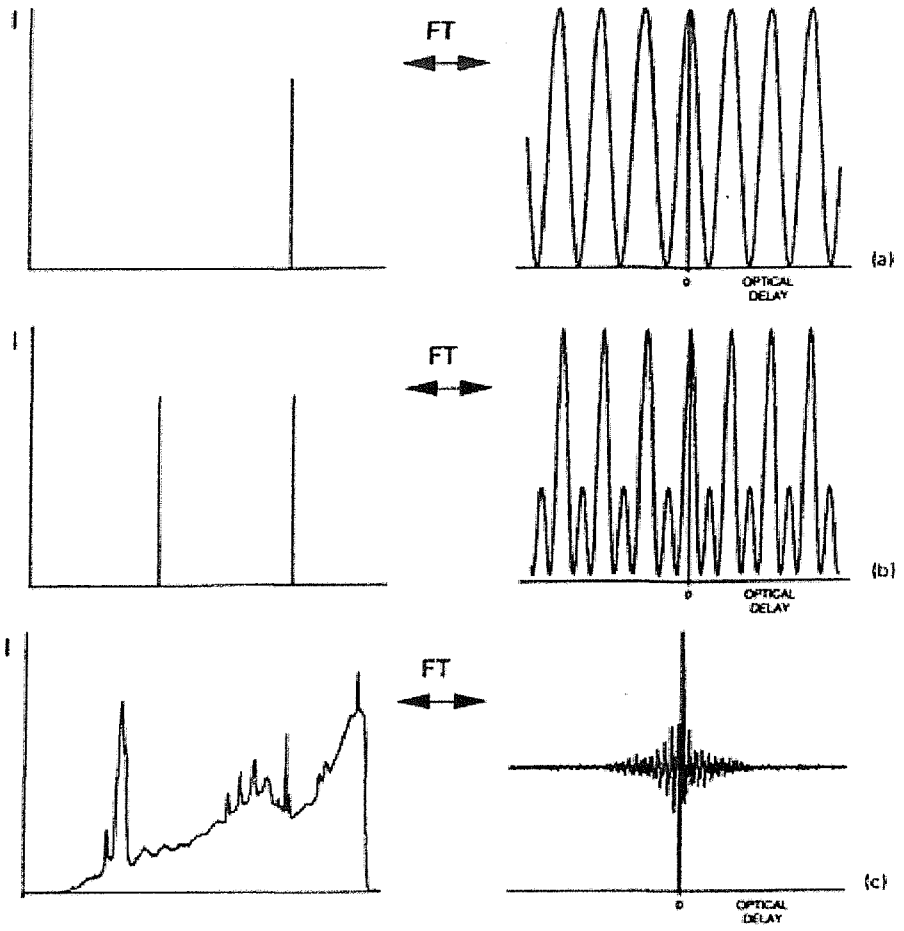


**Figure 1.5** Fourier transformation of a single frequency pulse (top), of two single frequency pulses (middle) and of a multifrequency pulse (bottom). Reproduced with permission from *Fourier Transform Raman Spectroscopy* by *Hendra, Jones & Warnes.*

The Fourier Transform process is then used to deconvolute this signal into different superimposed cosine functions, which is then presented as a signal as a function of frequency. Hence the interferogram is transformed into the spectrogram.

### The detector

Since photomultipliers are insensitive beyond 1 μm, solid state detectors are used in near-infrared experiments. Two popular detectors are the InGaAs detector and the Germanium detector. The former, operates at room temperature and to slightly longer wavelengths (and hence higher shifts). The latter, the Ge detector, needs cryogenic cooling but has a better signal to noise ratio.

### Filters

As the Raman signal is very weak compared with the elastic scattering (Rayleigh scattering), a good filter arrangement to block this frequency is essential. The filter system should 'cut in' as steeply as possible to allow Raman scattering to be recorded as close to the laser frequency as possible.

Optical filters may be used to block unwanted frequencies. The two most common types of optical filters are absorption or interference filters. Holographic optical filters are now common components in new Raman instrumentation.

In Fourier Transform systems electronic filtering may also be used.

### Comparison between dispersive and Fourier Transform Raman spectroscopy.

The use of an interferometer shows several advantages over a dispersive system:

*The Jacquinot Advantage*

Because Raman scattering is such a weak process, it is important that the scattered light is collected as efficiently as possible. The light enters via a large circular hole instead of a narrow slit in a dispersive instrument, thus allows more light to fall onto the interferometer. This means that the optical conductance will be larger by two orders of magnitude compared to grating spectrometers [30-32].

*The Felgett Advantage*

Both the interferometer and the spectrograph have an advantage compared with a monochromator when it comes to the amount of Raman scatter being analysed at the same time. A scanning monochromator is very inefficient in that only a small range of wavelengths of the light falls onto the detector, therefore each spectral element is measured sequentially. In the interferometer and the spectrograph every spectral element is measured simultaneously; the whole frequency range is scanned simultaneously. This is also known as the multiplex advantage [33].

*The Connes Advantage*

The signal to noise of spectra will improve as spectra are averaged. Dispersive systems are sensitive to mechanical wear, which will have an effect on the frequency accuracy, influencing the co-adding of the spectra. FT-instruments make use of a HeNe laser to monitor the change in optical path difference. The interferogram is digitised at the zero-crossings of the HeNe interferogram. The accuracy of sample data spacing is solely determined by the precision of the HeNe wavelength. This built-in, high precision is known as the Connes advantage [34].

In FT-Raman spectroscopy, one usually makes use of a Nd:Yag laser with an excitation at 1.064 μm. The use of such a near-infrared (NIR) laser suffers from a reduction in signal (Raman intensity) compared to a visible laser, because the Raman intensity is related to the fourth power of the excitation frequency. However, low photon energies in the near infrared are less likely to cause fluorescence of the sample. This allows the spectroscopist to use higher laser powers which partially compensates for the reduced efficiency.

A problem in FT-Raman spectroscopy is that most samples absorb to some extent in the NIR [35], resulting in sample heating [36]. Self-absorption of the Raman scattering [35, 37] is another problem especially when attempting quantitative analyses. There are also difficulties in studying samples at temperatures greater than 150 °C due to thermal blackbody emission from the sample [35]. Additionally, near-infrared detectors are much noisier than photomultipliers and CCD detectors, but in comparison an FT-instrument offers the multiplex advantage, which means faster scans, and the availability of higher powered lasers.

## 1.9 Vibrational Spectroscopy and Phase Changes

The reason for using vibrational spectroscopy to study different crystal structures is not immediately obvious. Most low level descriptions of the vibrational spectrum of a molecule start from the concept that the vibrating molecule is isolated. Thus group frequency analyses used in the infrared totally ignore intermolecular interactions. Even full co-ordinate analyses consider an isolated molecule in a vacuum. Now, the spectrum can be divided up into the section below 150 $cm^{-1}$ shift where we find the crystal lattice modes, the rest of the spectrum from 150 $cm^{-1}$ to around 3600 $cm^{-1}$ consists of internal modes and less apparent, overtones and combination bands. When comparing the Raman spectrum of a melt with that of the solid state, the bands in the melt are broader and of different relative intensity to those of the crystalline solid. The vibrations of a crystal are those of the unit cell, not of an isolated molecule hence the selection rules depend on the unit cell rather than the molecular point group. The component molecules are exposed to a rigid strictly defined but intense intermolecular force field hence a sharp spectrum is produced for the perturbed molecule, each band splitting due to the crystal effects. The melt produces broad bands characteristic of the

molecule but perturbed by the continuously varying intermolecular force field in which it finds itself. Thus, we have spectra due to:

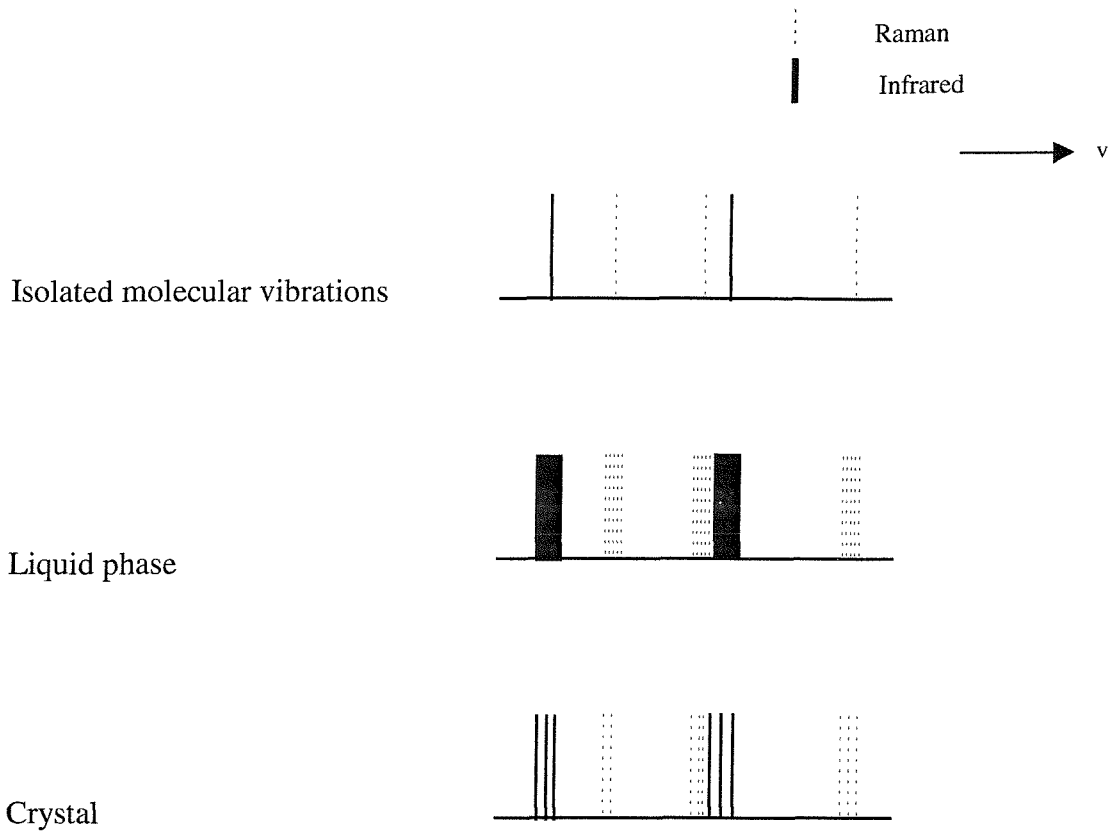


So the crystalline spectrum is more complex and much sharper than the relevant melt (or solution) and is dependent upon the crystal structure. In infrared spectra the same theory applies, but unfortunately the bands tend to be broader.

## 1.10 Raman Intensities

The study of Raman intensities enables us to make quantitative measurements by comparing the relative strengths of the spectra of the various samples. In theory, the intensity of Raman bands depends on a complex expression involving the polarizability tensor of a molecule. In practice, a simplified model is used so that Raman intensities can be studied in a way similar to absorption spectroscopy. The intensity can be expressed in an equation analogous to the Beer-Lambert law.

$I_{Raman} = XKVCI_0$

where $I_{Raman}$ : intensity of Raman band

$I_0$ : intensity of exciting radiation

V : volume of sample illuminated by the source and viewed by spectrometer

C : concentration of the sample

K : absolute Raman scattering cross section

X : a constant that includes experimental factors like spectrometer efficiency, change in focus,...

A big problem lies in the determination of V and K, for which values in the literature have varied considerably. In addition, the overall intensity of the whole recorded spectrum is determined by many experimental factors (X). Optical efficiency, method of illumination, wavelength response and the skill of the operator are important variables when comparing the absolute intensities of spectra recorded on different Raman spectrometers.

When sampling solids, even more parameters become important like particle size [38] and packing density. This is the reason why in theory quantitative Raman analyses are regarded as being impractical.

There are several methods to overcome these problems. Use of an internal or external reference are the most common. Cutler [39] and later Petty et al. [40] describe a method for correcting near-infrared emission spectra for variations in spectrometer response with wavelength. The method describes the use of the spectrum of a blackbody emitter as the correction curve. In a second paper, Petty et al. suggested the use of a standardised intensity scale for liquid spectra [41], where the recorded Raman spectra are standardised against the 1170 $cm^{-1}$ band in the external reference hexachlorobuta-1,3-diene. The effects of alignment, laser power and resolution on the appearance of the Raman spectra were demonstrated and the advantages of using a standardised intensity scale were proven.

Unfortunately, the use of the standard intensity scale has not taken off.

## 1.11 Raman Sampling

Raman sampling has a tremendous advantage compared to IR sampling in that there is virtually no sample preparation required. One can take a Raman spectrum while the sample is still in the sample bottle (provided it is transparent) and the presence of water is not a problem either. This is one of the advantages that makes Raman spectroscopy a popular technique.

The cells described here were used with the FT-Raman instrument, but it is possible the use them with a dispersive Raman instrument with a macropoint accessory.

### The spinning cell

Two types of spinning cells were used in this work. The first cell holds standard NMR tubes. The tubes are held at the bottom and they are rotated along their vertical axis. This cell is ideal for analysing solids and liquids.

A second type of spinning cell was used to analyse tablets. Tablets of different diameters can be held in the sampleholder. This cell also enables the user to use an external reference. The external reference slides into the path of the laser without disturbing the alignment of the sample. A photograph of the cell is shown in Figure 1.6.

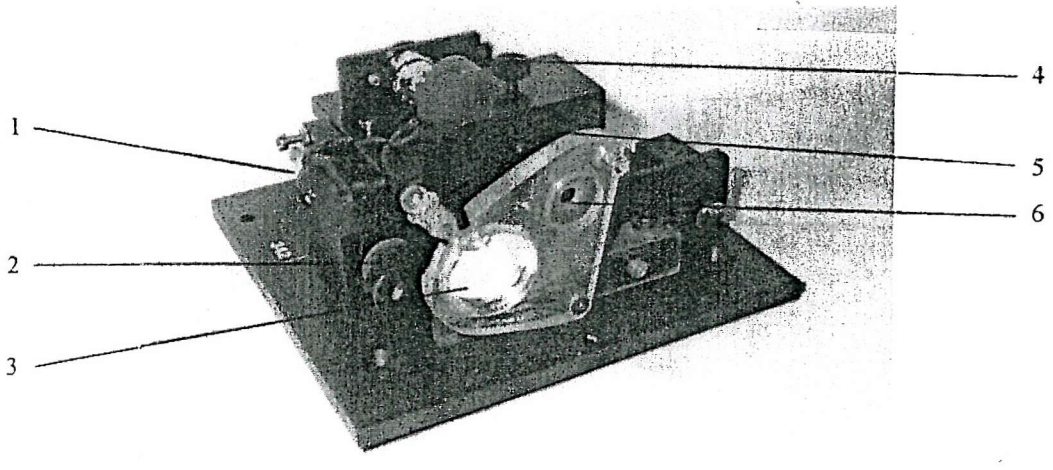


1. Motor controlling the translation
2. Lifting arm for translation
3. Reference cell
4. Motor controlling the rotation
5. Rotating sample holder
6. Hole through which the laser beam enters

**Figure 1.6** Photograph of the tablet analyser.

### The cold cell

For several experiments below room temperature, the cold cell was used. The user can perform measurements ranging from about –150°C to 60°C, depending on the refrigerant that is used. Since the system is temperature controlled, it is easy to monitor reactions. The samples are held in NMR tubes and it is therefore possible to analyse both solids and liquids.

### The hot cell

The hot cell is used for experiments ranging from room temperature up to around 150°C. Again, the system is temperature controlled. The cell holds different sizes of sample bottles and it is therefore practicable to study liquids and solids.

## *1.12 X-Ray Diffraction*

As radiation with a wavelength comparable to bond lengths is bombarded onto a crystal, diffraction occurs. Hence, this diffraction of waves by atoms and molecules can be used for structure determination.

### Single crystal diffraction

With X-Ray wavelengths comparable to the separation of lattice planes in a crystal, Max von Laue suggested that they might be diffracted when passed through a crystal. In these early experiments, the crystal was seen as stacks of reflecting lattice planes, separated by a distance d. It was found that bright reflection (constructive interference) occurs when the glancing angle follows Bragg law:

$n\lambda = 2d\sin\theta$ where $\theta$ is the glancing angle.

In practice, the experiment is performed by mounting a single crystal in the apparatus and rotate it until a reflection is detected.

### The powder method

This alternative technique was developed by Debye and Scherrer and relies on the fact that in a powder sample, some of the crystals will always be orientated so that they will satisfy Bragg's law. Hence different crystallites will have different planes complying to Bragg's law and as a result each will give rise to a cone of diffracted intensity with a different half-angle ($2\theta$).

## 1.13 References


[1] A. Brodin, A. Nyqvist-Mayer, T. Wadsten, B. Forslund and F. Broberg, J. Pharm. Sci, 1984, **73**, 4, 481

[2] B.R. Buchanan, M.A. Baxter, T. Show Chen, X. Qin and P.A. Robinson, Pharm. Res., 1996, **13**, 616

[3] D. Hughes, M.B. Hursthouse, R.W. Lancaster, S. Tavener, T.L. Threlfall, P. Turner, J. Pharm. Pharmacol., 1997, **49**, S4, 20

[4] D.C. Apperley, R.A. Fletton, R.K. Harris, R.W. Lancaster, S. Tavener and T.L. Threlfall, J. Pharm. Sci, 1999, **88**, 12, 1275

[5] J.T. Carstensen, Drug Dev. Ind. Pharm., 1984, **10**, 1277

[6] J.D. Mullins & T.J. Macek, J. Pharm. Sci, 1960, **49**, 245

[7] D. Giron et al, S.T.P. Pharma, 1988, **4**, 330

[8] H. Ando, Drug. Dev. Ind. Pharm., 1995, **21**, 2227

[9] D. Giron, Thermochim. Acta, 1995, **248**, 1

[10] A. Hakanen & E. Laine, Thermochim. Acta, 1995, **248**, 217

[11] E. Laine, J. Pirttimäki, R. Rajala, Thermochim. Acta, 1995, **248**, 205

[12] T. Steiner, W. Hinrichs, W. Saenger & R. Gigg, Acta Cryst., Sect.B, 1993, **49**, 708

[13] K. Ashizawa, J. Pharm. Sci, 1989, **78**, 256

[14] M. Epple & H.K. Cammenga, J. Therm. Anal., 1992, **38**, 619

[15] C.A. Deeley, R.A. Spragg & T.L. Threlfall, Spectrochim. Acta, 1991, **47A**, 1217

[16] F.W. Langkilde, J. Sjöblom, L. Tekenbergs-Hjelte & J. Mrak, J. Pharm.Biomed. Anal. 1997, **15**, 687

[17] W.F. Findlay & D.E. Bugay, J. Pharm.Biomed. Anal. 1998, **16**, 921

[18] J. Anwar, S.E. Tarling & P. Barnes, J. Pharm. Sci., 1989, **78**, 337

[19] G. Bettinetti, F. Giordano, G. Fronza, A. Italia, R. Pellegata, M. Villa & P. Ventura, J. Pharm. Sci., 1990, **79**, 470

[20] A. Smekal, Naturwiss., 1923, **11**, 873

[21] H.A. Kramers and W. Heisenberg, Z. Phys., 1925, **31**, 681

[22] C.V. Raman and K.S. Krishnan, Nature, 1928, **16**, 557

[23] G. Landsberg and L. Mandelstam, Naturwiss., 1928, **70**, 10

[24] D.N. Batchelder, Eur. Spectrosc. News, 1988, **80**, 28

[25] G.W. Chantry, H.A. Gebbie and C. Helsum, Nature, 1964, **203**, 1052

[26] T. Hirschfeld, "Laser Raman Gas Diagnostics", Plenum, New York, 1974

[27] T. Hirschfeld and B. Chase, Appl. Spectrosc., 1986, **40**, 2, 133

[28] D.B Chase, J. Am. Chem. Soc., 1986, **108**, 7485

[29] B. Schrader, A. Hoffmann, A. Simon, R. Podschadlowski and M. Tischer, J. Molec. Struct., 1990, **217**, 207

[30] G. Hansen, Optik, 1949, **1**, 227, 269

[31] V.A. Fassel, IUPAC Recommendation. V.4 I. Pure Appl. Chem., 1972, **30**, 653; Appl. Spectrosc., 1974, **28**, 398

[32] P. Jacquinot, J. Opt. Soc. Am., 1954, **44**, 761; P. Jacquinot, Infrared Phys., 1984, **24**, 99

[33] P. Felgett, J. de Physique et le Radium, 1958, **19**, 187

[34] J. Connes & P. Connes, J. Opt. Soc. Am., **56**, 1966, 896

[35] B. Schrader, A. Hoffmann and S. Keller, Spectrochim. Acta, 1991, **47A**, 9/10, 1135

[36] S.J.A Pope, Y.D. West, Spectrochim. Acta, 1995, **51A**

[37] I.A.M. Royaud, PhD thesis, Southampton University, 1990

[38] M.V. Pellow-Jarman, P.J. Hendra and R.J. Lehnert, Vibr. Spectrosc., 1996, **12**, 257

[39] D.J. Cutler, Spectrochim. Acta, 1990, **46A**, 2, 131

[40] C.J. Petty, G.M. Warnes, P.J. Hendra and M. Judkins, Spectrochim. Acta, 1991, **47A**, 9/10, 1179

[41] C.J. Petty, P.J. Hendra and T. Jawhari, Spectrochim. Acta, 1991, **47A**, 9/10, 1189

# Chapter 2 Sample Rotation in Raman Spectroscopy

## 2.1 Introduction

In this chapter we evaluate the use of sample rotators in Raman spectroscopy. Rotation of samples in Raman spectroscopy has become normal practice since the early 1990s. Commercial rotators, initially only able to hold powders but now also tablets, have been available since early 1996.

Brienne et al. reported in 1993 of a Spinning-Cell used to avoid decomposition of $Co_2(CO)_8$ by the laser [1]. The rotational speeds used in this work were fairly high (2000 rpm). Especially in FT-instruments, where a near infrared laser is used to probe the sample, sample heating will inevitably occur. Rotating of the sample will reduce this effect of sample heating, but in FT-instruments this periodic change in intensity of the scattering and background could lead to spurious lines appearing in the spectra. Salzer et al. [2,3] suggested the use of step-scan FT-NIR[8] Raman to avoid these problems of modulation and double modulation. However, the solution does not need to be as costly as this. When rotational speeds are kept reasonably low, good quality FT-spectra from rotating samples can be obtained. A good example is given in an article by Langkilde et al. who successfully performed quantitative analyses on a mixture of polymorphs while slowly spinning the samples [4]. Another article by Taylor and Langkilde describes the use of sample rotation to study the composition of several commercial pharmaceutical tablets [5].

## 2.2 Experimental

All FT-Raman spectra were acquired on a Perkin-Elmer System 2000 FT-Raman spectrometer which was equipped with a quartz beam splitter and an InGaAs detector, operating at room temperature. A Spectron continuous wave $Nd^{3+}$:YAG laser (1.064μm) provided the NIR excitation.

[8] NIR : near Infrared

The dispersive Raman spectra were obtained using a Renishaw Ramascope with HeNe excitation at 632.8 nm and CCD detection. Rotation in this instrument was performed after fitting a Ventacon Macropoint accessory.

Two types of rotator were used. One, designed to examine samples held in NMR tubes, the other to analyse tablets. The first, a prototype model SR-6 Ventacon system rotates the NMR tube held from above and at the same time moves the tube upwards and downwards. The periodicities of the two movements are independently controlled from the power supply, a model D-1 Ventacon Universal Power supply.

The second rotator used, was the prototype model T-1 Ventacon Pharmaceutical Tablet Analyser. The tablet, held in a cup, is rotated about a horizontal axis by one motor, whilst another motor controls the speed with which the tablet cup is moved up and down. Again, the periodicities are independently controllable from the power supply. Tablets may be firmly held in the cup or are allowed to tumble. Figure 2.1 shows how the tablet is sampled as the sample holder rotates and translates.

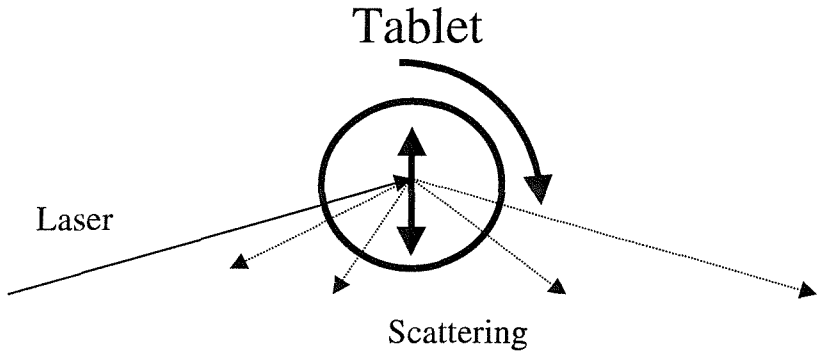


**Figure 2.1** The picture shows the movement of the tablet while recording the Raman spectra. One motor controls the vertical movement (shown by the vertical arrow), whereas another motor controls the rotational speed (shown by the other arrow).

## 2.3 Minimising sample heating by the laser

Sample heating by the laser has always been a problem in Raman spectroscopy, but since the availability of the near-infrared lasers this has become worse. The problem lies in the fact that all samples more or less absorb in the near infrared. In addition, in comparison with the higher energy visible lasers, higher laser powers are required.

An example is found in a compound used in a local anaesthetic formulation, prilocaine. An FT-Raman spectrum of the compound was recorded. The melting point of prilocaine is 38°C, thus it was transferred in the solid state into the sample holder. But after 10 scans at moderate laser power (200mW), the spectrum started to decrease in intensity. Bands broadened and after 2 minutes it was decided to halt the scanning. The sample had clearly started to melt.

It is difficult to estimate the degree of heating by the laser since it depends on certain characteristics of the sample in question like thermal conductivity, reflectivity and other variables like sampling time, laser power and the optics of the instrument.

In an attempt to measure the increase in temperature due to laser heating, Pope and West [6,7] used a phase transition in sodium molybdate known to occur at 112°C as a reference point. The Raman spectra of the two forms are easy to differentiate. In their experimental set-up a temperature rise of 40°C was measured when 125mW of laser power was used. However, in another experiment, performed on PTFE[9] by Lehnert [8], an increase in temperature of only 1°C per 100mW was found. Taylor and Langkilde reported of a temperature increase of at least 20°C when they recorded the spectrum of theophylline monohydrate using 800mW of laser power [5].

In 1995, Dent [9] made the suggestion to surround a heat sensitive sample with a good thermal conductor. In the same issue, Pope and West published a paper where several possibilities of using such good thermal conductors were explored [7]. Amongst others, NIR FT-Raman spectra were recorded of $KMnO_4$, graphite, $CuSO_4.5H_2O$ and $NiSO_4.xH_2O$ as nujol mulls between KBr, Quartz or Pyrex flats or as KBr or KCl discs.

A less time consuming solution would be to rotate the sample. The effect is shown in Figure 2.2 where the FT-Raman spectrum of prilocaine is recorded. The top spectrum was recorded while the powder was held stationary. The bottom spectrum was recorded whilst rotating the powder.

[9] PTFE: Polytetrafluoroethylene

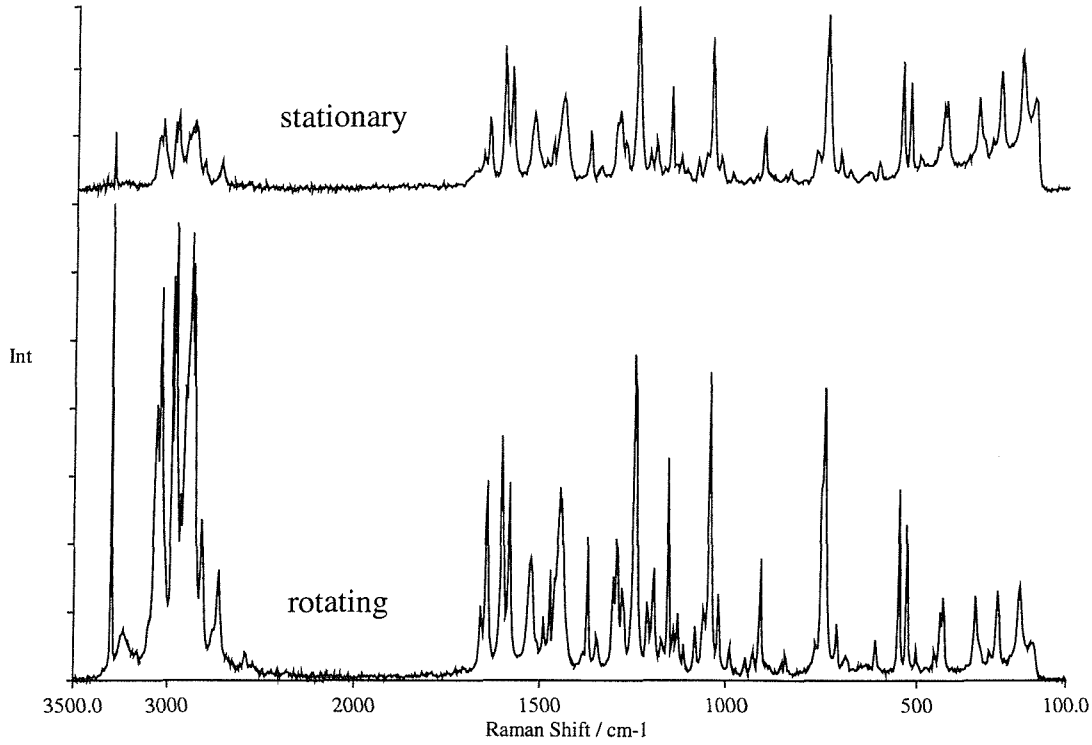


**Figure 2.2** The effect of heating by the laser on prilocaine. The top spectrum displays prilocaine, held in a solid sample holder. Because of constant heating by the laser, the sample has started to melt. In the bottom spectrum prilocaine is rotated in an NMR tube. Both spectra were recorded using 200mW of laser power.

The poor quality of the top spectrum of prilocaine is due to the component starting to melt.

Thus, avoiding sample heating by the laser is essential in order to get a good quality crystalline spectrum. Another class of samples where avoiding sample heating is important are compounds displaying polymorphism. Where samples display polymorphism, changing temperatures can induce phase changes.

But there is another advantage to rotating samples. A second reason why spectroscopists choose to rotate their samples is to avoid sub sampling.

## 2.4 Avoiding subsampling

Especially in the pharmaceutical industry where formulations in tablet form are being analysed, avoiding sub sampling is of major concern. Since the laser spot diameter is only small, varying from 0.1 to 1 mm, averaging over an area as large as possible is essential to avoid erroneous conclusions. In addition, the degree of subsampling will depend on the particle diameter of the components and the composition of the tablet.

An example of subsampling by recording stationary spectra is given in the following spectra of a tablet containing $K_2CrO_4$ and $Na_2SO_4$. Two FT-Raman spectra are recorded whilst the tablet is stationary. A third was recorded as the tablet was rotating. The spectra are displayed in Figure 2.3.

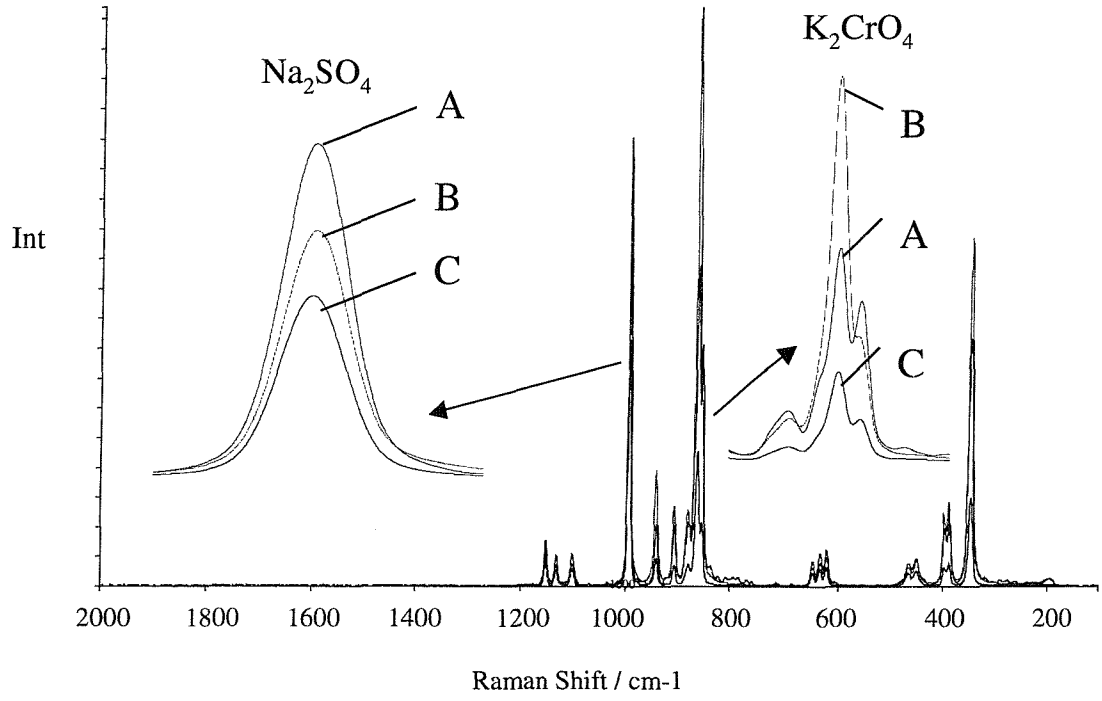


**Figure 2.3** FT-Raman spectra of a tablet containing $K_2CrO_4$ and $Na_2SO_4$. The spectra B and C were recorded from different points on the tablet whilst it was stationary. Spectrum A was recorded while the tablet was rotating. Laser power: 200mW, 4$cm^{-1}$ resolution, 20 scans.

Two regions, typical for one specific component within the tablet are enhanced in the figure. The band region specific for $K_2CrO_4$ expands from 900 $cm^{-1}$ to 820 $cm^{-1}$ and for $Na_2SO_4$ the band between 1005 $cm^{-1}$ to 980 $cm^{-1}$ was chosen.

Spectra B and C were recorded whilst keeping the tablet stationary. Spectrum B would suggest that there is more $K_2CrO_4$ than $Na_2SO_4$ present in the tablet compared with spectrum C. Spectrum A however shows an increased intensity of the $Na_2SO_4$ band compared with the $K_2CrO_4$ band, in accordance with spectrum C.

Therefore recording a single stationary spectrum would lead to erroneous interpretation of the composition of the tablet.

But there are risks associated with rotating samples both in FT and dispersive Raman instruments.

## 2.5 Rotation in Fourier Transform Instruments

The concept behind Fourier Transform instruments is as follows. An interferometer, often a Michelson interferometer (see the Introduction section, page 13) is used to split the collected light into two equal beams which recombine after one of them is subjected to an optical delay. This results in a complicated interference pattern as a function of optical delay. This is known as the interferogram. The Fourier Transform algorithm is then used to convert this time dependent interferogram into a frequency dependent signal, which we see as the spectrum.

### Spurious frequencies in FT-Raman spectra

As a sample is rotated, its scatter intensity will vary with rotational speed. Other factors influencing the intensity fluctuations are the particle size of the components and scan speed. This periodic change in intensity itself will produce a different beat frequency and if it happens to be in the frequency range in which the detector operates, it will be Fourier Transformed into a spurious signal.

Due to the characteristics of the detectors and mechanical limitations it is normal to restrict the rate of scan of the interferometer so that the bandwidth of the detector output lies in the audio frequency range. Scan speeds can be adjusted over fairly considerable limits but the detector output from the interferogram is normally kept within the range 250-5000 Hz in an FT Raman instrument and it is this audio signal that is subsequently transformed using the Fourier Transform algorithm.

This concept is made clear with the following example. Let us assume that the tablet rotates at 1500 rpm (or 25 Hz). If the instrument scan speed is set to 0.1 cm/s, this frequency translates to 25 $s^{-1}$ / 0.1 cm/s equals 250 $cm^{-1}$. This frequency (in wavenumbers) lies well below the detector cut-off which is around 5000 $cm^{-1}$ in our NIR instrument. If the rotational speed were to increase to 51 000 rpm (or 850 Hz), this frequency would translate to 8500 $cm^{-1}$ absolute wavenumbers, which would give a spurious line in the actual spectrum at around 900 $cm^{-1}$ frequency shift.

An example of the appearance of these spurious frequencies is given in Figure 2.4.

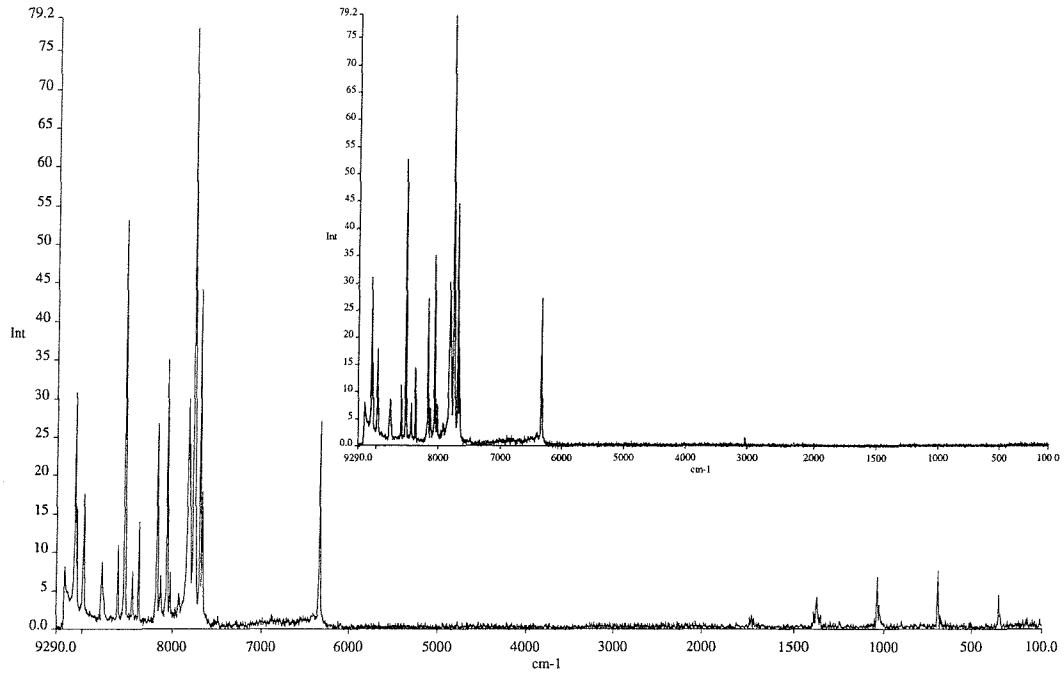


**Figure 2.4** FT-Raman spectra of maleic acid. The top spectrum is the stationary one, whereas the bottom spectrum is of maleic acid while rotating. Rotational speed is around 1600 rpm. The X-axis is in absolute wavenumbers.

The spurious lines in the bottom spectrum are clearly visible below 1500 $cm^{-1}$. Hence they do not disturb the actual Raman spectrum between 9394 $cm^{-1}$ and 6000 $cm^{-1}$. In Figure 2.5 the effect of increasing the rotational speed on the frequency of the spurious lines is demonstrated. A tablet containing metoprolol succinate is rotated at two different speeds (1690 rpm and 6760 rpm) and the FT-Raman spectra are recorded. For comparison, the stationary spectrum is also included.

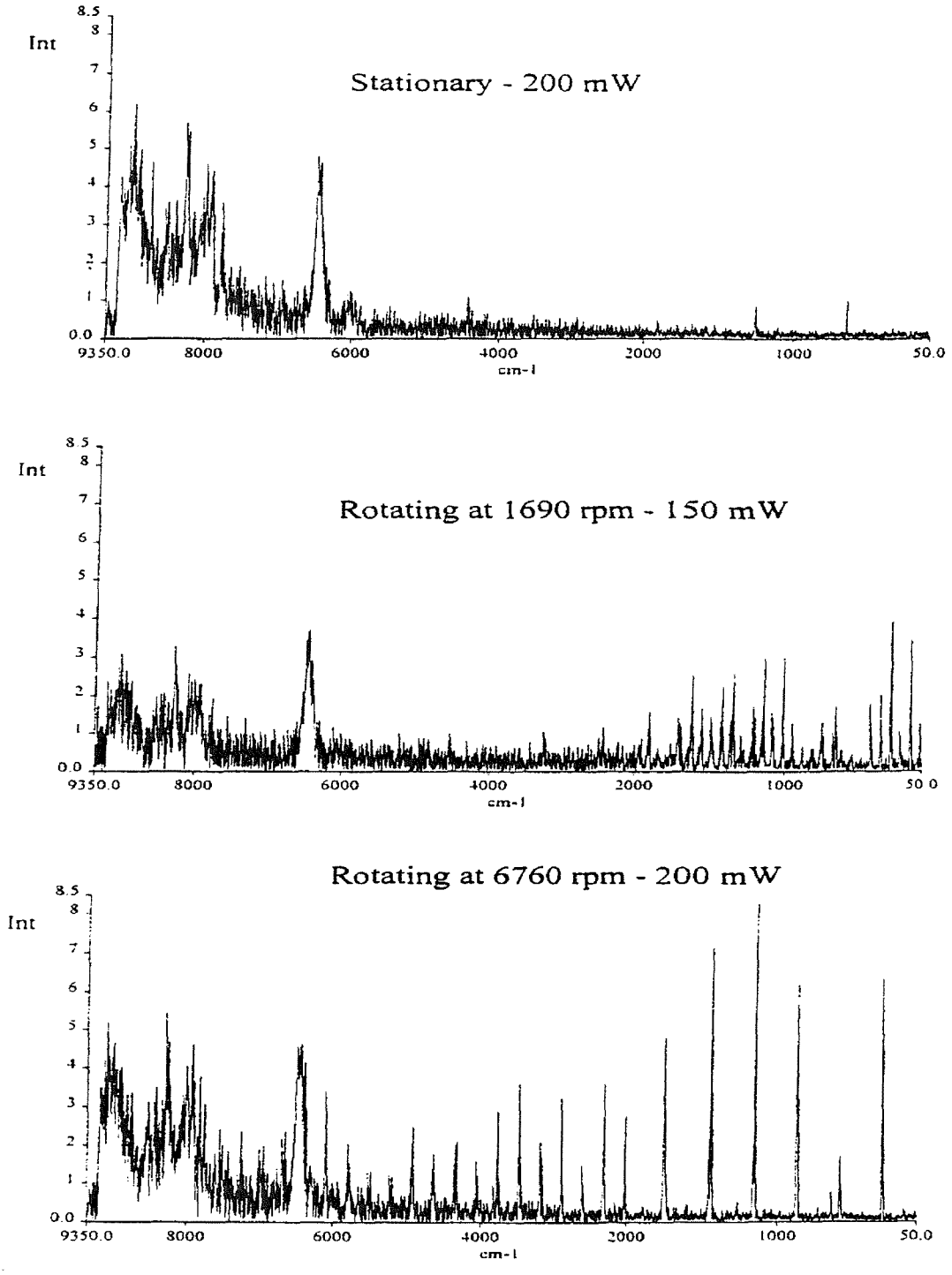


**Figure 2.5** Unshifted FT-Raman spectra of a tablet containing metoprolol succinate at different rotational speeds. The appearance of spurious bands in the spectra is clearly visible. At higher rotational frequency, the frequency of the spurious bands shifts towards higher wavenumbers. All spectra were obtained by co-adding 20 scans with 4 $cm^{-1}$ resolution. Reproduced with permission from [13].

Figure 2.5 shows that more than one spurious frequency band appears for each rotational speed. This is probably due to harmonics of the rotational frequency. These

harmonics are dependent on the particle size of the components, their composition, the laser spot size and on the quality of the rotator (off-axis tubes might induce spurious frequencies etc.).

### Appearance of side bands in FT-Raman spectra

It is known that modulation of the Raman scattering will produce side-bands to the main scattering bands, particularly if these are sharp and intense. R. Bennett specifically used modulation to remove thermal backgrounds [10,11]. By modulating the laser, the Raman spectrum was 'repeated' in the side bands, but this 'new' Raman spectrum was translated outside the region where thermal backgrounds are visible (from about 2000 $cm^{-1}$ to the detector cut-off at 3550 $cm^{-1}$). Hence it was possible to discriminate between the long lived, slow response thermal emission and the instantaneous Raman scattering. This shift of the Raman spectrum (or put differently as the side band frequency shift from the 'real' spectrum) depends on the modulation frequency. Bennett used a 526 Hz laser modulation hence the spectrum was repeated at $\nu \pm 526$ Hz.

Rotation of a sample in FT-instruments can be seen as a similar type of modulation. Cutler and Petty [12] pointed this out in their paper where again, they used pulsed lasers to reject long-lived backgrounds.

Since the surface of a tablet is never perfectly homogeneous (especially not in tablets containing more than one component), many frequency modulations will occur, resulting in side bands close in frequency to the main bands of the Raman spectrum. An example is shown in Figure 2.6 where an FT-Raman spectrum of $KMnO_4$ powder, whilst the sample is rotated, is displayed. This particular powder was chosen because as an inorganic powder, it has very sharp and very intense bands in its Raman spectrum. Therefore it would be easier to distinguish between peaks resulting from the Raman scattering and those resulting from rotation. From our previous arguments many side bands are expected to appear in the Raman spectrum, but Figure 2.6 shows that they are not as problematic. Overall, the noise level has only slightly increased.

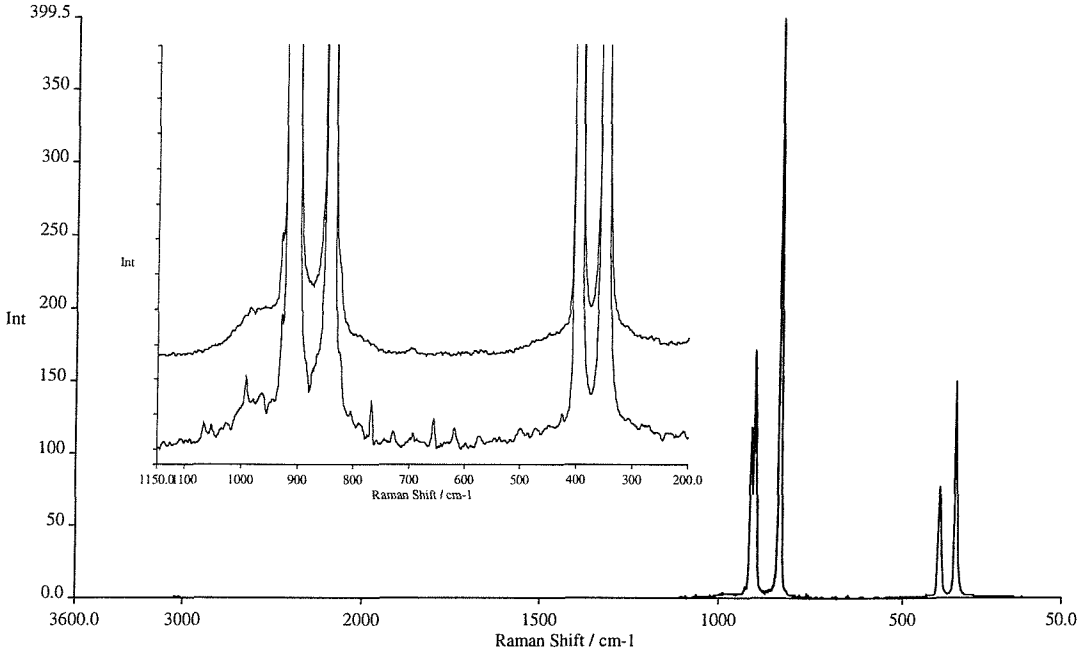


**Figure 2.6** Appearance of side bands in the FT-Raman spectrum of $KMnO_4$ powder. The top spectrum is that of $KMnO_4$ held stationary. The bottom spectrum is that of $KmnO_4$ whilst rotating. The side bands are clearly visible in the bottom spectrum, but their intensity is only 0.5% of the most intense peak in the spectrum. Both spectra are the result of 10 accumulations.

In addition to this sample of $KMnO_4$ powder, other powders and also tablets were studied while rotating. More specifically, the appearance of side bands was investigated as well as the possibility of increased noise levels. The results are summarised in Table 2.1.

**Table 2.1** Observations of the FT-Raman spectra of rotated samples with regards to the appearance of side bands and the increase of the overall noise level.

| Compound | Physical form | Appearance of side bands | Increase of noise level |
|---|---|---|---|
| $KMnO_4$ | powder | yes | yes |
| $Na_2SO_4$ | powder | yes | yes |
| Maleic acid | powder | no | yes |
| $Na_2SO_4$ | tablet | yes | yes |
| Maleic acid | tablet | no | negligible |

The spectrum of maleic acid whilst rotating is shown in Figure 2.7. As mentioned in Table 2.1, when rotating maleic acid powder in an NMR tube, no sidebands were visible, but a slight increase in the background noise level was observed.

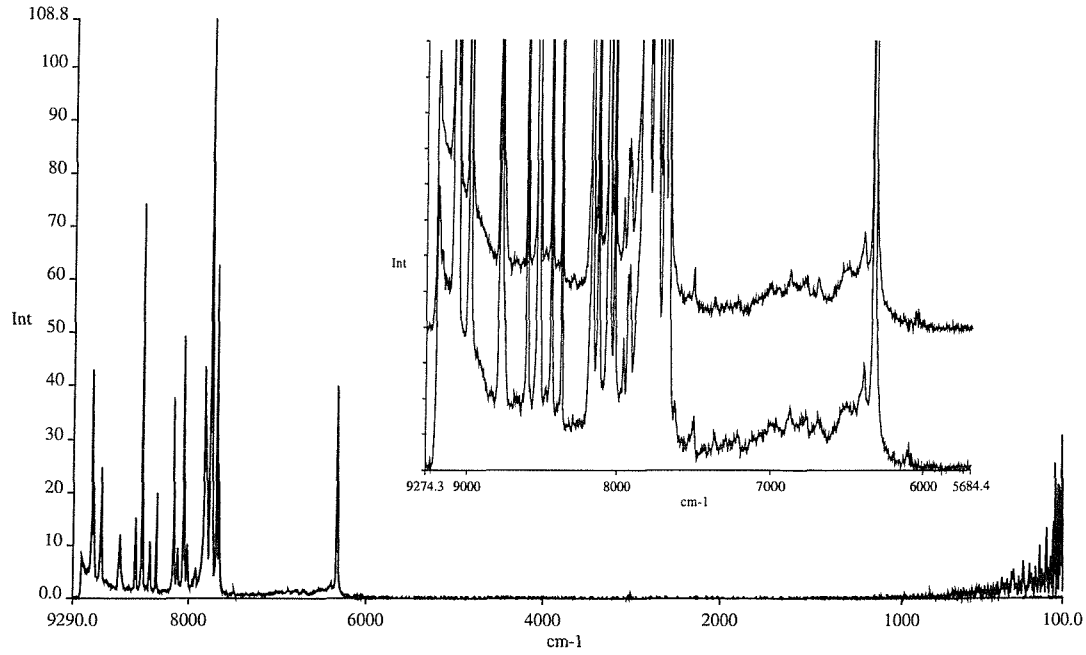


**Figure 2.7** Effect of sample rotation on the FT-Raman spectra is shown for maleic acid powder. The top spectrum is that of maleic acid held stationary. The bottom spectrum is that of maleic acid whilst rotating. There are no side bands visible in the spectrum of the rotating powder. Both spectra are the result of 10 accumulations. Note that the X-axis is in absolute wavenumbers instead of wavenumber shift.

In three papers by Salzer and Roland [1-3] a solution to the appearance of these spurious bands is presented. They suggest the use of step-scan spectrometers. But this solution is a very expensive one. The rotational frequency they used to show the appearance of spurious bands in the FT-Raman spectra was very high (up to 667 Hz). From our calculations, it is clear that simply by decreasing the rotational speed, the low wavenumber spurious lines can be avoided. In addition, the sidebands that are expected to show up in the actual Raman spectra are not always there. Most probably there will be a slight increase in the overall noise level, but by simply co-adding more scans this can be reduced.

Therefore, rotation of samples in FT-instruments at well below 1500 rpm can be considered as perfectly acceptable [13].

## 2.6 Rotation in dispersive Instruments

In dispersive instruments, no interferometer or Fourier Transformations are used to generate the spectra. Therefore, it would be tempting to conclude that rotating samples in dispersive instruments poses no problems, but one has to be careful.

There are other factors that influence the quality of the spectra in dispersive instruments. A first factor is fluorescence. Since dispersive instruments use higher energy lasers (usually visible lasers but UV lasers are also getting more common) than their FT- counterparts, the possibility of sample fluorescence is very real. In our experiment, a tablet containing $Na_2SO_4$ was rotated as the Raman spectrum was recorded. The compound is an inorganic white powder, not particularly prone to fluorescence. The spectra recorded while the tablet was stationary and rotating are shown in Figure 2.8.

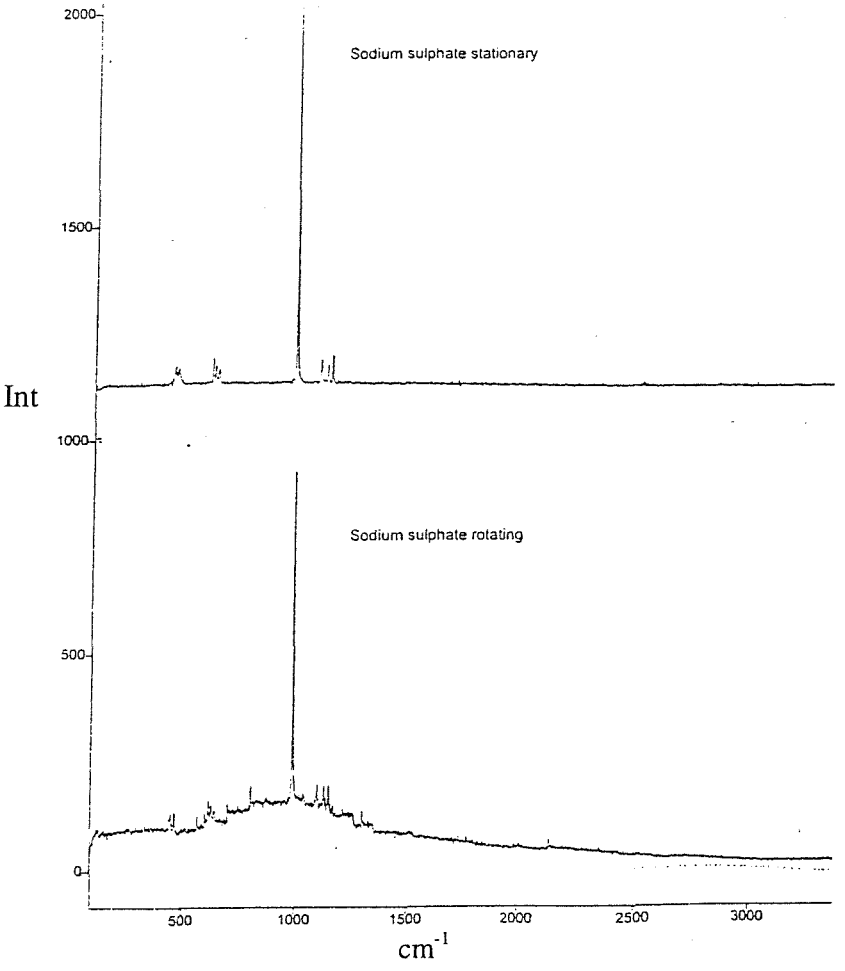


**Figure 2.8** Dispersive Raman spectra of a $Na_2SO_4$ tablet, both stationary (top) and rotated (bottom). The spectrum was recorded on the Raman microscope with the macropoint accessory fitted. The effect of fluorescence bleaching is shown in the top spectrum.

In the bottom spectrum, a fluorescent background is clearly visible, while it is absent in the stationary spectrum. The problem arises from fluorescence bleaching. Whilst keeping the tablet stationary, the fluorescence is bleached out of the spectrum.
When these experiments were repeated with other samples (both freshly prepared and old tablets), it was not possible to get any spectrum at all. Whether this was due to the fluorescence or the sensitivity of the pixels in the CCD detector not properly responding to the changes in the spectra with rotation is unclear, but it is quite clear that slow rotation can be problematic when using these instruments.

## 2.7 Conclusions

This work shows that it is perfectly acceptable to rotate samples in Fourier Transform Raman spectrometers as long as rotational speeds are kept reasonably low (below 1500 rpm). A small increase in the overall noise level is detected, but this can easily be reduced by increasing the number of co-added scans. In addition side bands can appear in the spectra but these have rather low intensities.
Rotation is acceptable in dispersive Raman instruments as long as one accepts that fluorescence is a limiting factor in the choice of samples.
In addition, one can opt for the step-scan interferometer.

## 2.8 References


[1] S.H. Brienne, R.D. Markwell, S.M. Barnett, I.S. Butler and J.A. Finch, Appl. Spectrosc., 47, (1993), 1131

[2] U. Roland and R. Salzer, Mikrochim. Acta, 14, (1997), 757

[3] R. Salzer, L. Sümmchen, U. Roland and R. Born, Spectrosc. Europe, 10/2 (1998), 8

[4] F.W. Langkilde, J. Sjöblom, L. Tekensbergs-Hjelte and Jonni Mrak, J. Pharm. Biomed. Anal., 15, (1997), 687

[5] L.S. Taylor and F.W. Langkilde, Jn Pharm. Sci., 89, 10, (2000), 1342

[6] S.J.A. Pope, Y.D. West, Spectrochim. Acta, 51A, (1995) 2027

[7] S.J.A. Pope, Y.D. West, Spectrochim. Acta, 51A, (1995) 2011

[8] R.J. Lehnert, Ph.D. Thesis, University of Southampton, 1994

[9] G. Dent, Spectrochim. Acta 51A, (1995), 1975

[10] R. Bennett, Spectrochim. Acta, 50A, (1994), 1813

[11] R. Bennett, Spectrochim. Acta, 51A, (1995), 2001

[12] D.J. Cutler, C.J. Petty, Spectrochim. Acta, 47A, (1991) 1159

[13] A.T.G. De Paepe, J.M. Dyke, P.J. Hendra and F.W. Langkilde, Spectrochim. Acta, 53A, (1997), 2261

# Chapter 3 Quantitative Analysis using FT-Raman Spectroscopy

## 3.1 Introduction

Problems associated with reproducibility in the Raman experiment have resulted in quantitative analysis using FT-Raman spectroscopy being regarded as difficult. However, despite the difficulties, Raman spectroscopy as a tool for quantification is gaining more and more popularity. The problems associated with reproducibility arise from sample properties e.g. refractive index, colour and scattering coefficients as well as instrumental variables like detector response and laser stability.

When analysing solid samples even more variables need to be controlled if repeatable intensity measurements are to be generated e.g. particle size [1,2], packing density and preferred orientation.

As a result using internal or external standardisation has become common practice. Back in the early 1990s, Hendra et al proposed the use of a standardised intensity scale for liquid spectra [3,4]. Schweinsberg and West used this external reference in the quantitative analysis of liquid mixtures [5].

Since these early experiments, many papers have appeared using Raman spectroscopy as a quantitative tool. Especially in the area of polymorphism, Raman spectroscopy has proved to be very useful. The use of some sort of chemometrics has been the core in most of the examples [6-8]. However simply the ratioing of two band regions within the spectrum has also proved successful [9].

Another area in which quantitative Raman spectroscopy is gaining much popularity is in the analysis of tablets. The usual method of tablet analysis is HPLC, but since this method is destructive and very time consuming, new alternatives have been investigated. Again, both the use of band ratios [10-12] and chemometrics [13] have been used in this area.

In this chapter the use of FT-Raman spectroscopy as an analytical tool is carefully evaluated. In the first stage, reproducibility of the intensity of the FT-Raman spectra was studied both for liquids and solids. In a second stage, calibration curves were

constructed for quantification of the composition of different sets of tablets. A considerable number of problems were encountered because we had to prepare the calibration sets of tablets ourselves. The biggest problem was that of sample inhomogeneity arising from mixing problems. The reasons for what seems to be a trivial requirement are explained.

In this work simple band ratios were used. A comparison is made between the results from internal standardisation with those from external standardisation.

## 3.2 Experimental

FT-Raman spectra were acquired on a Perkin Elmer System 2000 FT-Raman spectrometer, equipped with a quartz beam splitter and an InGaAs detector operating at room temperature. Two different lasers were used; a Spectron continuous wave $Nd^{3+}$:YAG laser and an Optomech solid state $Nd^{3+}$:YAG laser. Both lasers provide near infrared excitation at 1.064 μm. The Optomech device is of contemporary design and is solid state driven. Its output is steady and known to be noise free. The alternative laser, from Spectron is of much older design uses a xenon arc lamp as source and is water-cooled. The device incorporates a stabilisation system but its output does fluctuate over a seconds and minutes time scale. On the other hand its beam properties (divergence and phase) are far superior to the solid state device. The use of either laser will be clarified in the experimental description.

In addition, as a comparison, the Bruker RFS100 FT-Raman spectrometer at AstraZeneca Södertälje was used to repeat some of the results. This system uses a solid state $Nd^{3+}$:YAG laser giving near infrared excitation at 1.064 μm. As a detector system, a liquid nitrogen cooled Ge detector was used.

Unless otherwise stated, throughout this report, the Perkin Elmer System 2000 was used.

To analyse the tablets, a prototype model T-1 Ventacon Pharmaceutical Tablet Analyser was used.

To determine Raman band intensities both the height and area of the specific bands were estimated. Perkin Elmer Spectrum software was used for a first 'quick' estimation of heights and areas. In addition, Grams software was used to curvefit the bands before calculating the areas and heights.

## 3.3 Reproducibility of Raman band intensities

A series of averaging experiments were performed, both on the external reference and a moving (rotating and translating) tablet. This means that several FT-Raman spectra were recorded. Then, the reproducibility of areas and heights of certain bands were calculated by measuring the average intensity, standard deviation and coefficient of variance. As stated above, two software packages were available to us to estimate peak heights and areas. In the Perkin-Elmer Spectrum software the 'calculate area/height function' was used on the raw data. In addition, GRAMS software was available to us. Before using the 'calculate area/height function', the bands were curve fitted using a combination of Gaussian and Lorentzian peak shapes. Curvefitting the bands before calculating areas and heights would be expected to be more accurate. In order to test this hypothesis, a repeatability experiment was performed on the external reference used in this work, hexachlorobuta-1,3-diene. The results are discussed at a later stage.

The Ventacon tablet analyser used with the Perkin-Elmer spectrometer, incorporates an external reference sample. This consists of a sample cuvette holding hexachlorobuta-1,3-diene which can be placed between the tablet and the collection lens of the spectrometer. The rear face of the cuvette is silvered. A picture of the Tablet Analyser is shown in the Introduction section Figure 1.6 on page 20. The reason for choosing hexachlorobuta-1,3-diene as our external reference is threefold. Firstly, it is a liquid, hence we don't expect variations in Raman intensities due to particle size, packing density, preferred orientation,.. Secondly, since this compound is non-hydrogenic, there are no near-infrared absorption bands. Thirdly, this compound is a good Raman scatterer and there are non-overlapping bands that are easy to use as standard.

### Comparison between two software packages used for area and height calculations

As was mentioned above two different software packages were available to estimate Raman band areas and heights. To compare the applicability of the two packages to our experiments, a reproducibility test was performed on the external reference. Sixty spectra, consisting of one scan, were recorded and afterwards the two different packages were used to estimate the area and height of the 1220 - 1120 $cm^{-1}$ band. The

question we tried to answer is whether it is necessary to perform a time consuming curve fit before estimating band areas and height.

The FT-Raman spectrum of the external reference is shown in Figure 3.1.

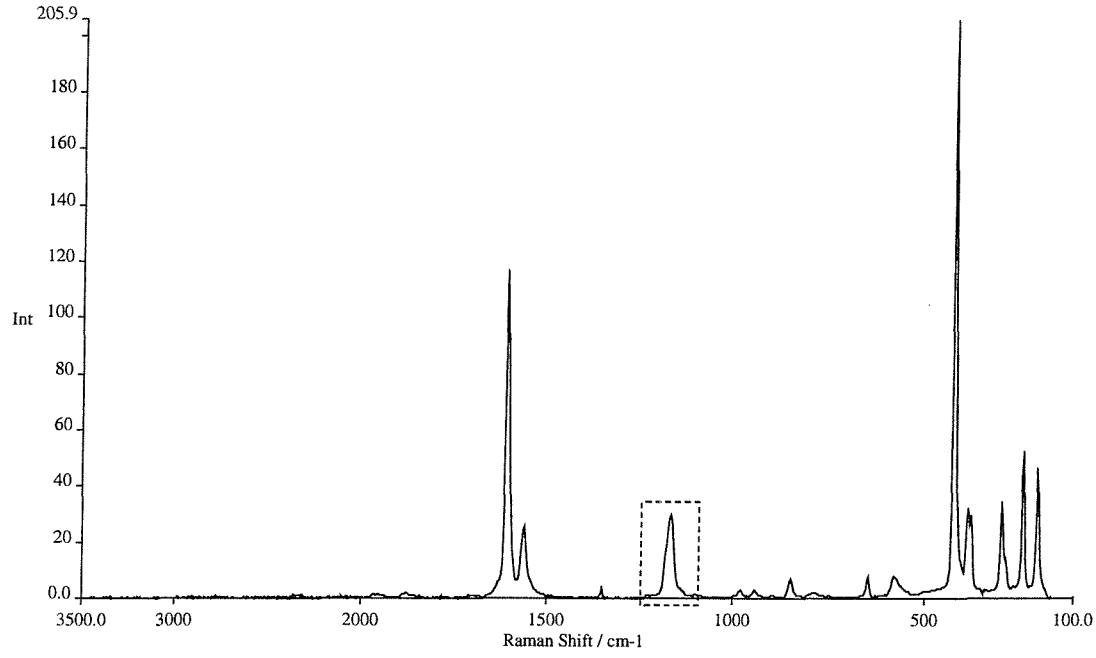


**Figure 3.1** FT-Raman spectrum of our external reference hexachloro-1,3-butadiene. The band region within the dotted box is the region used in our calculations. 200mW, 10 scans, 4 $cm^{-1}$ resolution.

The results of this reproducibility experiment are presented in Table 3.1.

**Table 3.1** Comparison of two different software packages used for height and area estimations of our FT-Raman bands. Coefficients of variance obtained from the reproducibility experiment on the Raman spectra of the external reference are presented. Sixty repeat measurements on hexachloro-1,3-butadiene were performed.

| Coefficient of variance values | | | |
|---|---|---|---|
| Curve fitted data before calculation of area and height | | Calculation of area and height without curve fitting | |
| Area | Height | Area | Height |
| 8.25 | 4.70 | 4.36 | 4.39 |

From the table of results, it is clear that for these spectra curve fitting before estimation of areas and heights does not give better results. One reason could be that

the band is relatively intense and the background noise is low. For low intensity and overlapping bands, curve fitting before estimation of band areas and heights is expected to give better results.
From these results, it was decided that no curve fitting is needed for our experiments where bands are usually intense and reasonably sharp.

### Liquid samples

In a first set of experiments, mixtures of cyclohexane and hexachlorobuta-1,3-diene were prepared. The sample holder used in these experiments allowed collection of FT-Raman spectra of this mixture, as well as the collection of FT-Raman spectra of an external reference (same principle as the tablet analyser described in the Introduction section of this thesis). The mixture, held in a cuvette, was left undisturbed as spectra of the external reference were recorded. As in the previous experiments, the external reference was hexachlorobuta-1,3-diene. This type of experiment allows us to evaluate both internal and external standardisation.
Several variables were changed in order to get the best reproducibility. The tested variables were:

- Scan speed (0.1 cm/s and 0.5 cm/s)
- Number of co-added scans per spectrum (10, 20 and 100 co-added scans)
- Laser power (200mW, 300mW and 400mW)
- Internal versus external standardisation
- Ratioing of single bands versus the use of the total spectrum

The reproducibility increases with increasing laser power, slower scan speed and increasing the number of co-added spectra, all as expected.
To enable the use of all the datapoints in the spectrum, a programme, called 'Polyfit' was written by Dr. West. By introducing spectra of the pure components, it estimates the composition of a spectrum that is supplied by the user.
The best results obtained from the different experiments are displayed in Table 3.2.

**Table 3.2** The reproducibility of FT-Raman intensities of a mixture of cyclohexane and hexachlorobuta-1,3-diene (50:50 %v/v) is presented. A comparison of the results, using external and internal standardisation and using a special spectrum recognition programme (uses the total spectrum in the calculations), is given. For the band ratios, only the results from heights are displayed.

| | Coefficient of variance (%) |
|---|---|
| Ratios of single bands | |
| Internal reference | ≤ 1.5 |
| External reference | ≤ 1.0 |
| Use of the whole spectrum | ≤ 0.5 |

From Table 3.2, it is clear that very good reproducibilities can be obtained from liquid samples, within 1.5 % coefficient of variance. The use of the entire spectrum gives better results than when a single band region is used, again as expected.

From the table, one would be tempted to suggest that the use of an external reference gives superior results to an internal reference. With the exception of where there are interactions between the two components, an internal standardisation should in theory always give better results. This somewhat surprising result is probably due to the overall relatively low quality of the spectra recorded.

In the next evaluation of liquid spectra, the quality of the spectra is higher, by using a better laser. Unfortunately the spectrum recognition programme 'Polyfit' that was used previously and that performed calculations using the entire Raman spectrum, was not available anymore.

It is important to have an idea of the reproducibility of the spectra of the external reference before we decide to effectively use it as an external reference in our quantitative analyses.

The different repeatability experiments performed on the external reference, using two different lasers, are described in Table 3.3. In some of the experiments, the external reference was moved in between recording of the different spectra. This means that the external reference was moved out of the path of the laser beam and then back again. This was done to mimic a real experiment where the external reference is moved out of the path of the laser beam in order to record the spectrum of the tablet.

**Table 3.3** A description of the different reproducibility experiments performed with the external reference is given. In the different experiments, the number of averaged spectra and the number of co-added scans per spectrum is varied, as well as moving the reference in between spectra as a complement to keeping it stationary. All spectra recorded with 200mW laser power.

| External reference | Number of averaged spectra | Number of co-added scans per spectrum |
|---|---|---|
| Optomech laser | | |
| Undisturbed | 10 | 10 |
| | 20 | 1 |
| Moved in between spectra | 20 | 1 |
| Spectron laser | | |
| Undisturbed | 10 | 1 |
| | 10 | 10 |
| | 10 | 100 |
| | 10 | 1 |
| | 10 | 10 |
| | 10 | 100 |

To calculate the repeatability of the Raman intensities, from all the spectra recorded, the average height and area were calculated for specific band regions, as well as the standard deviation and the coefficient of variance which is a good measure of the repeatability.

From the results of the experiments described in Table 3.3, the following conclusions can be drawn:

- the effect of sample movement on the reproducibility
- the influence of co-adding spectra

Co-adding spectra means reducing the noise hence better reproducibility is to be expected. The reproducibility of one scan spectra (time scale 12 seconds) are compared with spectra after co-adding 10 scans (time scale 2 minutes) and also after co-adding 100 scans (time scale 20 minutes).

The relative standard deviations of the different averaging experiments are presented in Table 3.4.

**Table 3.4** Coefficients of variance obtained from reproducibility experiment on the Raman spectra of the external reference are presented. The results reflect the reproducibility of the FT-Raman band heights.

| External reference | Number of averaged spectra | Number of scans/spectrum | Relative standard deviation (%) |
|---|---|---|---|
| Optomech laser | | | |
| undisturbed | 10 | 10 | < 1.5 |
| | 20 | 1 | < 1.5 |
| moved in between spectra | 20 | 1 | < 1.5 |
| Spectron laser | | | |
| undisturbed | 10 | 1 | 1.5 |
| | 10 | 10 | 2 |
| | 10 | 100 | 6 |
| | 10 | 1 | 1 |
| | 10 | 10 | 2.5 |
| | 10 | 100 | 20 |

For all the experiments on averaging of the external reference, we obtained relative standard deviations for 1 scan and 10 scan spectra of around 2%. From these results, we can conclude that the reproducibility of the external reference poses no problems. Even 1 scan spectra are sufficiently reproducible for our purpose.
Increasing the number of co-added scans per spectrum should improve the intensity reproducibility. From the table however we notice that 100 scan spectra, using the Spectron laser, show the worst reproducibility. This must be caused by the laser slowly decreasing its power output. This is shown in Figure 3.2 where the variation of the HCBD[10] area is given with time.

[10] HCBD : hexachlorobuta-1,3-diene

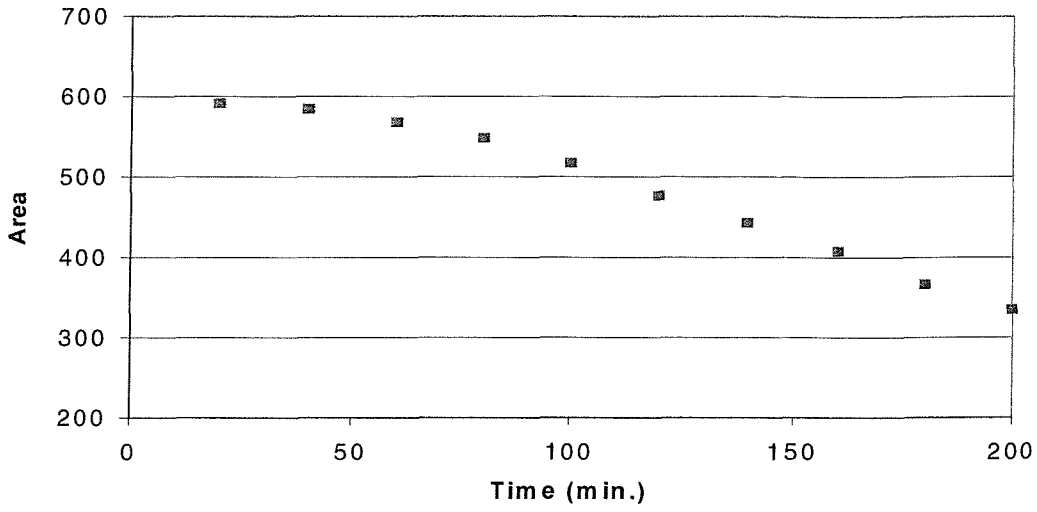


**Figure 3.2** The decrease in laser output with time shown by plotting the area of the external reference HCBD (1220 $cm^{-1}$ – 1120 $cm^{-1}$ band) against time. [Spectron laser]

When performing the quantitative analysis on different sets of tablets (see Section 3.5), 10 repeat spectra were recorded of the external reference. This allowed a further evaluation of the reproducibility of the external reference. This means that in between the spectra recorded of the tablets, a spectrum of the external reference was recorded. This spectrum consisted of 10 co-added scans and was usually recorded with 200mW laser power and 0.1 cm/s scan speed. The coefficients of variance tend to vary considerably. With a stable laser, coefficients of variance of less than 1% are obtainable. But a stable laser can become 'unstable' at any time of the day, resulting in coefficients of variance of more than 5%.

## Tablets

In a similar way as for the external reference, the repeatability of the FT-Raman spectra of tablets was studied.

Since it was impossible to obtain a set of commercial pharmaceutical tablets with a wide range of concentration of active material, it was decided to gravimetrically prepare the standard sets of tablets. This proved to be far more difficult than first anticipated. Because no specialist mixing equipment was available, the powders were simply mixed by hand with a mortar and pestle for a fixed timespan. A KBr tablet press was then used to compress the powders. A problem arose from inaccurate selection of the pressure for each tablet. The error on the press was around 500 kilos

on each selected weight. Hence the tablets used in our quantitative analyses were not compacted to an exactly similar degree.

Tablets with different components and varying composition (0 to 100% w/w%) were prepared. The following mixtures were selected:

- maleic acid and $Na_2SO_4$
- $K_2CrO_4$ and $Na_2SO_4$
- maleic acid and $K_2SO_4$

The advantage of using inorganic salts containing complex anions with high symmetry is the occurrence of strong bands corresponding to totally symmetric vibrations of the anion.

To avoid the problems related to sample inhomogeneity, while recording the spectra, the tablets were spun and moved along the vertical axis to obtain the best average sampling. The tablets were rotated (240 rpm) and translated (5 rpm) while scanning. The tablets were not fixed in the sample holder, i.e. they were tumbling. The different experiment performed on the tablets, using two different lasers, are summarised in Table 3.5.

**Table 3.5** The different reproducibility experiments performed on different tablets are described. In the different experiments, the number of averaged spectra and the number of co-added scans per spectrum is varied.

| Components in tablet | Number of averaged spectra | Number of co-added scans per spectrum |
|---|---|---|
| Optomech laser | | |
| $K_2CrO_4$ and $Na_2SO_4$ | 10 | 1 |
| | 10 | 10 |
| Spectron laser | | |
| $Na_2SO_4$ | 10 | 1 |
| | 10 | 10 |
| | 10 | 100 |
| $K_2CrO_4$ | 10 | 1 |
| | 10 | 10 |
| | 10 | 100 |

Peak areas and heights were estimated, more specifically the regions of interest were

- 934-742 $cm^{-1}$ and 425-200 $cm^{-1}$ for $K_2CrO_4$
- 1005-980 $cm^{-1}$ for $Na_2SO_4$

The results on reproducibility from the tablets are shown in Table 3.6. In addition, the results using the two different lasers are compared.

**Table 3.6** Coefficients of variance obtained from reproducibility experiment on the Raman spectra of the different tablets are presented. The results reflect the reproducibility of the FT-Raman band heights.

| Components in tablet | Number of averaged spectra | Number of co-added scans per spectrum | Relative standard deviation (%) |
|---|---|---|---|
| Optomech laser | | | |
| $K_2CrO_4$ and $Na_2SO_4$ | 10 | 1 | 3 - 10 |
| | 10 | 10 | 1 - 5 |
| Spectron laser | | | |
| $Na_2SO_4$ | 10 | 1 | <1 |
| | 10 | 10 | 3 |
| | 10 | 100 | 8 |
| $K_2CrO_4$ | 10 | 1 | 1.5 |
| | 10 | 10 | 1 |
| | 10 | 100 | 2 |

From the reproducibility experiments on the tablets it is clear that there are differences in reproducibility when using the two different lasers. The Optomech laser shows better reproducibility when increasing the number of scans per spectrum. Co-adding 10 scans per spectrum should be sufficient to get reproducible results. The Spectron laser shows good short-term stability. The reproducibility of 1 scan spectra is very good, better than 98%. For longer scan times, it shows again reduction in power output.

As with the external reference, the most important test of reproducibility was performed when recording spectra of the calibration set for later quantitative analysis. Using the Perkin-Elmer FT-Raman system, in between the spectra of the tablet, a spectrum of the external reference was recorded. For the Bruker system, no external reference was used.

Our observations are the same as from the reproducibility experiments on the external reference. When the laser is stable, the reproducibility of the tablets is very good with a coefficient of variance of less than 1%. But when the laser is unstable, the coefficient can be as high as 10%. It is expected that the reproducibility figures would improve when the entire spectrum is used in the calculations instead of a small part of the spectrum.

In addition, since the tablets were loose in their mounts, increased noise levels are to be expected, resulting in lower reproducibility.

### Reproducibility after external standardisation

The reason for using an external reference is so that the spectra of the tablets can be corrected for laser instability and other instrumental factors. Hence it is expected that correcting the Raman intensity from a tablet by ratioing it with the Raman intensity of the external reference will improve the reproducibility. This was tested by calculating the coefficient of variance of the Raman spectra after recording a series of 10 spectra (each spectrum contains 10 co-added scans).

Our results are based on band heights calculations. When the laser is stable (reproducibility of the tablet with a coefficient of variance varying from 1 to 1.5 %) ratioing with an external reference will reduce the reproducibility.

When the reproducibility of the Raman intensity of the tablet has a coefficient of variance of between 1.5 and 2.5 %, ratioing with the external reference will result in better reproducibility most of the time but the improvement varies (up to 50%).

Correcting with an external reference when the *reproducibility of the external reference* has a coefficient of variance of 1 to 1.5% gives best results.

With a tablet Raman intensity reproducibility smaller than 97.5 %, ratioing usually decreases the coefficient of variance, probably because the low reproducibility is caused by another effect.

So it is very difficult to assess the best practice and hence the validity of the external reference in our quantitative experiments.

### Reproducibility after internal standardisation

The reproducibility of the ratio of band intensities (of the analyte over that of the internal reference) really allows one to assess the feasibility of quantitative analysis using FT-Raman spectroscopy. The reproducibility of the two band regions (1 for the analyte, the other for the internal reference) should be the same unless one is of low intensity and the other of high.

Unfortunately if the intensity of a peak of one component has a deviation with time towards lower values and the variation of the intensity of the other component drifts towards higher values, then the deviation from the average value of the ratios will be larger than that of both components. One component drifting towards lower intensities with time, while the other drifts towards higher intensities would suggest non-linearity of some sort. However when one component is present in high concentrations, while the other is present in a very low concentration, the noise on the lower intensity band could well result in an 'apparent' non-linearity.

Other causes of non-linear effects could be like detector sensitivity changes with frequency and the non-linearity of the detector. In the whole analysis presented so far and following, it is assumed that the output of the detector versus signal is linear. The InGaAs and Ge detectors used in these instruments are on the limit of practicability and hence the linearity is relatively poor. The most difficult characteristic to cope with is that the dark impedance of good detectors can exceed 200 MOhm. Detecting and amplifying in this current range is extremely difficult particularly as the frequency is raised.

## 3.4 *Influence of packing density on FT-Raman intensities*

Before quantitative analysis on tablets using FT-Raman spectroscopy could be attempted, a determination of the influence of packing density on the Raman intensity was performed.

Three sets of four tablets were prepared. For each tablet 1 gram of maleic acid was weighed and transferred into a 16 mm KBr die. The different sets were prepared by varying the pressure used for compression. A first set was compressed with 3 tons of force. The other sets of four tablets were compressed with 6 and 9 tons of force respectively. All tablets were compressed for 2 minutes. The accuracy of the force

measurement of the tablet press was not very good (error of 0.5 tons) and the force tended to decrease after a while.

FT-Raman spectra were recorded while the tablet was rotating and translating. For each tablet, 10 repeat spectra were recorded in order to monitor reproducibility of the spectra. In addition, an external reference was used, as described in the 'reproducibility section'. It proved to be quite a challenge to keep the laser stable to record all twelve tablets in one day. Subsequently, the experiments were repeated on the Bruker FT-Raman instrument.

As with the reproducibility measurements, a specific band region in the spectrum was selected and the area and height of the bands were estimated. The results from both instruments are presented in Table 3.7.

**Table 3.7** The influence of the packing density on the Raman intensity is presented. The results obtained from two different spectrometers are compared. The Bruker values are the average of the measurements on 4 different tablets. The Perkin Elmer values are the average of 3 different tablets. (*only two different tablets)

| | | Bruker instrument | | Perkin Elmer instrument | | | |
|---|---|---|---|---|---|---|---|
| | | Absolute Raman Intensity | | Absolute Raman Intensity | | External reference corrected Raman Intensity | |
| | | height | Area | height | Area | height | Area |
| 3 tons | Average | **13.6** | **721.0** | **55.4** | **2667.0** | **1.8** | **3.3** |
| | Standard deviation | 0.4 | 19.0 | 1.4 | 64.4 | 0.1 | 0.1 |
| | Coefficient of Variance | 3.3 | 2.6 | 2.6 | 2.4 | 4.2 | 2.8 |
| 6 tons | Average | **13.3** | **707.7** | **50.3** | **2414.8** | **1.7** | **2.6** |
| | Standard deviation | 0.4 | 19.3 | 2.2 | 106.4 | 0.1 | 0.1 |
| | Coefficient of Variance | 3.2 | 2.7 | 4.3 | 4.4 | 4.9 | 3.5 |
| 9 tons | Average | **13.0** | **689.0** | **52.7*** | **2537.8*** | **1.7*** | **3.1*** |
| | Standard deviation | 0.3 | 15.2 | 1.0 | 48.5 | 0.0 | 0.2 |
| | Coefficient of Variance | 2.4 | 2.2 | 2.0 | 1.9 | 0.6 | 7.6 |

At first sight, on increasing the packing force, there seems to be a decrease in Raman intensity. But this conclusion might be erroneous since the error bars on the average values for the different weights overlap for all values. This means that a slight deviation from the chosen compression weight does not have a profound effect on the Raman intensity. On the other hand, many of the relative standard deviations are rather high (> 2%). Even on the newer Bruker spectrometer, where laser stability would still be expected to be very good, none of the values are below 2%.

Whether the low reproducibility is due to rotation of the tablet or due to the differences in packing is not clear. From these results it is clear that the reproducibility from tablets that are supposed to be 'identical', varies with at least 2%.
The use of chemometrics might be able to give us a better insight into the problem i.e. it might be possible to contribute the low reproducibility to the differences in packing or to the limitations in the technique itself.

## 3.5 Quantitative Analysis

In this section, the results on quantitative analysis using FT-Raman spectroscopy on both tablets and a formulation containing local anaesthetics is presented.

### A Local Anaesthetic Block Copolymer System

Different formulations with different amounts of a eutectic mixture of lidocaine and prilocaine were prepared, ranging from 3% to 7% (w/w%) in aqueous solution. In addition, 22% (w/w%) of block copolymers are present in the solution as excipients. Four different sets of formulations in this concentration range were prepared. FT-Raman spectra were recorded on the Bruker RFS100 spectrometer. The samples were rotated while scanning. For each spectrum, 1000 scans were co-added, 700mW laser power was used and the instrument was set to 4 $cm^{-1}$ resolution.
Different band areas in the spectra of the formulations, due to the various components were used in the calculations. Figure 3.3 shows a typical spectrum of the formulation where the areas of importance are highlighted.

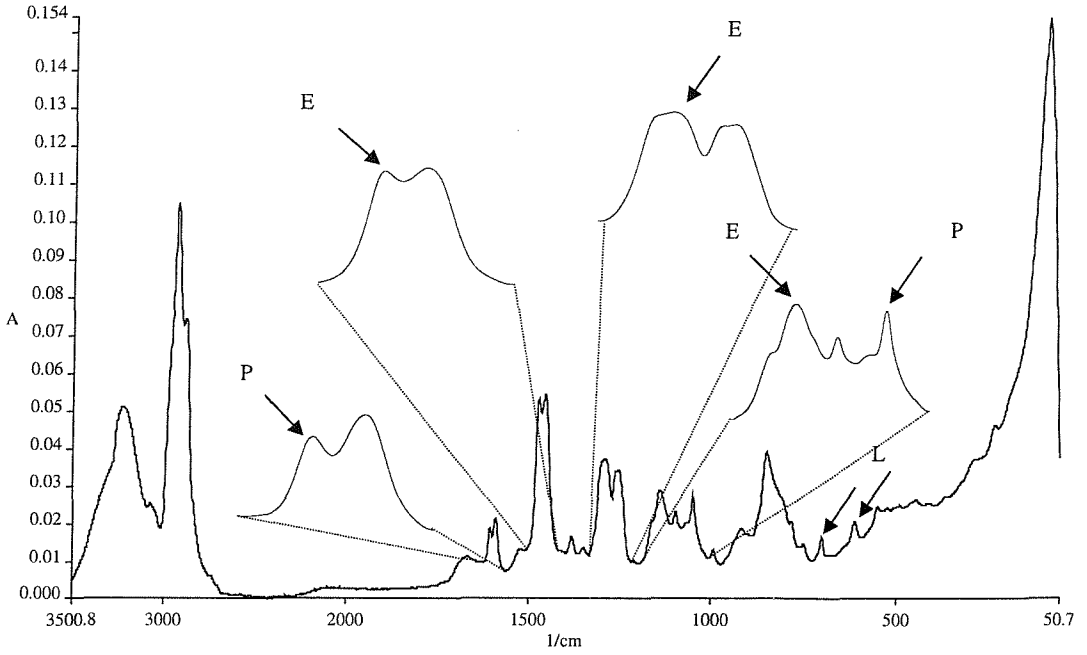


**Figure 3.3** FT-Raman spectrum of the formulation. The peaks selected for calculations are shown. P: prilocaine, L: lidocaine and E: excipients

Two of the bands chosen, representative of the excipients, at 1286 $cm^{-1}$ and 1475 $cm^{-1}$ are very sensitive to intermolecular interactions [14]. It was therefore essential to rotate the formulations in order to minimise sample heating which could in turn induce micellization.

Since most of the bands shown in Figure 3.3 consist of overlapping peaks, curve fitting the bands before area and height estimation was essential.

As might be expected, the *absolute* areas and heights of the different components are not linearly related to the amount of sample present due to instrument variables. Using an internal reference (the band regions of the excipient) showed improved linearity, but only for one particularly chosen ratio of bands. Out of the following combinations tested:

- 706 $cm^{-1}$ (lidocaine)/ 1286 $cm^{-1}$ (excipient) versus w/w% eutectic mixture
- 706 $cm^{-1}$ (lidocaine)/ 1475 $cm^{-1}$ (excipient) versus w/w% eutectic mixture
- 619 $cm^{-1}$ (lidocaine)/ 1286 $cm^{-1}$ (excipient) versus w/w% eutectic mixture
- 619 $cm^{-1}$ (lidocaine)/ 1475 $cm^{-1}$ (excipient) versus w/w% eutectic mixture
- 1606 $cm^{-1}$ (prilocaine)/ 1286 $cm^{-1}$ (excipient) versus w/w% eutectic mixture
- 1606 $cm^{-1}$ (prilocaine)/ 1475 $cm^{-1}$ (excipient) versus w/w% eutectic mixture
- 1046 $cm^{-1}$ (prilocaine)/ 1286 $cm^{-1}$ (excipient) versus w/w% eutectic mixture

- 1046 $cm^{-1}$ (prilocaine)/ 1475 $cm^{-1}$ (excipient) versus w/w% eutectic mixture
- 706 $cm^{-1}$ (lidocaine)/ 1130 $cm^{-1}$ (excipient) versus w/w% eutectic mixture
- 619 $cm^{-1}$ (lidocaine)/ 1130 $cm^{-1}$ (excipient) versus w/w% eutectic mixture
- 1606 $cm^{-1}$ (prilocaine)/ 1130 $cm^{-1}$ (excipient) versus w/w% eutectic mixture
- 1046 $cm^{-1}$ (prilocaine)/ 1130 $cm^{-1}$ (excipient) versus w/w% eutectic mixture

only 1606 $cm^{-1}$ (prilocaine)/ 1286 $cm^{-1}$ (excipient) versus w/w% eutectic mixture showed a linear relationship in all four sets of formulations with a correlation coefficient of 0.99 or better. In three of the sets of formulations, the following plot 1606 $cm^{-1}$ / 1475 $cm^{-1}$ versus w/w% component also had a correlation coefficient of better than 0.99.

These results are presented in Table 3.8.

**Table 3.8** Calibration lines were constructed and the correlation coefficients ($R^2$) are displayed for the different sets of formulations. Only the heights of the Raman bands were used in the regression analysis. All values below 0.98 are omitted. * 1 datapoint was rejected

| | Correlation coefficient after linear regression for formulation | | | |
|---|---|---|---|---|
| Ratio of bands | Set1 | Set2 | Set3 | Set4 |
| 619 $cm^{-1}$ (lidocaine) / 1130 $cm^{-1}$ (excipient) | | | 0.9998* | 0.99* |
| 1606 $cm^{-1}$ (lidocaine) / 1130 $cm^{-1}$ (excipient) | | 0.99 | 0.998* | 0.999* |
| 619 $cm^{-1}$ (lidocaine) / 1286 $cm^{-1}$ (excipient) | | | | 0.98 |
| 619 $cm^{-1}$ (lidocaine) / 1475 $cm^{-1}$ (excipient) | | 0.99 | | |
| 1606 $cm^{-1}$ (prilocaine) / 1286 $cm^{-1}$ (excipient) | 0.99 | 0.998 | 0.998 | 0.996 |
| 1606 $cm^{-1}$ (prilocaine) / 1475 $cm^{-1}$ (excipient) | 0.98 | 0.998 | 0.998 | 0.997 |
| 1046 $cm^{-1}$ (prilocaine) / 1286 $cm^{-1}$ (excipient) | | | | 0.9993* |
| 1046 $cm^{-1}$ (prilocaine) / 1475 $cm^{-1}$ (excipient) | | | | 0.98 |

As was found before, band heights give better correlation than when the areas are used. The linear relationship of the prilocaine region over a band region of the excipients is shown in Figure 3.4.

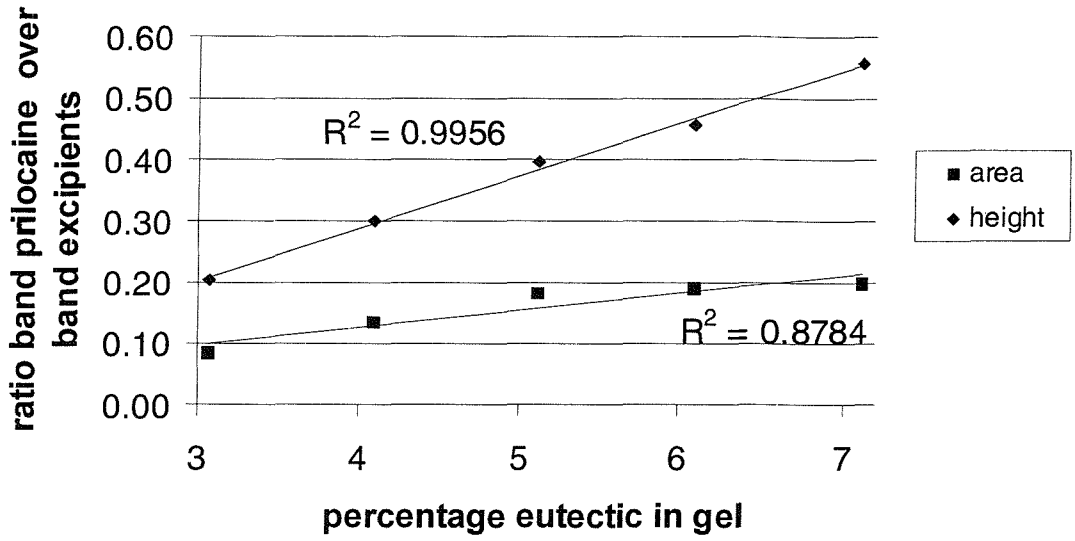


**Figure 3.4** Calibration graph from the quantitative analysis on the formulations. The ratio of the band of prilocaine (1606 $cm^{-1}$) over that from the excipients (1286 $cm^{-1}$) is plotted against the percentage eutectic mixture in the formulation. Linear regression is applied and the correlation coefficients ($R^2$) are presented.

The fact that a linear correlation of the band height with concentration is found seems promising. However, the linear relationship shows a different slope and intercept in the different sets of formulations. The relative standard deviation of the average slope is 2 %.

This error of 2% is too large an error for the concentration range we have studied. One possible explanation for the changes in slopes for the different sets of formulations could be due to errors in integration or changing instrument response.

## Tablets

Many different sets of tablets were prepared. The specifications of each set are presented in Table 3.9.

**Table 3.9** The different sets of tablets used in our quantitative analyses are presented below. In addition to the components of the tablets it is also indicated when the powders were sieved prior to compaction.

| | Component A | Component B | Restricted particle size |
|---|---|---|---|
| Set 1 | Maleic acid | $Na_2SO_4$ | Yes |
| Set 2 | Maleic acid | $Na_2SO_4$ | No |
| Set 3 | $K_2CrO_4$ | $Na_2SO_4$ | No |
| Set 4 (in triplicate) | Maleic acid | $K_2SO_4$ | No |

The composition of all sets of tablets varied from 0% to 100% w/w%. The powders were hand mixed for 2 minutes and then compressed, using a KBr die. The pressure used to make the tablets was in all cases 5 tons on an 8 mm diameter dye (about 10 Kbar). FT-Raman spectra were recorded and areas and heights of some selected bands were estimated. Bands within the spectra used for quantitative analyses were chosen with the following comments in mind :

- The band should be reasonable strong in the spectrum
- The sample should not have a near infrared absorption band at the same frequency
- The band should be due to one component only, the avoidance of band overlap

The average of 10 spectra (ten scans each) was calculated and the band heights and areas were plotted to construct the calibration curve.

### Tablets containing mixtures maleic acid and $Na_2SO_4$.

Spectra of the different tablets containing maleic acid and $Na_2SO_4$ were recorded, peak areas and heights were estimated, more specifically the regions that were used in our calculations are 1800-1500 $cm^{-1}$ for maleic acid and 1005-980 $cm^{-1}$ for $Na_2SO_4$. The region 1220-1120 $cm^{-1}$ in the spectrum of the external reference was used as a reference.

Details of the peak regions used in our calculations are given in Figure 3.5.

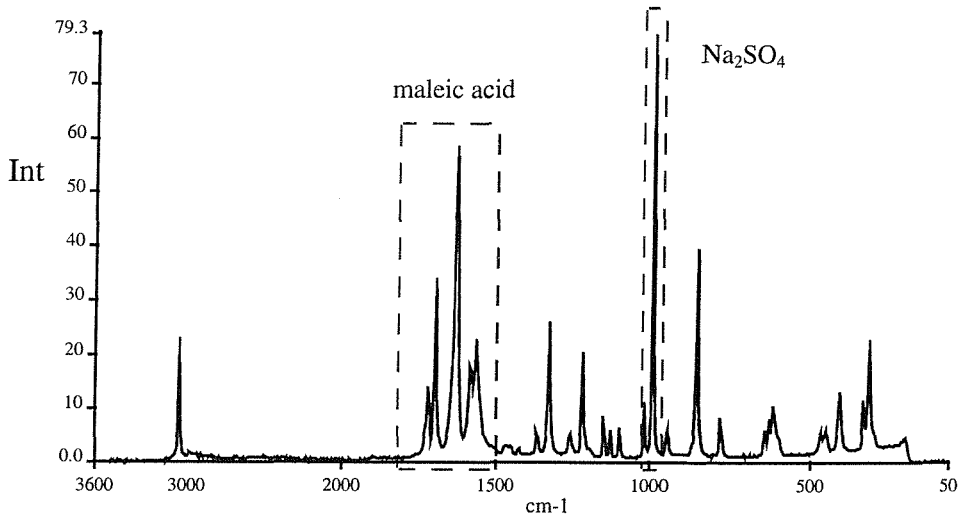


**Figure 3.5** Raman spectrum of a mixture maleic acid/$Na_2SO_4$. The peaks selected for calculations are 1800 - 1500 $cm^{-1}$ for maleic acid and 1010 - 980 $cm^{-1}$ for $Na_2SO_4$.

The different experiments performed are described in Table 3.10. It will be noted that mixtures of sieved and unsieved powders are included in the experiments. The number of averaged spectra per tablet and the number of scans per spectrum are also defined. A spectrum of the external reference was recorded before and after each spectrum of a tablet. The number of scans of the external reference was also varied. Note that the time to record 100 scans (equal to 10×10 scans in previous experiments) takes about 20 minutes when 0.1 cm/s interferometer scan speed is used.

**Table 3.10** Summary of the different experiments performed in order to construct the calibration curves for the quantitative analysis.

| | Tablet | | | External reference |
|---|---|---|---|---|
| | No. of tablets | No. of averaged spectra per tablet | No. of co-added scans per spectrum | No. of co-added scans per spectrum |
| Unsieved | 7 | 10 | 10 | 10 |
| | 11 | 1 | 100 | 3 |
| Sieved 210-300 µm particle size | 11 | 10 | 10 | 10 |
| | 13 | 10 | 10 | 3 |
| | 13 | 1 | 100 | 3 |

Peak areas and heights were estimated and the intensity ratios against the external reference and then internally were calculated. All spectra were recorded using 200mW of laser power.

*Internal reference*

The results when using internal reference procedures are summarised in Table 3.11.

**Table 3.11** Calibration lines were constructed and the correlation coefficients ($R^2$) are displayed for the different experiments. (*1 tablet rejected in the calibration curve)

| No. of spectra per tablet | No. of scans per spectrum | Correlation Coefficient ($R^2$) when using internal standardisation | |
|---|---|---|---|
| | | Area | Height |
| | Non Sieved | | |
| 10 | 10 | 0.9998 | 0.9999 |
| 1 | 100 | 0.994 | 0.994 |
| | Sieved | | |
| 10 | 10 | 0.997* | 0.994* |
| 10 | 10 | 0.984* | 0.985* |
| 1 | 100 | 0.997* | 0.996* |

From Table 3.10, it is clear that experiments 2 and 5 are identical except that sieved powders were used in the latter experiment. Experiments 1 and 3 are also clearly related and we see that sieving reduces the quality of the data.

When comparing experiments 3 and 4, it is clear that reducing the signal to noise ratio of the external reference by reducing the number of co-added scans per spectrum appears to ruin the results in experiment 4, but this does not happen in experiments 2 or 5. Why experiment 4 should be so poor in output is not clear.

*External reference*

Peak areas and heights, ratioed with the external reference were plotted against the absolute weight of the corresponding component. Linear regression and curved regression were then applied. The correlation coefficients, when 2$^{nd}$ order regression was applied, were in 3 of the 5 experiments better than 0.995, compared with values

below 0.98 for linear regression. The results when using an external reference are summarised in Table 3.12.

**Table 3.12** Calibration curves were constructed and the correlation coefficients ($R^2$) are displayed for the different experiments. (* 1 tablet was rejected in the calibration curve)

| Correlation Coefficients ($R^2$) when using external standardisation | | | |
|---|---|---|---|
| Experiment | | Maleic Acid | $Na_2SO_4$ |
| Non Sieved | | | |
| 1 | Area | 0.981 | 0.997* |
| | Height | 0.982 | 0.997* |
| 2 | Area | 0.968 | 0.998* |
| | Height | 0.967 | 0.998* |
| Sieved | | | |
| 1 | Area | 0.943 | 0.994* |
| | Height | 0.942 | 0.995* |
| 2 | Area | 0.949 | 0.964 |
| | Height | 0.952 | 0.965 |
| 3 | Area | 0.978 | 0.983* |
| | Height | 0.979 | 0.981* |

Table 3.12 reveals that in all the calibration experiments the correlation for maleic acid is worse than that for $Na_2SO_4$, almost certainly because the $Na_2SO_4$ is so strong a scatterer introducing sharp bands whilst the band for maleic acid is broad and weaker. The regression curves for both $Na_2SO_4$ and maleic acid, corrected by an external reference, are displayed in Figure 3.6.

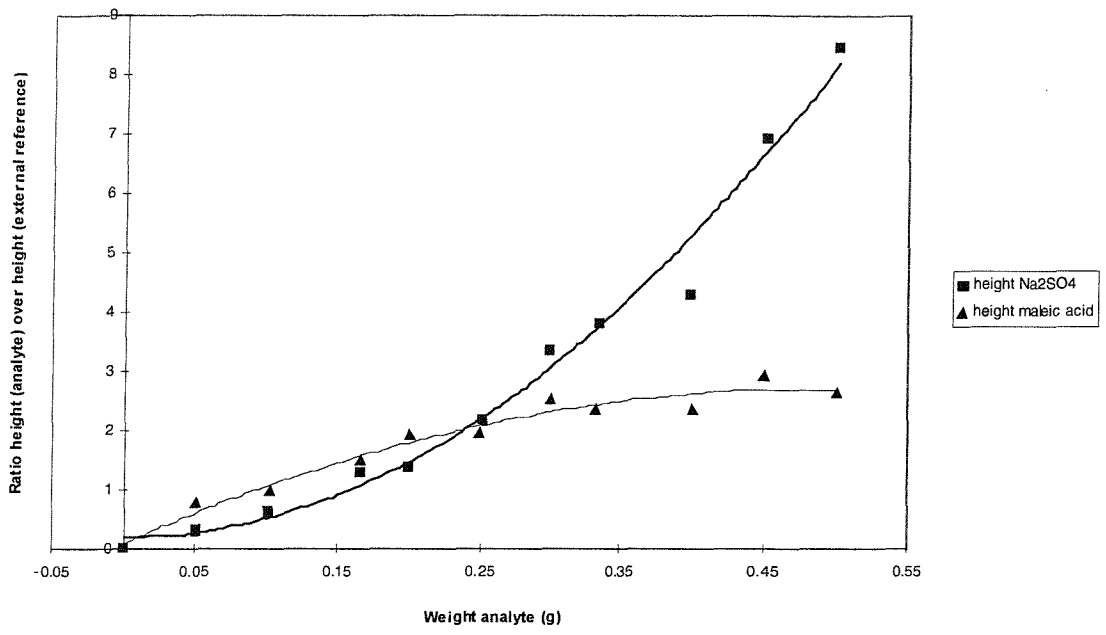


**Figure 3.6** Calibration graph, displaying the FT-Raman heights $Na_2SO_4$ and maleic acid against their weight. The band heights of $Na_2SO_4$ and maleic acid were corrected by an external reference.

The reason for obtaining a second order regression line is dependent on the difference in densities and compressabilities of the two components in the tablets. Tablets with a higher concentration of maleic acid are thicker compared to the lower concentration ones (due to the lower density and a compressibility factor). Corrections were made to allow for the reduced mass per unit of volume viewed by the instrument, but this did not give a linear regression. Therefore for correcting this curved regression, more parameters should be included e.g. compressability and the scattering properties versus particle size.

In order to reduce this deviation from linearity of the calibration curve, two components of similar density were then chosen.

## Tablets containing mixtures $Na_2SO_4$ and $K_2CrO_4$.

A new set of tablets was prepared from $Na_2SO_4$ and $K_2CrO_4$ powders. These two particular powders were chosen because they are both strong Raman scatterers and they have a similar density, (2.68 for $Na_2SO_4$ and 2.732 for $K_2CrO_4$). Spectra were

recorded, peak areas and heights were estimated, more specifically the regions of interest were 934-742 $cm^{-1}$ and 425-200 $cm^{-1}$ for $K_2CrO_4$ and 1005-980 $cm^{-1}$ for $Na_2SO_4$. More details of the peak regions used in the calculations are given in Figure 3.7.

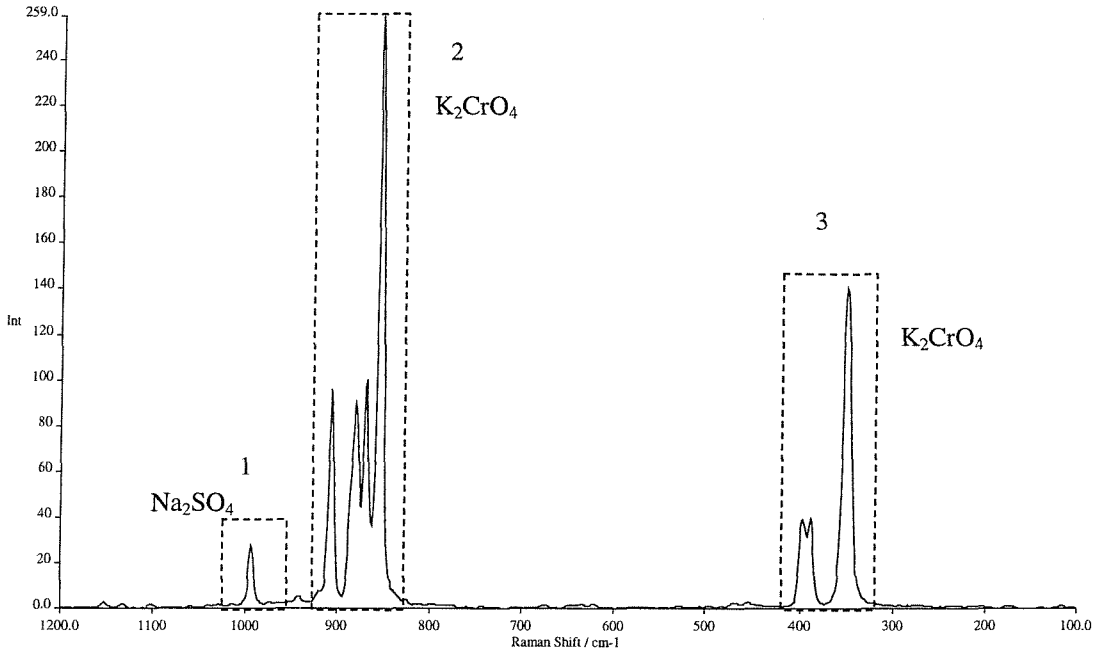


**Figure 3.7** Raman spectrum of a mixture $K_2CrO_4$ and $Na_2SO_4$. The peaks selected for calculations are 1: 1005-980 $cm^{-1}$, 2: 934-742 $cm^{-1}$ and 3: 425-200 $cm^{-1}$. Laser power : 200mW

A set of 14 tablets was prepared. For each tablet, 10 spectra, consisting of 10 co-added scans each, were recorded. In between these spectra, those of the external reference were recorded, again using co-addition of 10 scans in each spectrum.

*Internal reference*

Results from internally ratioing the two components are summarised in Table 3.13. The ratio of band regions $K_2CrO_4$ over $Na_2SO_4$ were plotted against the ratio of weights of $K_2CrO_4$ over $Na_2SO_4$. Linear regression was applied and the correlation coefficients calculated. The tablet with the second largest $K_2CrO_4$ concentration was left out of the calculations.

**Table 3.13** Calibration curves were constructed and the correlation coefficients ($R^2$) are displayed for the different experiments.

| | Correlation Coefficient ($R^2$) when using internal standardisation | |
|---|---|---|
| | Ratio band regions 425-200 / 1005-980 $cm^{-1}$ | Ratio band regions 934-742 / 1005-980 $cm^{-1}$ |
| Areas | 0.995 | 0.996 |
| Heights | 0.997 | 0.994 |

Figure 3.8 shows a calibration graph when the internal ratio 425-200 $cm^{-1}$/1005-980 $cm^{-1}$ was plotted against the weight ratio $K_2CrO_4$ over $Na_2SO_4$.

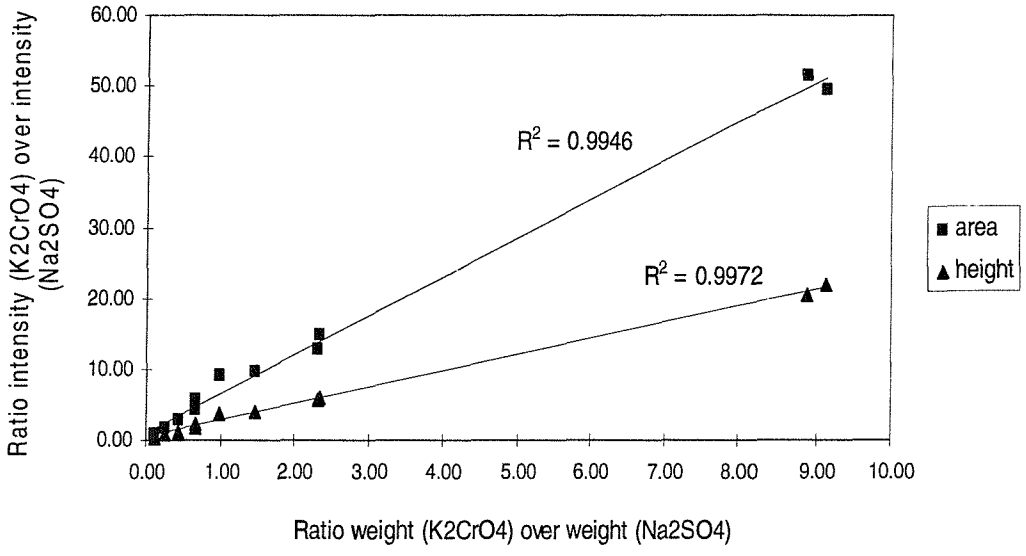


**Figure 3.8** Calibration graph, displaying the ratio of FT-Raman heights of $K_2CrO_4$ (425-200 $cm^{-1}$) over $Na_2SO_4$ (1005-980 $cm^{-1}$) against the ratio of their weights $K_2CrO_4$ over $Na_2SO_4$ (internal standardisation).

*External reference*

In the spectrum of the external reference, the following two peak regions were used in our calculations: 1220-1120 $cm^{-1}$ and 1700-1500 $cm^{-1}$. Band areas and heights from the tablet components were ratioed with the band areas and heights of the external reference. These figures were plotted against the weight of the particular component. Calibration lines were constructed and the correlation coefficients calculated.

In this experiment, there seemed to be no correlation between the Raman intensity and the concentration. It must be said that the reproducibility of Raman intensities was low, even for the external reference, relative standard deviations below 2% were rare. It is thought that this is mainly due to the laser being unstable.

A first glance at the regression line reveals that the deviations get larger as the concentration of $K_2CrO_4$ increases. The correlation coefficients for linear regression are low 0.84 to 0.89 for $K_2CrO_4$, from 0.89 to 0.91 for $Na_2SO_4$. Therefore it was decided to focus on that part of the calibration curve, showing more linear behaviour. The results are given in Table 3.14. Tablets displaying very poor reproducibility (RSD[11] > 5%) were rejected.

[11] RSD: relative standard deviation

**Table 3.14** Calibration lines were fitted, correlating the ratio of the tablet Raman intensity over that of the external reference with the weight of the compound in the tablet. The correlation coefficients ($R^2$) are given for the different band regions used. For the regression lines regarding $Na_2SO_4$ intensities, 8 tablets were used, for $K_2CrO_4$ 6 tablets were used.

| Correlation Coefficients ($R^2$) when using external standardisation | | | |
|---|---|---|---|
| Correlation of ratio of bandregions against the following values : | | | |
| | | Correlation coefficient ($R^2$) | Linear region (%w/w $K_2CrO_4$) |
| Band region of the external reference 1220-1120 $cm^{-1}$ | | | |
| $Na_2SO_4$ | | | |
| | Area | 0.940 | 0 - 90 |
| | Height | 0.924 | |
| $K_2CrO_4$ | | | |
| 934-742 $cm^{-1}$ | Area | 0.992 | 0 - 70 |
| | Height | 0.991 | |
| 425-200 $cm^{-1}$ | Area | 0.987 | |
| | Height | 0.986 | |
| Band region of the external reference 1700-1500 $cm^{-1}$ | | | |
| $Na_2SO_4$ | | | |
| | Area | 0.918 | 0 - 90 |
| | Height | 0.902 | |
| $K_2CrO_4$ | | | |
| 934-742 $cm^{-1}$ | Area | 0.991 | 0 - 70 |
| | Height | 0.988 | |
| 425-200 $cm^{-1}$ | Area | 0.985 | |
| | Height | 0.984 | |

The calibration line showing the weight $K_2CrO_4$ plotted against the ratio of the height of the $K_2CrO_4$ band over the height of the external reference is shown in Figure 3.9.

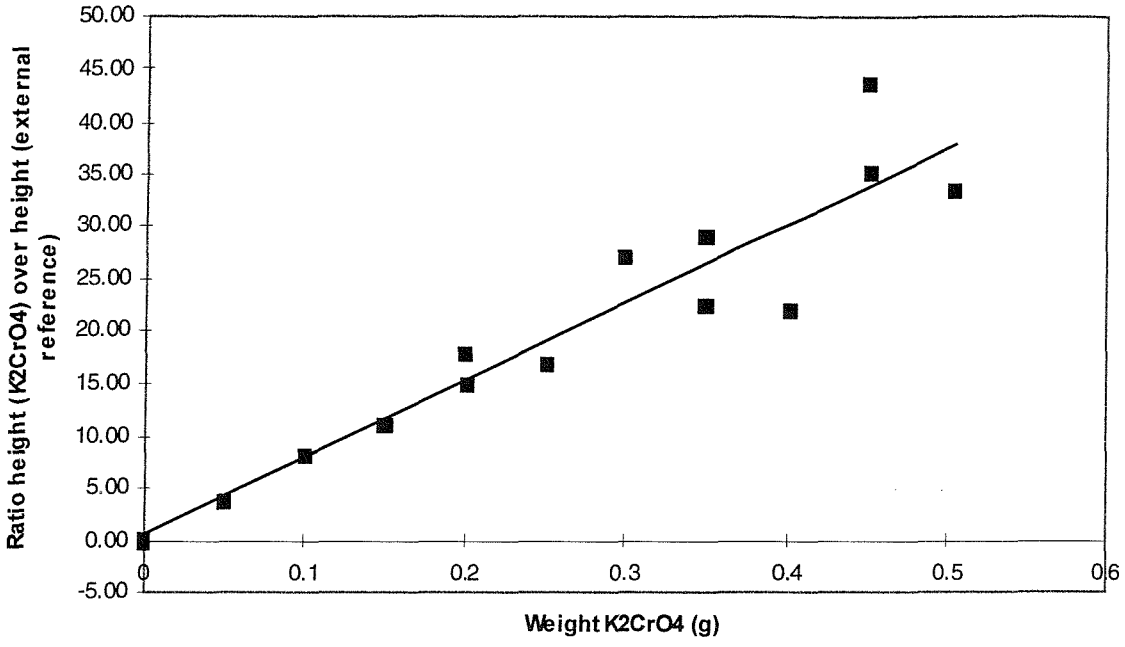


**Figure 3.9** Calibration graph, displaying the ratio of FT-Raman heights of $K_2CrO_4$ (425-200 $cm^{-1}$) over the external reference (1220-1120 $cm^{-1}$) against the weight of $K_2CrO_4$.

From Figure 3.9, it is clear that the excessive curvature of the correlation graph in Figure 3.6 has decreased.

By replacing maleic acid by $K_2CrO_4$ we succeeded in reducing the curvature, but at the expense of acceptable internal standardisation. Hence it was decided to use maleic acid again in the next set of tablets, but $Na_2SO_4$ was replaced by $K_2SO_4$ powder since this component is less sensitive to hydration.

### Tablets containing mixtures maleic acid and $K_2SO_4$.

Three new sets of tablets was prepared from maleic acid and $K_2SO_4$ powder.

To avoid incomplete mixing of the powders before compression into tablets, the next sets of tablets were carefully mixed (for 10 minutes) by adding the compound in the largest amount to the compound in the smallest amount in steps, as described by Langkilde et al. and Taylor and Langkilde [9,15].

Another factor expected to give bad results could be due to the compression of the tablets. Even when the mixing of the powders has been done thoroughly, when transferring the powders into the KBr die, separation could occur. The amplitude of the error introduced in this way was evaluated by recording FT-Raman spectra of both sides of some of the tablets.

To assess the error due to laser instability, in addition to the spectra recorded with the Perkin Elmer System 2000 FT-Raman spectrometer, the experiments were repeated on the Bruker FT-Raman spectrometer. In this system, the laser is expected to be more stable because it is newer.

Spectra were recorded, peak areas and heights were estimated. Details of the peak regions used in the calculations are given in Figure 3.10.

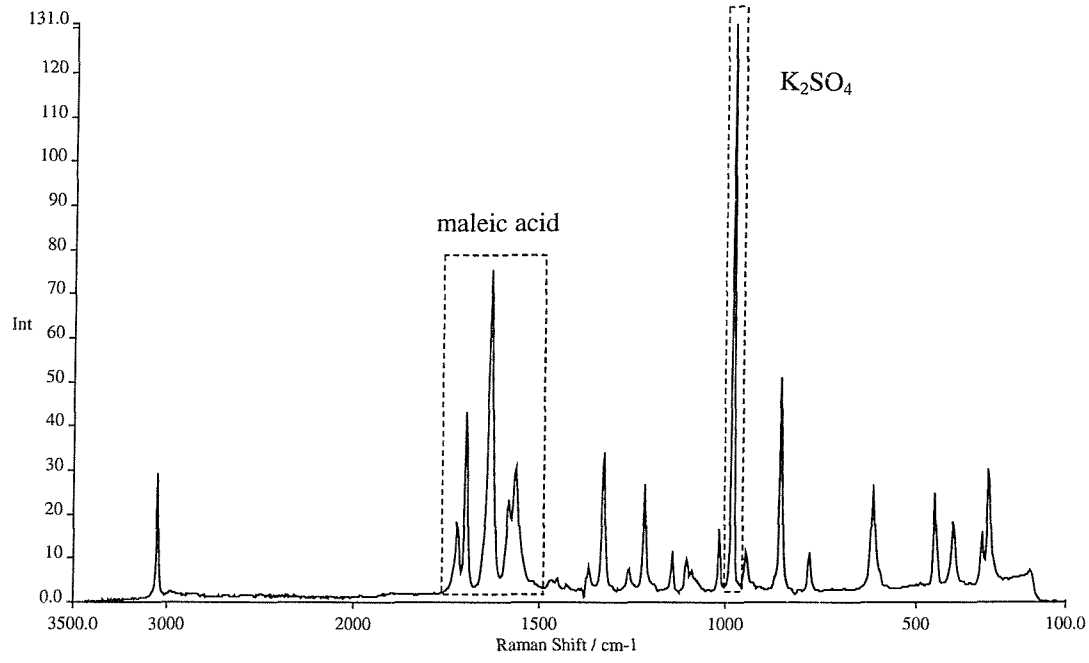


**Figure 3.10** Raman spectrum of a mixture maleic acid and $K_2SO_4$. The peaks selected for calculations are 1790 - 1490 $cm^{-1}$ for maleic acid and 1000 - 970 $cm^{-1}$ for $K_2SO_4$.

For each set, 9 tablets were prepared; 7 tablets containing mixtures and 2 tablets consisting of 1 pure component. For each tablet, 10 spectra, consisting of 10 co-added scans each, were recorded. In between these spectra, those of the external reference were recorded, again using co-addition of 10 scans in each spectrum. For the experiments using the Bruker system, no external reference was used.

*Internal reference*

The ratio of band intensities of $K_2SO_4$ over maleic acid (area and height) was plotted against the ratio of weights of $K_2SO_4$ over maleic acid. For each set of tablets, a linear trendline was fitted. The correlation coefficients, using the two different Raman spectrometers are displayed in Table 3.15.

**Table 3.15** Calibration curves were constructed and the correlation coefficients ($R^2$) are displayed for the different experiments.

| | Correlation Coefficient ($R^2$) when using internal standardisation | |
|---|---|---|
| | Height | Area |
| | Perkin-Elmer system | |
| Set 1 | 0.995 | 0.991 |
| Set 2 | 0.999 | 0.995 |
| Set 3 | 0.994 | 0.996 |
| | Bruker system | |
| Set 1 | 0.986 | 0.962 |
| Set 2 | 0.997 | 0.983 |
| Set 3 | 0.997 | 0.997 |

For all three sets of tablets, 1 tablet of each set was left out of the calculations as an outlier. It is surprising that the 3 tablets left out all had the same concentration.
Both sets 2 and 3 show good results for both spectrometers. However it is strange that for internal standardisation, different slopes are found for the linear regression. This is to be expected when comparing the results of the two different spectrometers, but we would expect a similar slope for the sets recorded on the same spectrometer. The different slopes for correlation of bandheights with concentration are displayed in Table 3.16.

**Table 3.16** Comparison of the different slopes from the calibration lines for the different spectrometers. The calibration tablets were made up from $K_2SO_4$ and maleic acid.

| | Slope from trendline |
|---|---|
| Perkin-Elmer system | |
| Set 1 | 0.748 |
| Set 2 | 0.909 |
| Set 3 | 0.874 |
| Bruker system | |
| Set 1 | 0.635 |
| Set 2 | 0.828 |
| Set 3 | 0.705 |

The reason for different slopes could be detector response, instrumental factors, changing scattering properties with slight misalignment of the tablet analyser.

*External reference-Perkin Elmer system*

As for the previous experiments, in the spectrum of the external reference, the following peak region was used in our calculations: 1220-1120 $cm^{-1}$. Band areas and heights from the tablet components were ratioed with the band areas and heights of the external reference. These figures were plotted against the weight of the particular component. Calibration lines were constructed and the correlation coefficients calculated.

There is no relation between the Raman intensities from maleic acid and the concentration. The reason for this is unclear since the reproducibility of the tablets was around 98%. For $K_2SO_4$, it is clear from the graphs that a second order curve fits the data best. As with the internal reference results, the same tablets were left out of the calculations. Results when an external reference was used, are summarised in Table 3.17.

**Table 3.17** Calibration lines were constructed and the correlation coefficients ($R^2$) are given for the different experiments attempted. External standardisation of the $Na_2SO_4$ Raman intensities versus the weight of $K_2SO_4$.

| | Correlation Coefficient ($R^2$) when using external standardisation | |
|---|---|---|
| | Height | Area |
| | Perkin-Elmer system | |
| Set 1 | 0.991 | 0.987 |
| Set 2 | 0.996 | 0.983 |
| Set 3 | 0.978 | 0.973 |

The calibration curve showing the weight of $K_2SO_4$ plotted against the ratio of the height of the $K_2SO_4$ band over the height of the external reference is shown in Figure 3.11.

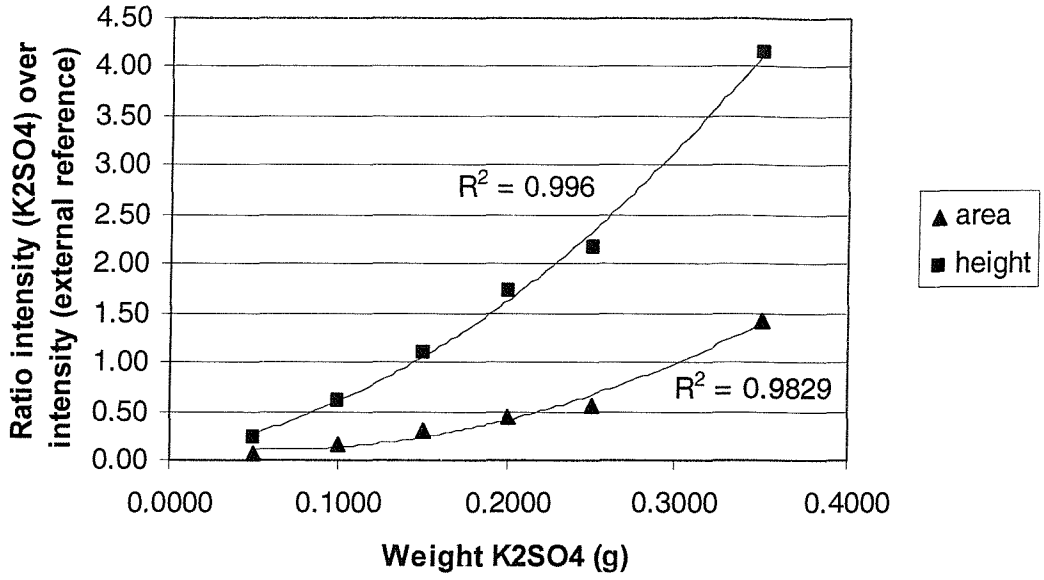


**Figure 3.11** Calibration graph, displaying the ratio of FT-Raman heights of $K_2SO_4$ over the external reference against the weight of $K_2SO_4$.

## Evidence of de-mixing before compression

As was mentioned before, the powders that were carefully mixed might de-mix during or after being transferred into the KBr die. FT-Raman spectra recorded of both sides of a tablet should provide evidence for this. From 5 tablets, spectra were recorded from both sides using the Bruker spectrometer. The differences in intensities (presented as band heights) of the different components in the tablets are shown in Table 3.18.

**Table 3.18** Comparison of heights and the ratio of heights (of the 2 components in a tablet) for the two sides of the tablet. Average means that an average value from 10 spectra was taken.

| Concentration $K_2SO_4$ in tablet (w/w %) | Concentration maleic acid in tablet (w/w %) | Side A of tablet | Side B of tablet | Approximate variation between both sides (%) |
|---|---|---|---|---|
| 12 | 88 | | | |
| Average height band $K_2SO_4$ | | 0.18 | 0.14 | 30 |
| Average height band maleic acid | | 1.3 | 1.17 | 10 |
| Average ratio of heights | | 0.14 | 0.12 | 15 |
| 13 | 87 | | | |
| Average height band $K_2SO_4$ | | 0.15 | 0.21 | 30 |
| Average height band maleic acid | | 1.37 | 1.34 | 2.5 |
| Average ratio of heights | | 0.11 | 0.16 | 30 |
| 37 | 63 | | | |
| Average height band $K_2SO_4$ | | 0.70 | 0.74 | 5 |
| Average height band maleic acid | | 1.34 | 1.02 | 25 |
| Average ratio of heights | | 0.52 | 0.72 | 30 |
| 75 | 25 | | | |
| Average height band $K_2SO_4$ | | 2.68 | 2.25 | 20 |
| Average height band maleic acid | | 0.67 | 0.88 | 25 |
| Average ratio of heights | | 4.00 | 2.56 | 35 |
| 100 | 0 | | | |
| Average height band $K_2SO_4$ | | 4.63 | 4.8 | 5 |

These differences in spectral intensities between the different sides of the tablets are proof of de-mixing of the powders before compression into tablets.

Since the FT-Raman systems have a penetration depth less than 1.5 mm and the tablet thickness varies from 3 to 5 mm, it is impossible to obtain good quantitative results. It is expected that, at best, only half of the tablet is sampled in these experiments. This would have been sufficient if no de-mixing had occurred.

## 3.6 Conclusions

Several conclusions can be drawn from these results.

Reproducibility

Provided that the laser is stable, the Raman spectra of liquids (including the external reference used in the quantitative analyses) are reproducible within 98.5%. The reproducibility of the FT-Raman spectra of the tablets varied considerably, from 99% to 95%. The reason for this variation is probably due to the fact that the tablets were not fixed into the sample holder, this made the tablet 'tumble' instead of 'smooth', stable rotation.

Use of external standardisation

The value of using external standardisation to correct for instrumental variables is questionable. It was found that when the instrument is stable (relative standard deviation $\leq$ 1.5%), external standardisation is not necessary. When the reproducibility from tablet to tablet is around 98%, our external reference enhances the reproducibility. But when the tablet reproducibility falls below 97.5%, ratioing against an external reference only makes the results worse, because either the laser is very unstable in the short term, or other factors become important like the tablet moving in and out of focus,...

Quantitative Analysis

a) *Internal standardisation*

The results obtained from the construction of the calibration curves for the different sets of formulations containing local anaesthetics are promising. When plotting the ratio of the 1606 $cm^{-1}$ band from prilocaine over the 1286 $cm^{-1}$ band of the excipients against the percentage of eutectic mixture present in the formulation, a correlation coefficient higher than 0.99 was obtained in all 4 sets of formulations. One problem that needs to be solved is the fact that the slopes for these regression lines varied from one to the other. This could be due to integration errors or some other instrument variables. It is expected that the use of chemometric procedures will improve these results.

For the quantitative analyses on the different sets of tablets, correlation coefficients were usually higher than 0.99.

For some sets of calibration samples a tablet was rejected. The reason for these outlier values was thought to be due to mixing problems when preparing the tablets.

b) *External standardisation*

The values of the correlation coefficients after external standardisation of the band intensities are much lower than those when using internal standardisation. This is not surprising. The values of the correlation coefficients vary considerably depending on the composition of the tablets. Tablets containing a hard inorganic compound and a softer organic compound give better correlation between the FT-Raman intensities and the concentration than the tablets made up from two hard inorganic compounds. For the inorganic-organic mixtures, tablets prepared from non sieved powder gave better results in terms of correlation coefficient than those prepared from sieved powder. On average, correlation coefficients higher than 0.99 were obtained for the inorganic-organic mixtures. For the set of tablets made up from two inorganic compounds there was no linear relation over the total concentration range. It seemed that there was a linear relation over the concentration range up to 70% w/w% $K_2CrO_4$. Correlation coefficients of 0.99 were obtained.

It seems that good correlation coefficients are obtainable from external standardisation. But the reproducibility of these graphs is still questionable.

Band area versus band height

It seems that for these experiments, band height gave better results both in the reproducibility experiments as in the construction of the calibration graphs. Exceptions were found in the set of tablets made up from $K_2CrO_4$ and $Na_2SO_4$. Here band areas clearly gave better results than the use of band heights. The reason for this is that the bands in $K_2CrO_4$ are very intense and sharp hence increasing the effect of integration errors on the calculated height.

Influence of packing density

There was an influence of packing density on the FT-Raman spectra of maleic acid tablets. Tablets compressed using 9 tons on a 16 mm KBr die showed around 5% reduction in Raman intensity, compared with the tablets compressed using 3 tons of weight. This value is only an average value and could vary because the relative standard deviations for the average Raman intensities at the different compressions tend to be rather high (2% or more).

## 3.7 References


[1] M.V. Pellow-Jarman, P.J. Hendra and R.J. Lehnert, Vibr. Spectrosc., **12**, (1996), 257

[2] P. Ascarelli, E. Cappelli, G. Mattei, F. Pinzari, S. Martelli, Diamond and Related Materials, **4**, (1995), 464

[3] C.J. Petty, P.J. Hendra and T. Jawhari, Spectrochim. Acta, **47A**, 9/10, (1991), 1189

[4] T. Jawhari, P.J. Hendra, H.A. Willis and M. Judkins, Spectrochim. Acta, **46A**, 2, (1990), 161-170

[5] D.P. Schweinsberg and Y.D. West, Spectrochim. Acta, 53**A**, (1997), 25-34

[6] T.M. Hancewicz and C. Petty, Spectrochim. Acta, **51A**, (1995), 2193-2198

[7] C.M. Deeley, R.A. Spragg and T.L. Threlfall, Spectrochim. Acta, **47A**, (1991), 1217

[8] A.M. Tudor, S.J. Church, P.J. Hendra, M.C. Davies and C.D. Melia, Pharm. Res., **10**, 12, (1993), 1772

[9] F.W. Langkilde, J. Sjoblom, L. Tekensbergs-Hjelte, J. Mrak, J.Pharm.Biomed.Anal., **15**, (1997), 687

[10] C.G. Kontoyannis, J.Pharm.Biomed.Anal., **13**, 1, (1995), 73

[11] C. Wang, T.J. Vickers, C.K. Mann, J.Pharm.Biomed.Anal., **16**, (1997), 87

[12] S.E.J. Bell, D.T. Burns, A.C. Dennis, L.J. Matchett and J.S. Speers, Analyst, **125**, (2000), 1811

[13] I. Jedvert, M. Josefson and F. Langkilde, J. NIR Spec, **6**, (1998), 279

[14] C. Guo, L. Huizhou, W. Jing, C. Jiayong, J. Colloid Interface Sci, **209**, (1999), 368

[15] L.S. Taylor & F.W. Langkilde, J. Pharm. Sci., **89**, 10, (2000), 1342

# Chapter 4 Study of a Local Anaesthetic System

## 4.1 Introduction

In the pharmaceutical industry it is very important to make sure that the drug is administered in the most suitable way. Not only is the amount of active substance very important, but also its bioavailability, stability and solubility which in turn will affect how the drug will be formulated and subsequently administered. In our study of a local anaesthetics system, the dosage form is carefully chosen. The two active materials prilocaine and lidocaine form a eutectic mixture [1] that results in a melting point lower than that of either of the two actives. Since the eutectic mixture is liquid at room temperature it has been possible to formulate an effective local anaesthetic preparation for topical application. As excipients, two polymers in aqueous solution are added, which results in an easily applicable gel. It is important to know what the effect is of the excipients on the two actives and that is why we have made a start in a study of the possible interactions using vibrational spectroscopy.

The effect of changes in conformation on vibrational spectra has been extensively studied in the Polymer [2,3] and biological fields [4,5]. Since both lidocaine and prilocaine possess a secondary amide group, it was interesting to compare our findings with those from the literature on e.g. proteins [6-7]. The most powerful tool to study protein structures is X-ray diffraction. However, practically all protein molecules in biological systems are in aqueous solution and it is questionable whether the conformational structure of the protein determined by X-ray diffraction is similar to that of the protein in solution. Therefore techniques like Raman and fluorescence spectroscopy have gained much popularity.

## 4.2 Experimental

FT-Raman spectra were acquired on a Perkin Elmer System 2000 FT-Raman spectrometer, equipped with a quartz beam splitter and an InGaAs detector operating

at room temperature. An Optomech continuous wave $Nd^{3+}$:YAG laser (1.064μm) provided the NIR excitation.

For the mapping experiments, a Renishaw Raman microscope, was used. A HeNe laser provided visible excitation at 632.8 nm. A CCD detector is incorporated in the spectrometer.

The absorption infrared spectra were recorded on the Perkin Elmer System 2000 FT-IR and Paragon spectrometers. The System 2000 was equipped with a MIR TGS detector and an optimised KBr beamsplitter. The Paragon system uses a LITA detector and a KBr beamsplitter.

The ATR infrared spectra were recorded on a Bio-Rad FTS 135 spectrometer, equipped with the 'Golden Gate' accessory. The detector was a DTGS detector. Some additional experiments were performed on a Bio-Rad FTS 3000 spectrometer at AstraZeneca in Mölndal, Sweden. This instrument was equipped with a Specac hot stage 'Golden Gate' accessory.

A Ventacon Raman hot cell was used to record high temperature Raman spectra. In addition a Ventacon infrared hot cell was used for the high temperature infrared work. For the low temperature work a Ventacon C-1 cold cell was used.

## 4.3 Characterisation of a local anaesthetic system

The local anaesthetic system studied consists of two active substances in an aqueous solution of block copolymers. The two active components are lidocaine and prilocaine and their chemical structures are displayed in Figure 4.1. They form a eutectic mixture that melts at 18°C.

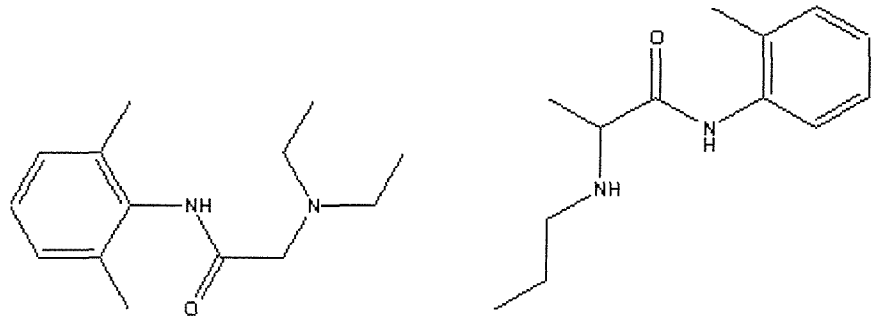


**Figure 4.1** Chemical structures of lidocaine (left) and prilocaine (right)

The two block copolymers in this formulation are Pluronic F68 and F127. They are polyethyleneoxide-polypropyleneoxide-polyethyleneoxide tri-block copolymers. More specifications about these block copolymers are given at a later stage.
The FT-Raman and infrared spectra of the two actives and block copolymers separately and in the formulation were recorded and are discussed below.
As mentioned in the introduction, the two active materials contain a peptide group in their molecular structure. This group shows a number of characteristic vibrational frequencies. In addition it is very susceptible to hydrogen bonding.
A peptide group gives rise to many different vibrational frequencies, such as the amide I to III bands that arise from in-plane vibration of the peptide bond. In addition, there is the amide IV frequency that is due to the bending mode of the CONH group. The amide V to VII bands arise from the out-of-plane vibrations. Among these, the amide I (carbonyl stretching) and amide III bands are most often correlated with the structural properties of the proteins since they are quite distinctive in the Raman spectra [6].

### Lidocaine

Lidocaine is a white, crystalline material with a melting point of 67°C. The FT-Raman and infrared spectra of the crystalline material and the melted material were recorded. and are displayed in Figures 4.2 and 4.3.

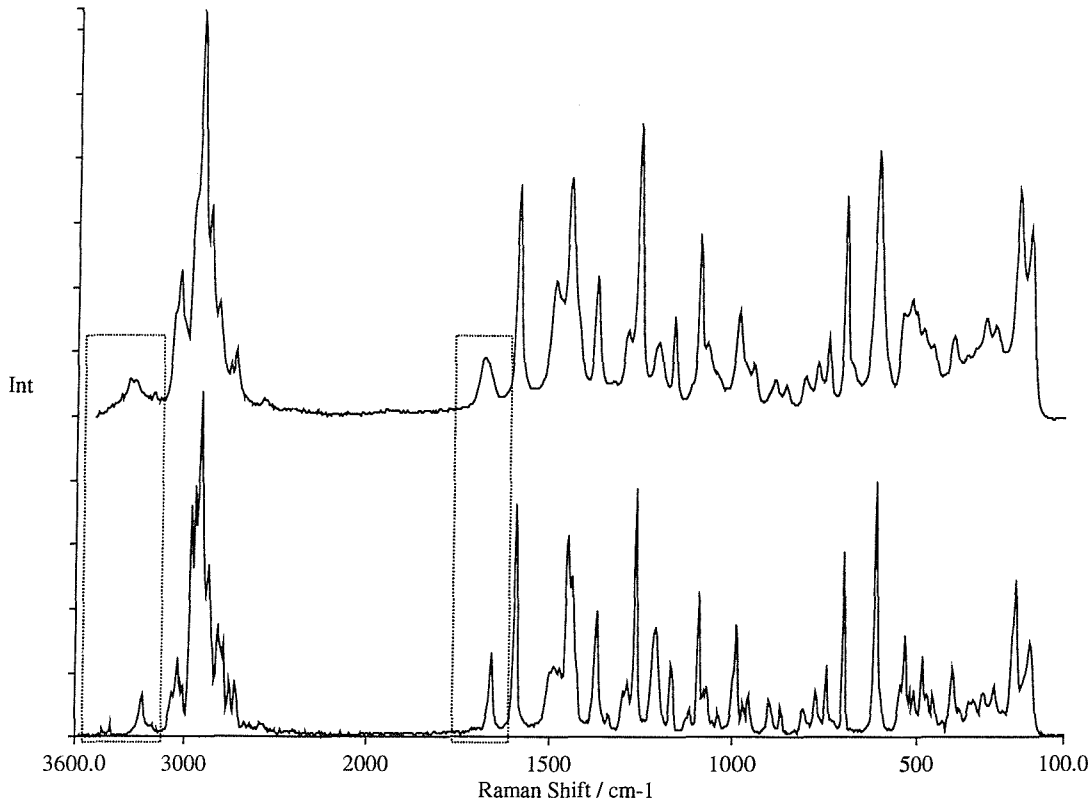


**Figure 4.2** FT-Raman spectrum of lidocaine in the molten state (top) and as a crystalline material (bottom). The regions in the spectrum of particular interest are boxed in.

On melting of lidocaine, the bands in the spectrum get less intense and tend to broaden. The NH stretching frequencies (above 3100 $cm^{-1}$) and the carbonyl stretching frequencies (above 1620 $cm^{-1}$) have shifted towards lower wavenumbers in the solid state spectrum of lidocaine. This could be an indication of hydrogen bonding. For comparison, the absorption infrared spectra are displayed below in Figure 4.3.

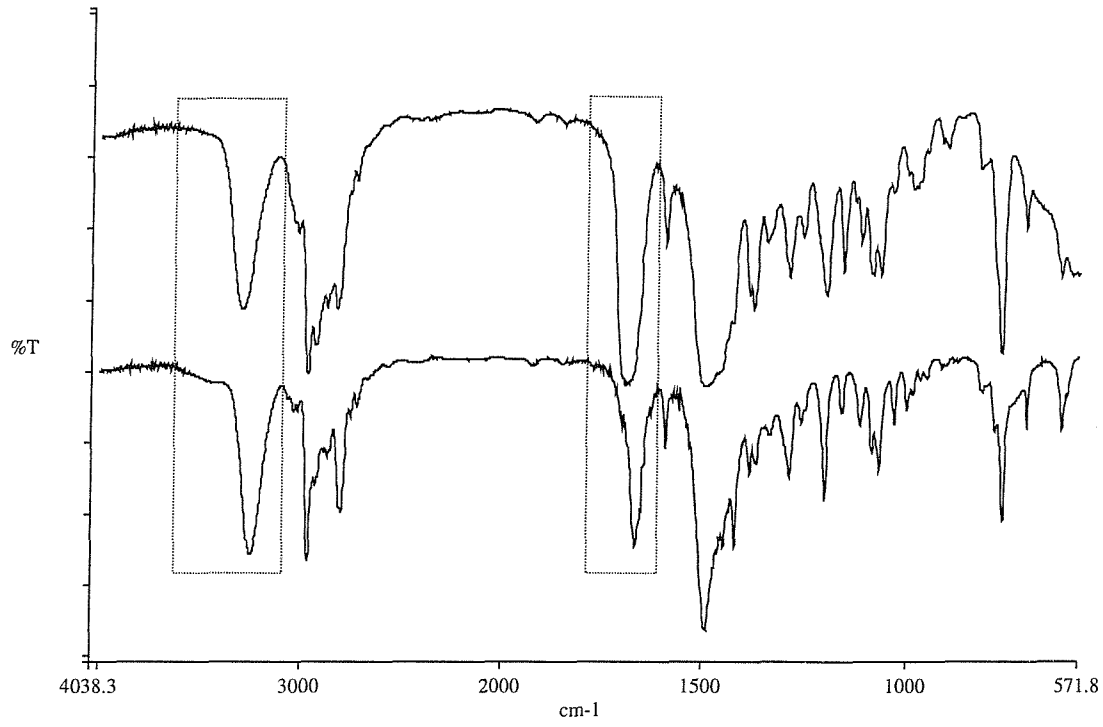


**Figure 4.3** Infrared absorption spectra of lidocaine in the molten state (top) and as a crystalline material (bottom). The spectra of lidocaine were recorded as a powder between KBr flats. The regions in the spectrum of particular interest are boxed in.

The conclusions from the Raman data with regard to the frequency shifts of the stretching vibrations sensitive to hydrogen bonding on melting also apply to the infrared spectra. In the spectrum of the crystalline material, there is a low intensity background at the high frequency side of the 3255 $cm^{-1}$ band. This could well be an indication of hydrogen bonding.

The ATR spectra of lidocaine (not displayed here) show similar changes in the spectra on melting.

In Table 4.1, the most important vibrational frequencies of crystalline lidocaine are listed.

**Table 4.1** Tentative assignment of the vibrational frequencies in the Raman and infrared spectra of crystalline lidocaine. v: stretching, s: strong, m: medium, w: weak, vw: very weak, br: broad

| Infrared frequency ($cm^{-1}$) | Raman frequency ($cm^{-1}$) | Tentative assignment |
|---|---|---|
| 3444vw br | | vNH hydrogen bonded |
| | 3414vw | Free vNH |
| 3255br | 3243 | vNH bonded in trans form |
| | 3185 | Overtone of C-N |
| 1669s | 1663 + 1673w | C=O bonded (amide I) |
| 1630w | | C=O |
| 1618w | | Benzene C=C |
| 1593m | 1594s | Benzene C=C |
| 1492 | 1488 | C-H in plane bending |
| 1264 | 1265 | C-N stretching (amideIII) |
| 1035 | 1037 | C-H in plane bending |
| 765 | | CH out of plane bend |
| | | 1,2,3 tri-substituted benzene |

When examining the solution infrared spectra, it can be deduced from the NH stretching vibrations that the amide group in lidocaine is in the trans form. The frequency of the NH stretching shifts towards higher frequencies when dissolved (3255 $cm^{-1}$ crystalline to 3319 $cm^{-1}$ in solution), compared with the crystalline spectrum.

In addition, the carbonyl stretching frequency has shifted to a higher frequency in the solution spectrum (1669 $cm^{-1}$ in the crystalline material to 1690 $cm^{-1}$ in solution).

## Prilocaine

Prilocaine is a white powder with a melting point of 38°C. As with lidocaine, the infrared and Raman spectra of the crystalline material and the melted material were recorded. The FT-Raman and infrared spectra are displayed in Figures 4.4 and 4.5.

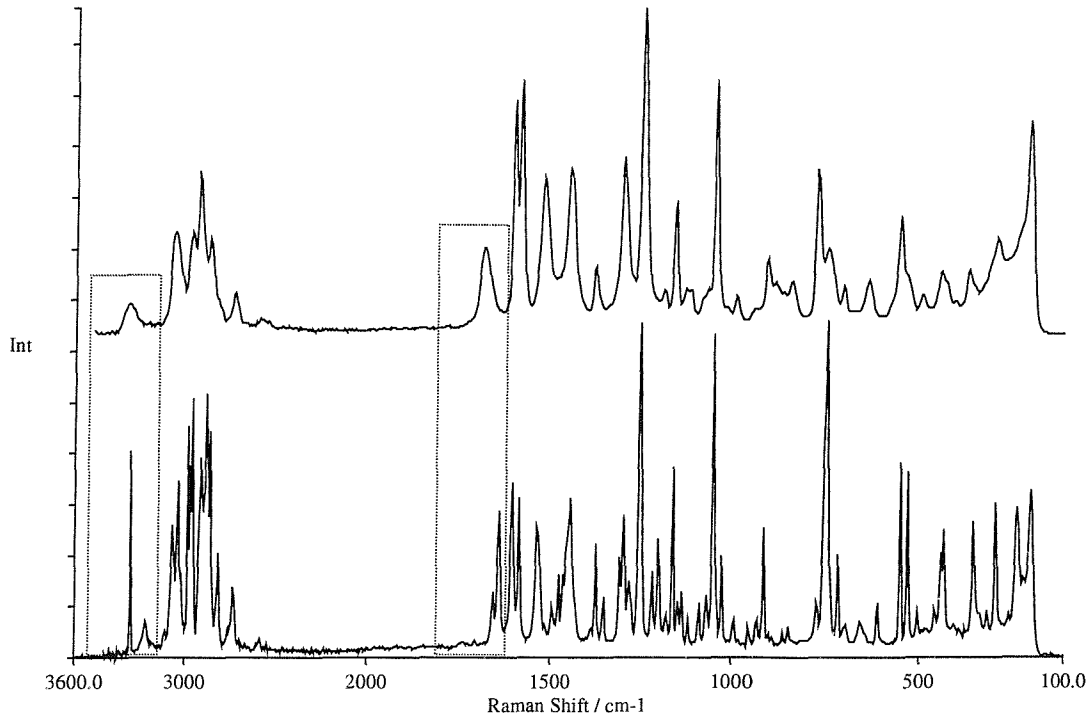


**Figure 4.4** FT-Raman spectrum of prilocaine in the molten state (top) and as a crystalline material (bottom). The regions in the spectrum of particular interest are boxed in.

The spectra of lidocaine and prilocaine are quite similar in appearance, which is what we would expect. However, in the NH stretching region the spectra are very different. Prilocaine has a very sharp band at 3302 $cm^{-1}$. In addition, there are two relatively weak bands around 3414 $cm^{-1}$ and 3219 $cm^{-1}$. In the region around 1600 $cm^{-1}$, we notice two doublets. The highest frequency bands are due to the carbonyl stretching, the others to the aromatic ring system.

The absorption infrared spectra are displayed in Figure 4.5.

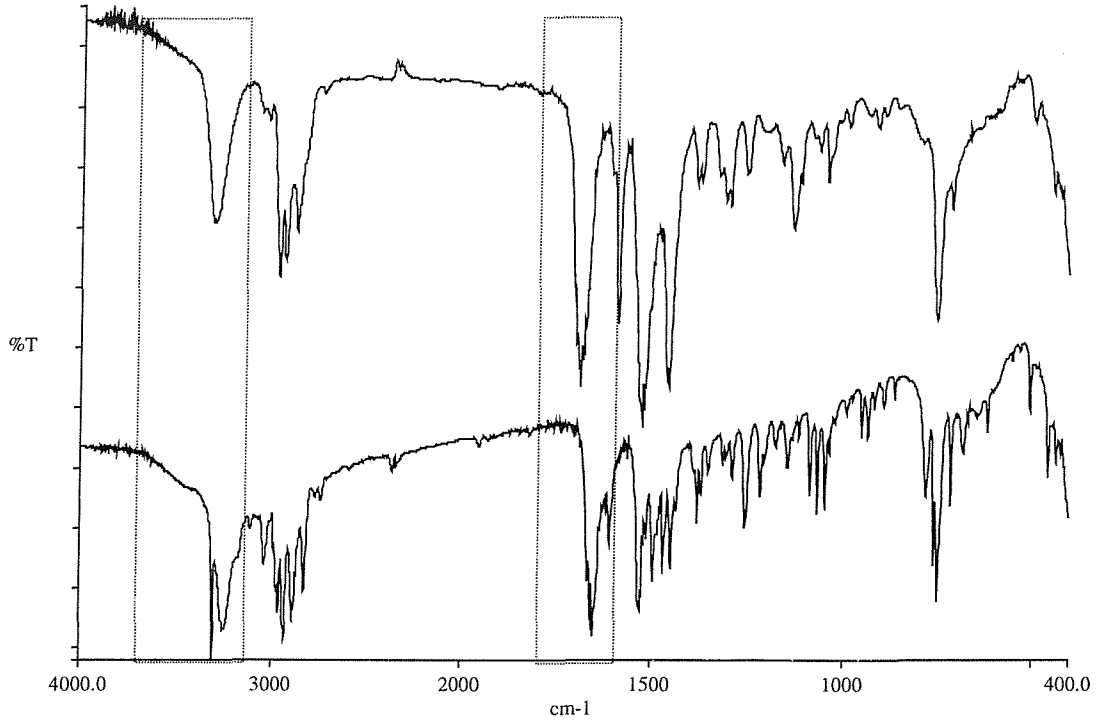


**Figure 4.5** Infrared absorption spectra of prilocaine in the molten state (top) and as a crystalline material (bottom). The spectra of prilocaine were recorded between KBr flats. The regions in the spectrum of particular interest are boxed in.

In the solid state spectrum of prilocaine, there are two distinct NH stretching frequencies. The higher frequency band is very sharp and would suggest that there is no hydrogen bonding to this NH group. A second, broader, lower frequency band is observed at 3251 $cm^{-1}$ and this is expected to be due to a hydrogen bonded NH group. In Table 4.2, the most important vibrational frequencies of crystalline prilocaine are listed.

**Table 4.2** Tentative assignment of the vibrational frequencies in the Raman and infrared spectra of crystalline prilocaine. s:strong, vs: very strong, m: medium, w:weak

| Infrared frequency ($cm^{-1}$) | Raman frequency ($cm^{-1}$) | Tentative assignment |
|---|---|---|
| 3370wbr | | H-bonded trans amide νNH |
| | 3414w | |
| 3304s | 3302s | Secondary amine |
| 3251 | 3219br | νNH |
| ±3166 | | Cis amide νNH |
| 3106 | 3109 | Overtone of the 1550 band |
| 1664s | 1660s | C=O |
| 1654vs | | C=O (amide I) H-bonded |
| 1647vs | 1642s | C=O (amide I) H-bonded? |
| 1618m | | Benzene C=C |
| 1606s | 1607s | Benzene C=C |
| 1587 | 1587 | Benzene C=C |
| 1526 | | NH bend (amide II) |
| 1491 | 1477 | C-H in plane bending |
| | | Should be doublet |
| 1038 | | C-H in plane bending |
| | | Should be doublet |
| 760 | 762 | CH out of plane bend |
| 751s | 755s | NH wag or CH out of plane bend |

Again, the evidence for a trans amide configuration can be found in the NH stretching region of the solution infrared spectra. In Figure 4.6 three solution infrared spectra, using a non polar solvent, are displayed with different concentrations. On increasing the concentration, the trans-NH stretching frequency is expected to shift towards lower wavenumbers, whereas the cis-NH stretching frequencies should remain constant. From the solution infrared spectra at different concentrations, a frequency shift is observed therefore the amide group is in the trans conformation.

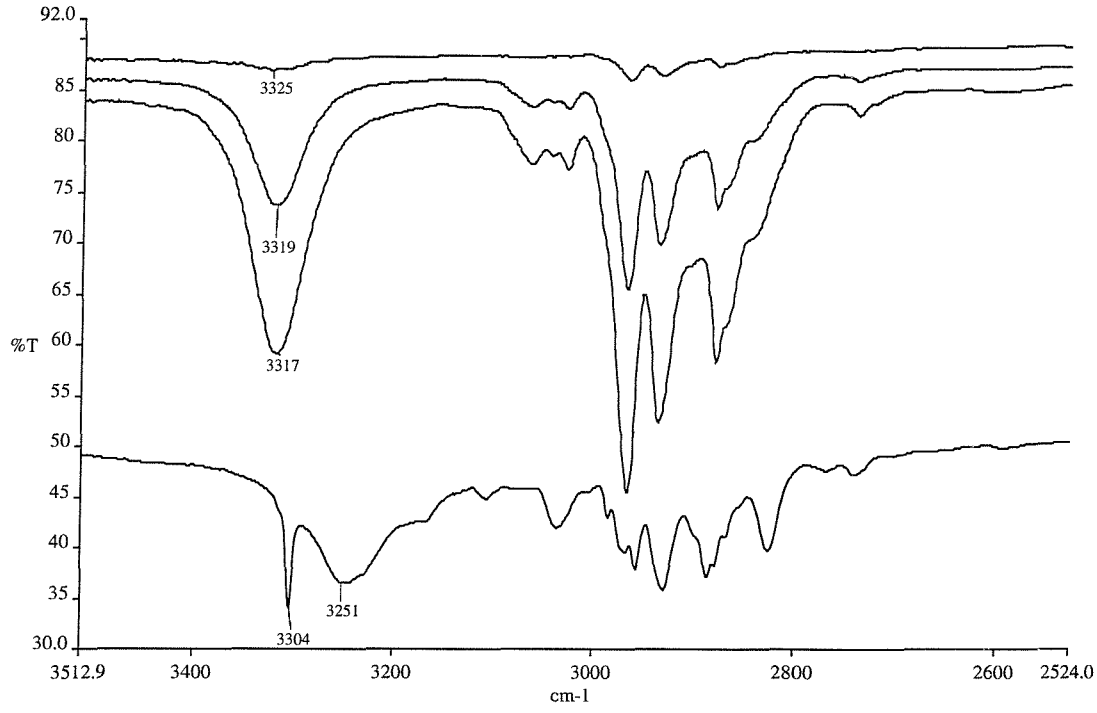


**Figure 4.6** The upper three infrared spectra are those of prilocaine in $CCl_4$, the top spectrum being the lowest concentration one. The concentration increases in the second spectrum and the highest concentration is found in the third spectrum. The bottom spectrum is the absorption infrared spectrum of crystalline prilocaine. As the concentration of prilocaine increases, the NH stretching frequency moves towards lower frequencies.

In addition, the carbonyl stretching frequency has shifted towards higher wavenumbers in solution (from 1654 $cm^{-1}$ in the crystalline material to 1694 $cm^{-1}$ in solution). It is more difficult to assign the amide II band (around 1550 $cm^{-1}$) in prilocaine even when comparing the spectrum with the solution infrared spectra. On increasing the concentration of prilocaine, this band is expected to shift towards higher frequencies as the hydrogen bonding increases.

## Eutectic mixture of lidocaine and prilocaine

The FT-Raman spectrum of the eutectic mixture in the molten state is shown in Figure 4.7. Even though the melting point of the eutectic mixture is not problematically low, at 18°C, it proved impossible to get the eutectic mixture solidified. Even after quenching it in liquid nitrogen, in the time required (± 10 s) to transfer it into a cryo-cell, it had melted again. Nevertheless, a spectrum was recorded at -100°C and is displayed together with the spectrum of the melt in Figure 4.7.

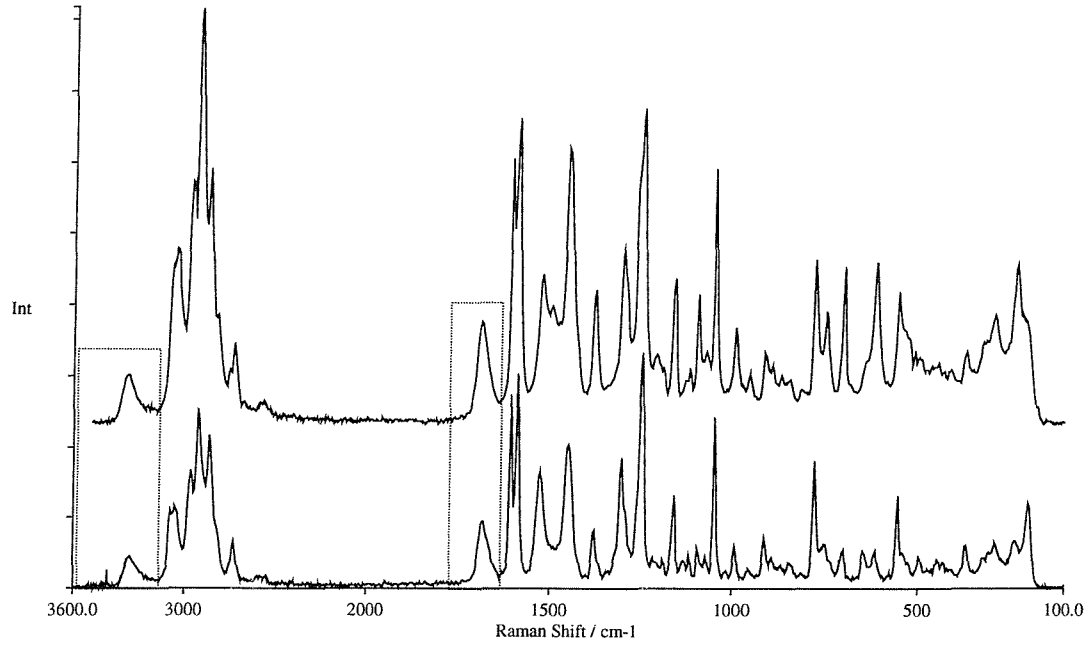


**Figure 4.7** FT-Raman spectrum of the eutectic mixture of lidocaine and prilocaine in the molten state (top) and as a more crystalline material at -100°C (bottom). The regions in the spectrum of particular interest are boxed in.

There are some clear differences between the two spectra in Figure 4.7. The most prominent differences are displayed in Table 4.3.

**Table 4.3** The changes in the FT-Raman spectra on cooling the eutectic mixture of lidocaine and prilocaine are presented. The frequencies are compared with those from the spectra of pure crystalline lidocaine and pure crystalline prilocaine.

| Intensity decreases on cooling vibrational frequencies ($cm^{-1}$) | Lidocaine vibrational frequencies ($cm^{-1}$) | Prilocaine vibrational frequencies ($cm^{-1}$) |
|---|---|---|
| 1500 | | |
| 1096 | 1096 | |
| 992 | 990 | 994 |
| 753 | 753 | 754 |
| 706 | 705 | |
| 618 | 616 | 616 |
| intensity increases | | |
| 198 | 197 | 197 melt |

When the eutectic sample is transferred into the cold cell very rapidly and a one scan spectrum is recorded, a sharp band in the NH stretching region around 3478 $cm^{-1}$ is apparent. This frequency is much higher than the sharp band in crystalline prilocaine (3302 $cm^{-1}$) and much higher than the highest frequency in lidocaine (3414 $cm^{-1}$). This high frequency is a sign of a very strong NH bond, where no weakening by hydrogen bonding occurs. Another very weak feature is present at 3441 $cm^{-1}$. Again this is a rather high frequency which suggests that there is no weakening of the NH stretching through hydrogen bonding. As more scans are accumulated, these bands disappear. The reason for this could be heating by the laser.

Another question one needs to ask is whether the eutectic spectrum at -100°C is a crystalline one or that of a glass?

For comparison, the infrared reflection spectra are shown in Figure 4.8.

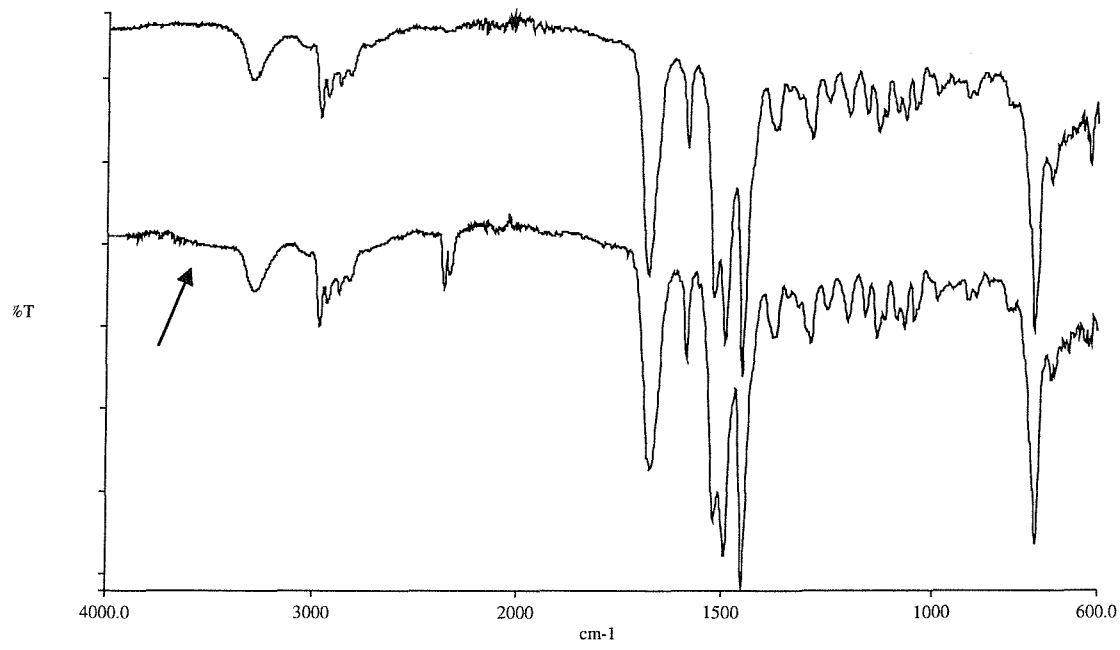


**Figure 4.8** ATR spectra of the eutectic mixture of lidocaine and prilocaine. The top spectrum is that of the melted eutectic, whereas in the bottom spectrum the eutectic has been cooled down to around 7°C.

The most prominent difference between the two ATR spectra is the appearance of some hydrogen bonding (indicated by the arrow in Figure 4.8) in the spectrum of the cooled eutectic.

Absorption infrared spectra were also recorded of the eutectic mixture. It was surprising that in some of the spectra signs of hydrogen bonding at high frequencies (~3500 $cm^{-1}$) appear but not in others.

In Table 4.4 the Raman and infrared vibrational frequencies in the eutectic mixture of lidocaine and prilocaine are compared.

**Table 4.4** Tentative assignment of the vibrational frequencies in the Raman and infrared spectra of the eutectic mixture of lidocaine and prilocaine below its melting point. s:strong, m: medium, br: broad, v: stretching

| Infrared frequency ($cm^{-1}$) | Raman frequency ($cm^{-1}$) | Tentative assignment |
|---|---|---|
| 3470br | | νNH secondary amine |
| 3294br | (3314 + 3260)br | νNH trans mono substituted amides |
| 3080 | 3080 | |
| 1683sbr | (1690 + 1671)br | C=O (amide I) |
| | 1607s | Benzene C=C |
| 1587s | 1589s | Benzene C=C |
| 1525s | 1524m | NH bend secondary amine |
| 1292m | | CN stretching (amide III) |
| 769 | 785 | tri-substituted benzene |
| 755 | 754 | di- or tri-substituted benzene |

## Excipients in the formulation containing local anaesthetics

The excipients in the formulation are Pluronic F127 and F68 (also known as Lutrol® F127 and F68). Pluronic is the family name for a group of polyethyleneoxide-polypropyleneoxide block copolymers, also called poloxamers. These block copolymers show reverse gelling effects in water, which means that they are low viscosity fluids at room temperature and rigid elastic gels at body temperature [8,9]. This reversible sol-gel property allows cool solutions to flow onto the skin or into the wound before warming to form a gel. Other advantages of these excipients are their capacity to solubilize hydrophobic compounds in water [8,10,11] and their low toxicity.

Some physico-chemical properties of the two block copolymers are given in Table 4.5.

**Table 4.5** Physico-chemical properties of the block copolymers F68 and F127.

| Properties | F68 | F127 |
|---|---|---|
| Average Molecular Weight (g/mol) | 8400 | 12600 |
| Percentage of EO (w/w%) | 80 | 70 |
| Melting pour point (°C) | 52 | 56 |

Many studies have been performed on conformation changes in aqueous solutions of these polyethyleneoxide-polypropyleneoxide block copolymers [12-14]. Chen-Chow and Frank showed evidence that the gel-state of Pluronic F127 consists of a large population of micelles, forming a viscous isotropic liquid crystal [15].
FT-Raman spectra of the block copolymers alone and in aqueous solution are shown in Figure 4.9. The total concentration of these block copolymers in the aqueous solution is 22% w/w%.

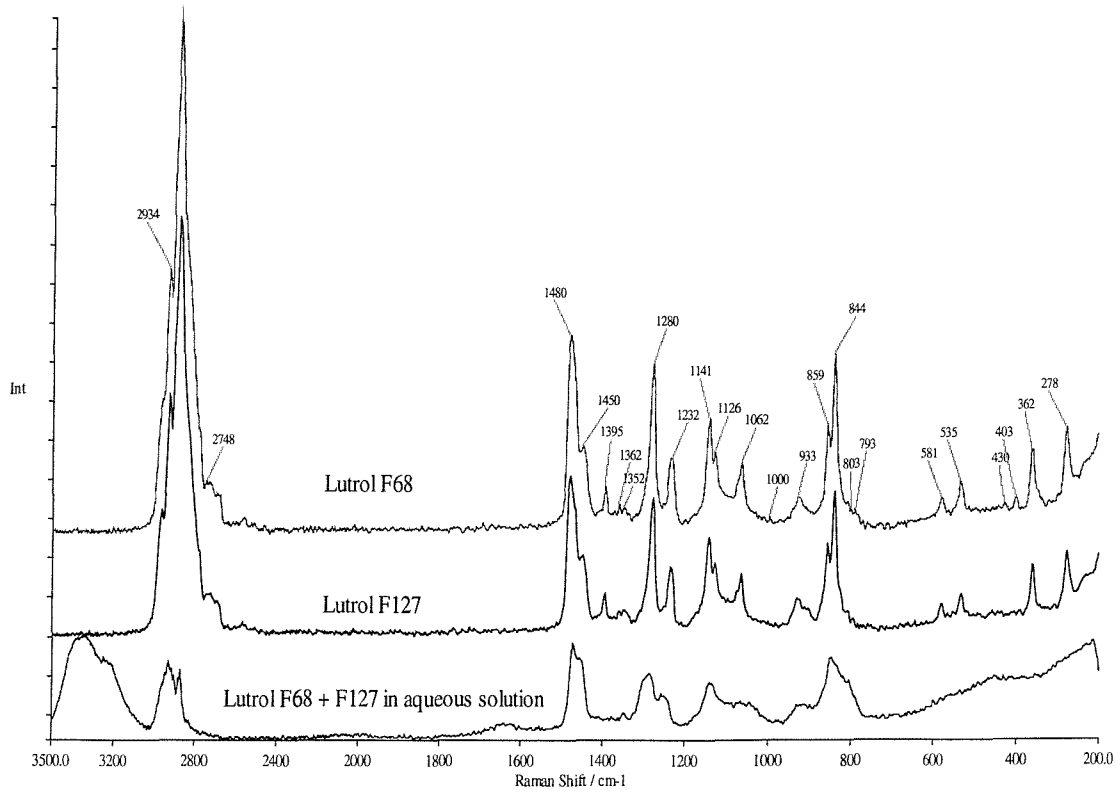


**Figure 4.9** FT-Raman spectra of the block copolymers alone and in aqueous solution.

From Figure 4.9, it is clear that dissolving the two polymers in water has a large effect on the spectrum. At the high frequency region, we see clear evidence of the water OH stretching. The band in this region looks quite asymmetric which indicates the presence of different states of solubilized water molecules [16]. Furthermore, in the fingerprint region, bands have decreased in intensity and have broadened. More details of the conformation of these block copolymers in aqueous solution are given at a later stage.

### The formulation containing local anaesthetics

The anaesthetic system that was studied consists of a eutectic mixture of lidocaine and prilocaine in an aqueous solution of two PEO[12]-PPO[13]-PEO block copolymers (Pluronic F127 and F68). The Raman spectrum of the formulation is shown in Figure 4.10.

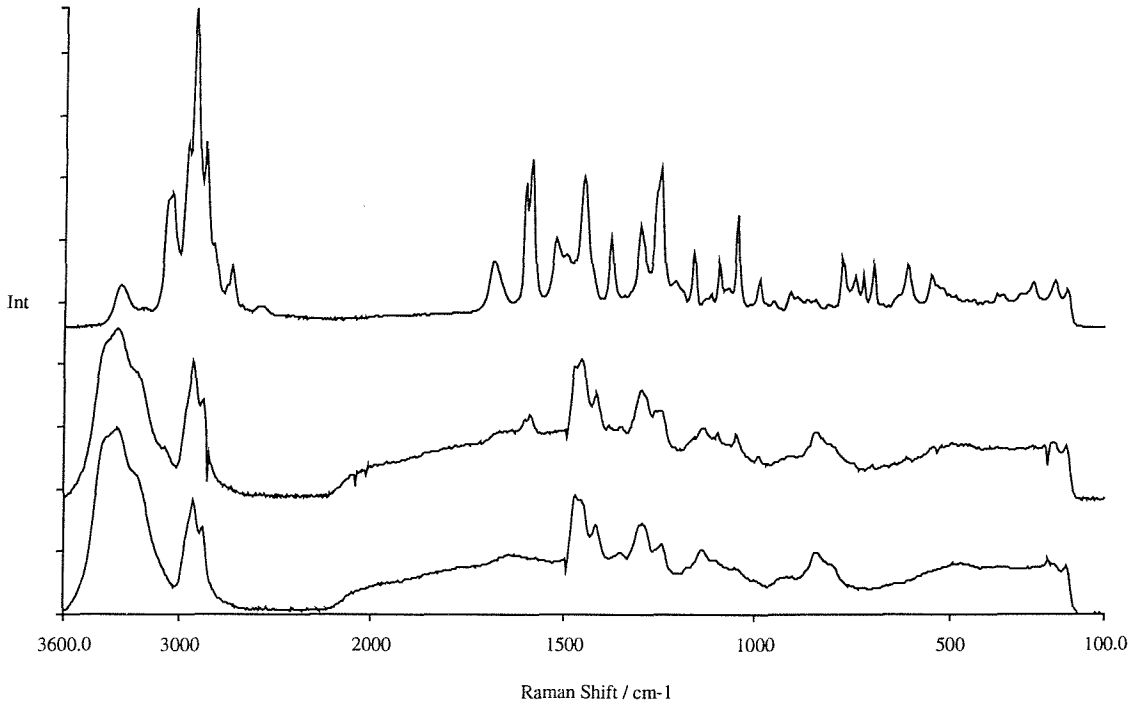


**Figure 4.10** FT-Raman spectra of the eutectic mixture of lidocaine and prilocaine (top), of the formulation (middle spectrum) and of the two block copolymers in aqueous solution (bottom).

When comparing the spectrum of the formulation with that of the aqueous solution of block copolymers, it is clear that the spectrum of the block copolymer system

[12] PEO: polyethyleneoxide
[13] PPO: polypropyleneoxide

containing local anaesthetics is dominated by the excipients. In order to be able to study interactions with the eutectic mixture, bands specific to lidocaine and prilocaine in the formulation need to be identified. The band regions in the formulation due to the eutectic mixture of lidocaine and prilocaine are displayed in Table 4.6.

**Table 4.6** Band regions in the formulation that are due to the actives lidocaine and prilocaine. √-shift means that the band could be a band of the active that shifted.

| Band region ($cm^{-1}$) | due to lidocaine | due to prilocaine |
|---|---|---|
| 1606 | | √ |
| 1591 | √ - shift | √ - shift |
| 1382 | | √ - shift |
| 1096 | √ - shift | |
| 1048 | | √ |
| 992 | √ - shift | √ - shift |
| 706 | √ | |
| 619 | √ | √ - shift |
| 554 | | √ |
| 229 | | √ - shift |

## 4.4 Interactions between lidocaine and prilocaine

As was mentioned above, when lidocaine and prilocaine are mixed together they form a eutectic mixture. By simply bringing the two powders in contact at room temperature, they start to form this liquid oil which is the eutectic mixture. But what interactions are there between lidocaine and prilocaine? When studying the molecular structures, hydrogen bonding between the two is most likely. Therefore, infrared and Raman spectra were recorded from melted lidocaine, prilocaine and their eutectic mixture. When there are no interactions between lidocaine and prilocaine, the sum of their vibrational spectra should be identical to the spectrum of the eutectic mixture. Since it proved impossible to crystallise the eutectic mixture, the spectra were compared in the liquid phase (melts).

## Infrared Data

Both absorption and reflection (ATR) infrared spectra were recorded.

### Absorption infrared spectra

The spectra of lidocaine, prilocaine and the eutectic mixture were all recorded while melted. The substances were dispersed onto KBr flats after which they were transferred into an infrared hot-cell.

The spectra of lidocaine and prilocaine were added together and compared with the infrared spectrum of the eutectic mixture. The absorption infrared spectra are shown in Figure 4.11.

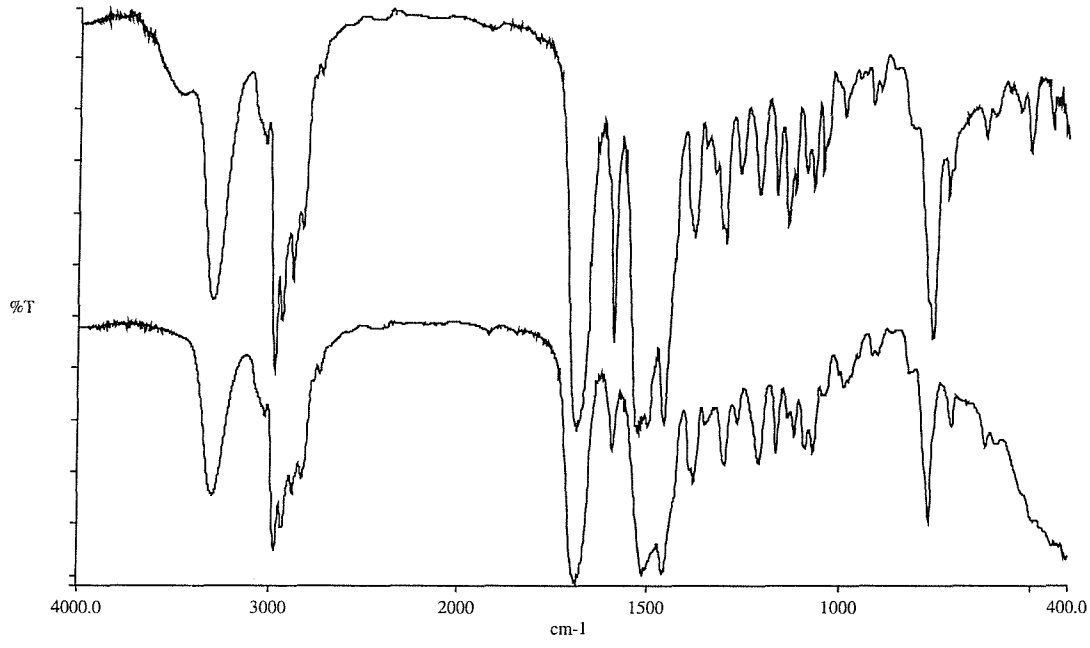


**Figure 4.11** Absorption Infrared spectra of the eutectic mixture of lidocaine and prilocaine (top spectrum) and the sum of the spectra of lidocaine and prilocaine (bottom spectrum). All spectra were recorded above the melting point of the components.

There are many differences between the two spectra, especially in the fingerprint region. Changes in relative intensities being the most common changes observed. In addition a broad band due to hydrogen bonded NH groups is observed in the spectrum of the eutectic mixture. To study the effect of hydrogen bonding, bands involved in hydrogen bonding, like the NH stretching and carbonyl stretching bands, need to be compared. Since these bands may hide underlying bands, it was essential to curvefit the data. The differences between the absorption infrared spectrum of the

eutectic mixture of lidocaine and prilocaine and the sum of the separate spectra of lidocaine and prilocaine are summarised in Table 4.7. In this table only the bands directly involved in hydrogen bonding have been included.

**Table 4.7** Comparison of the sum of the absorption infrared spectra of lidocaine and prilocaine with the spectrum of the eutectic mixture. All the spectra are in the melt phase. s: strong, br: broad, m: medium

| Sum spectra lidocaine and prilocaine vibrational frequencies ($cm^{-1}$) | Eutectic mixture vibrational frequencies ($cm^{-1}$) | Attributed to |
|---|---|---|
| - | 3491br | Hydrogen bonded NH stretching |
| 3312s | 3307s | NH stretching |
| 3267m | 3267m | NH stretching |
| 1692 | 1691 | C=O |
| 1666 | 1670 | C=O |

After curvefitting the NH stretching bands, the absorption IR data shows increased NH hydrogen bonding in the spectrum of the eutectic mixture, in comparison with the sum of the two components. A very broad background is present around 3491 $cm^{-1}$ in the spectrum of the eutectic mixture. In addition the NH stretching band around 3312 $cm^{-1}$ in the sum of the spectra of lidocaine and prilocaine has shifted towards lower frequencies in the eutectic mixture. This is expected as the NH group becomes involved in hydrogen bonding [17].

After curvefitting the carbonyl stretching band, two underlying bands are found. One of them is shifted to higher wavenumbers in the eutectic mixture (compared with the sum of the spectra of lidocaine and prilocaine). This would suggest that there is less hydrogen bonding. The other band only shifts over 1 wavenumber towards lower frequencies. A shift in the carbonyl stretching frequency to lower wavenumbers is expected when the group gets involved in hydrogen bonding.

It was also found that there is a variation in the absorption spectra of the eutectic mixture from one experiment to the other. In some spectra, the broad background in the NH stretching region was absent. This would imply that if there is hydrogen bonding, it is quite weak.

ATR spectra

The ATR spectrometer used was equipped with a hot stage. Therefore it was possible to record the ATR spectra of the samples in the melt phase.

The ATR spectra recorded from the eutectic mixture lidocaine and prilocaine and the sum of the spectra of lidocaine and prilocaine, all in the molten state are shown in Figure 4.12.

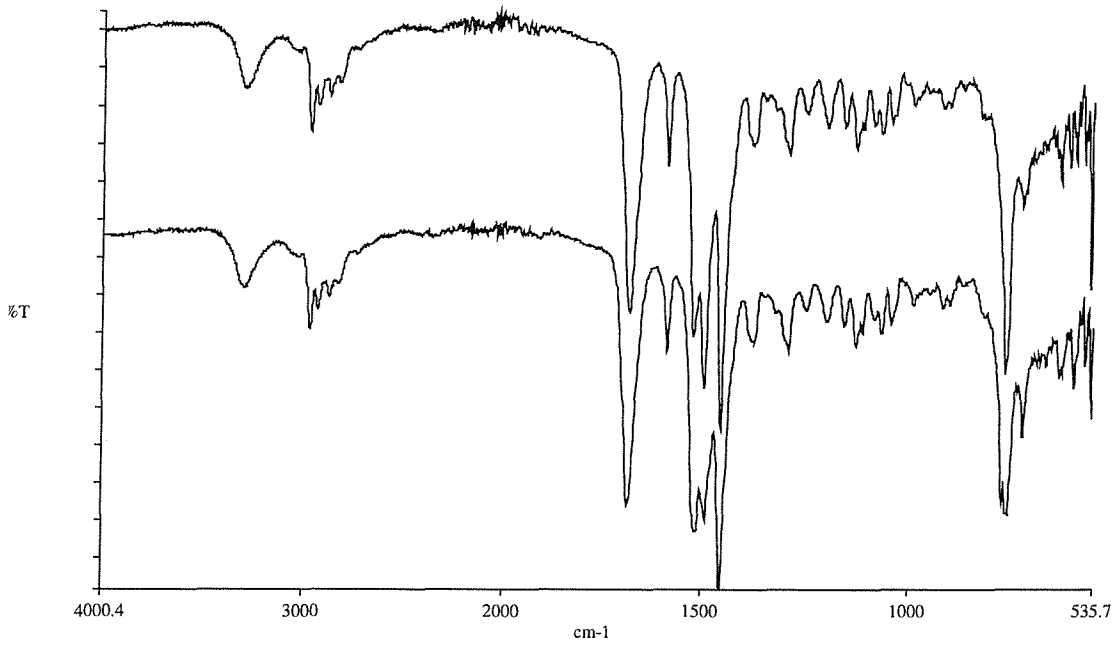


**Figure 4.12** ATR Infrared spectra of the eutectic mixture of lidocaine and prilocaine (top spectrum) and the sum of the spectra of lidocaine and prilocaine (bottom spectrum). All spectra were recorded above the melting point of the components.

After curvefitting the NH and carbonyl stretching bands, some evidence of hydrogen bonding in the eutectic mixture appeared. The shifts in frequency compared with the sum of the spectra of lidocaine and prilocaine were at most 2 wavenumbers.

In the fingerprint region, some differences in relative intensities were observed. The change in relative intensity of the two bands at 1521 $cm^{-1}$ and 1493 $cm^{-1}$ is the most obvious change, more specific the intensity of the 1493 $cm^{-1}$ band has increased when forming the eutectic mixture. This band is due to skeletal deformations, more specific the N-alkyl deformation. Another possibility is that this band is due to the amide II bending frequency, at lower frequency than usual.

Some interesting conclusions can be drawn from the ATR data of the eutectic mixture below its melting point. At lower temperatures (7°C), it seems like a hydrogen

bonding background starts to appear (see also Figure 4.8). There is no sign of H-bonding background in the spectra of the crystalline components lidocaine and prilocaine.

The shifts in carbonyl and NH stretching frequencies in the spectrum of the eutectic mixture, compared with the sum of the spectra of its components in the melt phase are summarised in Table 4.8.

**Table 4.8** Comparison of the sum of the ATR infrared spectra of lidocaine and prilocaine with the spectrum of the eutectic mixture. s: strong, m: medium, w: weak

| Sum spectra lidocaine and prilocaine vibrational frequencies ($cm^{-1}$) | Eutectic mixture vibrational frequencies ($cm^{-1}$) | Attributed to |
|---|---|---|
| 3310w | 3309w | NH stretching |
| 3280m | 3278m | NH stretching |
| 1684s | 1683s | C=O |
| 1660w | 1659w | C=O |

Both the NH and carbonyl stretching frequencies are lower in the ATR spectrum of the eutectic mixture of lidocaine and prilocaine than in the sum of the spectra of the two components. The vibrational frequencies of both groups involved in hydrogen bonding are expected to soften as the hydrogen bond becomes stronger.

Solution Infrared data

The active components separately as well as their eutectic mixture were dissolved in $CCl_4$ and transferred to a solution infrared cell. The solution infrared spectra of the eutectic mixture and of the sum of the spectra of lidocaine and prilocaine are shown in Figure 4.13.

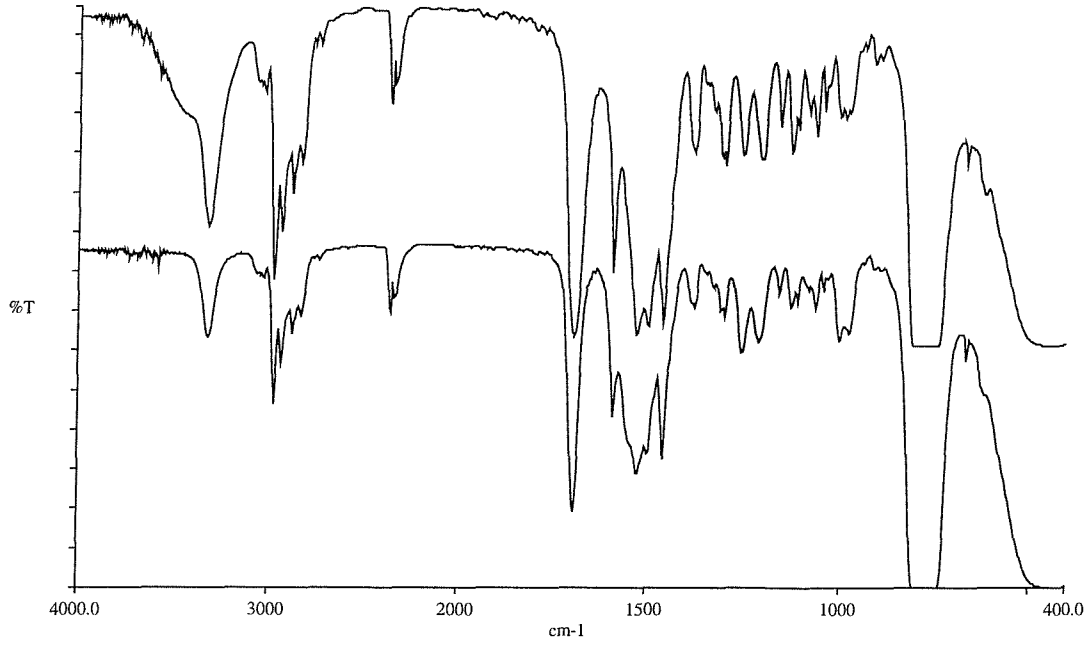


**Figure 4.13** Absorption Infrared solution spectra of the eutectic mixture of lidocaine and prilocaine (top spectrum) and the sum of the spectra of lidocaine and prilocaine (bottom spectrum). All spectra were recorded in $CCl_4$.

When comparing the sum of the solution spectra of lidocaine and prilocaine with that of the eutectic in solution, there are a few marked differences. The largest difference is found in the NH stretching region. Both lidocaine and prilocaine in $CCl_4$ have a relatively intense band around 3319 $cm^{-1}$. The eutectic mixture of the two, on the other hand, shows considerable band broadening at the high frequency side of the 3318 $cm^{-1}$ band. This could be an indication of hydrogen bonding between lidocaine and prilocaine. There are other differences between the two spectra in Figure 4.13, but since we are most interested in studying hydrogen bonding, these have been ignored at this stage. The differences in the NH and carbonyl stretching frequencies between the different spectra are summarised in Table 4.9.

**Table 4.9** Comparison of the sum of the solution infrared spectra of lidocaine and prilocaine with that of the eutectic mixture. s: strong, w: weak, br: broad

| Sum spectra lidocaine and prilocaine | Eutectic mixture | Attributed to |
|---|---|---|
| - | 3555w br | Hydrogen bonded NH stretching |
| 3319s | 3318s | NH stretching |
| 3289w br | 3277w br | NH stretching |
| 1693 | 1693 broader and less intense | C=O |

Compared with the stretching frequencies obtained from the absorption and ATR infrared spectra, the frequencies from these solution infrared studies lie much higher. As these compounds go into solution in a non polar solvent, their vibrational frequencies will shift more towards values of the free molecule.
The shift of the NH stretching frequency towards lower frequencies in combination with the band broadening suggests that there is hydrogen bonding in the eutectic mixture.

### Raman Data

FT-Raman spectra were recorded of the eutectic mixture of lidocaine and prilocaine and of the separate components. A Raman hot cell was used to record the spectra of the compounds in the melt phase.
The Raman spectra of the eutectic mixture of lidocaine and prilocaine and the sum of the spectra of lidocaine and prilocaine are compared in Figure 4.14.

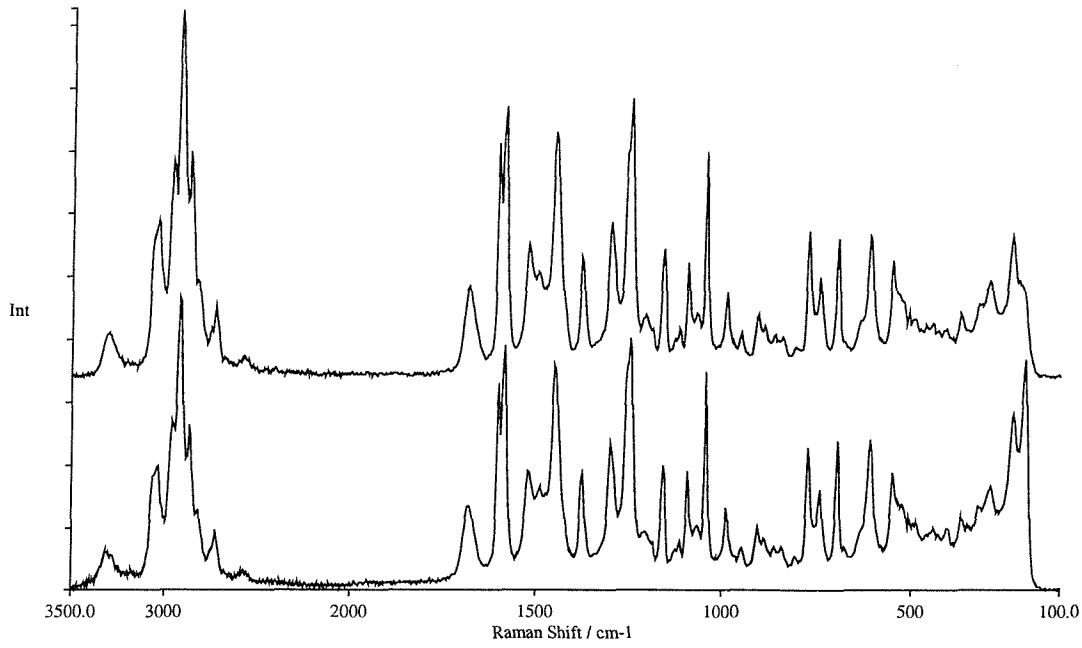


**Figure 4.14** FT-Raman spectra of the eutectic mixture of lidocaine and prilocaine (top spectrum) and the sum of the spectra of lidocaine and prilocaine (bottom spectrum). All spectra were recorded above the melting point of the components.

Curvefitting the NH and carbonyl stretching bands reveals the presence of two underlying bands for both groups. In the eutectic mixture, the bands have shifted to higher frequencies in comparison with the sum of the spectra of lidocaine and prilocaine. This would suggest that there is less hydrogen bonding in the eutectic mixture compared with the separate compounds. These shifts are summarised in Table 4.10.

**Table 4.10** Comparison of the sum of the Raman spectra of lidocaine and prilocaine with the spectrum of the eutectic mixture. br: broad, w: weak

| Sum spectra lidocaine and prilocaine vibrational frequencies ($cm^{-1}$) | Eutectic mixture vibrational frequencies ($cm^{-1}$) | Attributed to |
|---|---|---|
| 3313 | 3315 | NH stretching |
| 3227br w | 3263br | NH stretching |
| 1689 | 1690 | C=O |
| 1668w | 1670w | C=O |

Even though the spectra look very similar, other differences are visible. For example, the Raman data shows a shift of 4 $cm^{-1}$ from 1492 $cm^{-1}$ in the sum of the spectra of lidocaine and prilocaine to 1496 $cm^{-1}$ in the spectrum of the eutectic mixture. The 1492 $cm^{-1}$ band is more prominent in lidocaine than in prilocaine.

The fact that there are differences between the spectra suggests that there are some kind of interactions.

It is surprising however that the infrared data would suggest increased hydrogen bonding in the eutectic mixture, whereas the Raman data would suggest less hydrogen bonding in comparison with the sum of the spectra of the two components lidocaine and prilocaine.

The Raman data suffers from the same problem that the NH stretching is weak. This makes it more difficult to observe changes in this region.

One must be careful when drawing conclusions from these vibrational spectra. There seems to be a contradiction in the results from the Raman data compared with the results from the infrared data. However, the infrared extinction coefficient is very sensitive to conformational changes and other influences, whereas the Raman scattering cross section remains fairly unchanged. Therefore when the evidence of hydrogen bonding would have been observed in the Raman spectra, it would have been more significant. The increased high frequency background, observed in the infrared spectra could be an indication of hydrogen bonding, but it will be a very weak effect. This explains why this apparently hydrogen bonding was not observed in all the absorption spectra recorded of the eutectic mixture.

Since these results dealing with the possibility of interactions between lidocaine and prilocaine were inconclusive, it was decided to study the components in their crystalline state. Evidence for hydrogen bonding should be more clearly seen in the crystalline state.

### ATR data from the crystalline materials

In this experiment, ATR spectra were recorded from simple mixtures of crystalline lidocaine and prilocaine. At the start of the experiment, some solid prilocaine was transferred onto the diamond crystal, after which lidocaine powder was added. As the eutectic mixture started to form, the infrared spectra were recorded. After each spectrum, more lidocaine was added and a new spectrum was recorded.

The ATR spectra of prilocaine, lidocaine, the mixtures (after adding more and more lidocaine powder) and the eutectic mixture are shown in Figures 4.15 and 4.16. For clarity, the spectra have been split into two separate spectra. A first spectrum focuses onto the high frequency region that contains CH and NH stretching frequencies. The second set of spectra shows the fingerprint region.

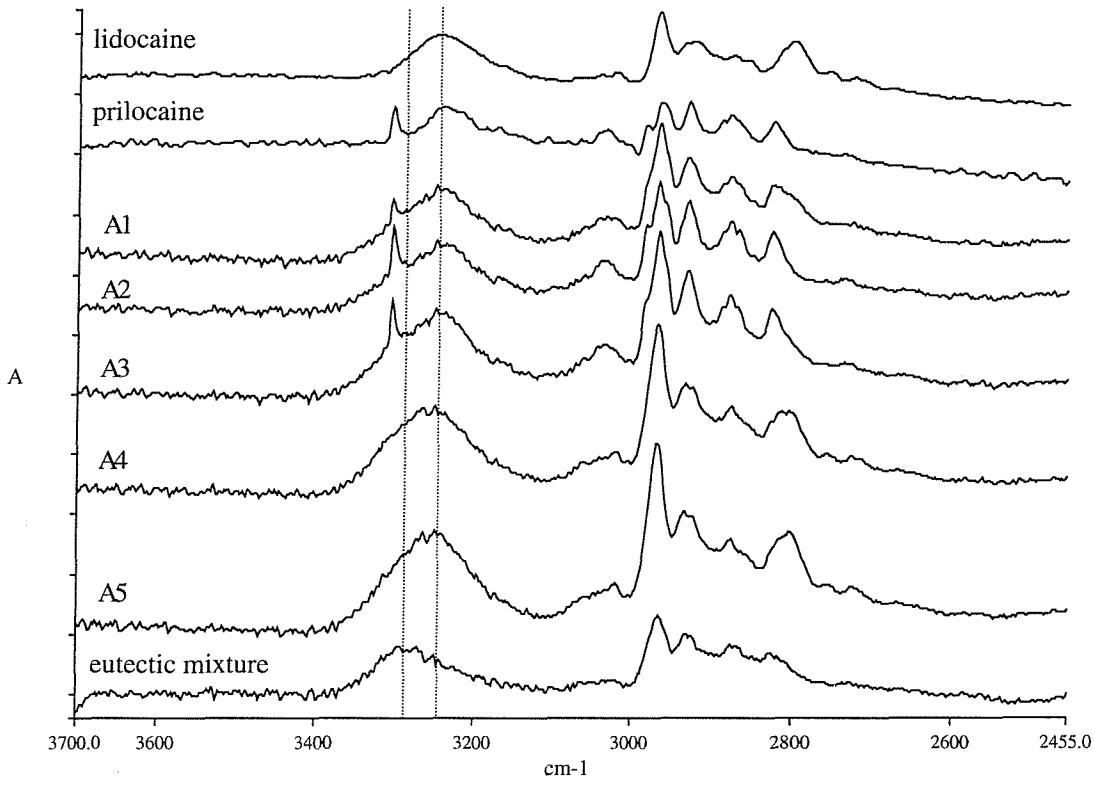


**Figure 4.15** ATR spectra of lidocaine, prilocaine, their eutectic mixture and 'other mixtures' A1 to A5. The spectra are displayed in absorbance units. From spectra A1 to A5, more and more lidocaine was added to prilocaine powder on the ATR crystal. The band of particular interest is the NH stretching around 3250 $cm^{-1}$.

In addition, the fingerprint region is shown in the following set of spectra.

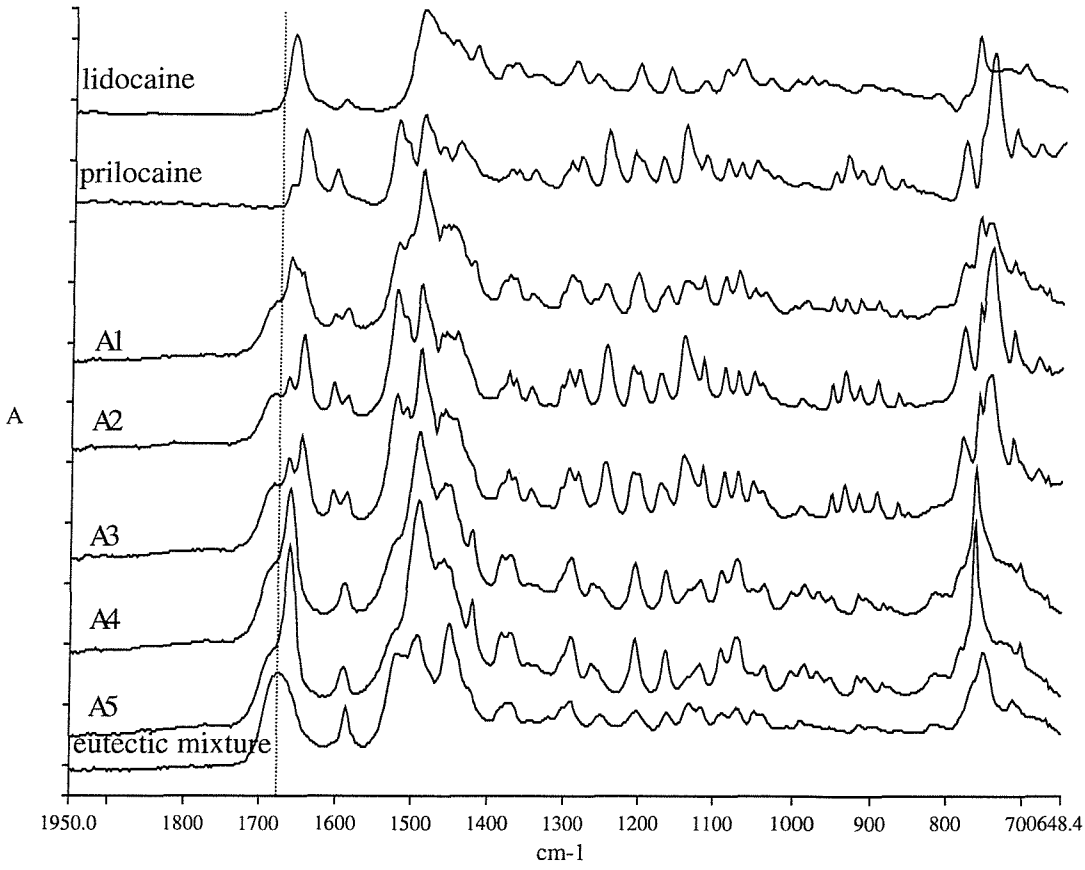


**Figure 4.16** ATR spectra of lidocaine, prilocaine, their eutectic mixture and 'other mixtures' A1 to A5. From spectra A1 to A5, more and more lidocaine was added to prilocaine powder on the ATR crystal. The band of particular interest is the carbonyl stretching around 1680 $cm^{-1}$.

From these ATR spectra it is clear that there are interactions between lidocaine and prilocaine as they form the eutectic mixture. As we are most interested in the changes in hydrogen bonding between the different infrared spectra, these specific bands were curvefitted. The shifts of the ATR bands that are sensitive to hydrogen bonding on adding more and more crystalline lidocaine to the mixture, are displayed in Table 4.11.

**Table 4.11** Changes in NH and carbonyl stretching ATR frequencies as crystalline lidocaine is added to crystalline prilocaine (spectra A1 to A5). The figures for pure lidocaine, prilocaine and the eutectic mixture are added as a reference. s: strong, w: weak, br: broad, sh: shoulder

| Spectrum | NH stretching frequencies ($cm^{-1}$) | | Carbonyl stretching frequencies ($cm^{-1}$) | | |
|---|---|---|---|---|---|
| Lidocaine | - | 3242br | - | 1662 | 1650 |
| Prilocaine | 3305s | 3235br | - | 1666 | 1645 |
| A1 | 3304s | 3248br | 1693 | 1659 | - |
| A2 | 3303s | 3246br | 1686 | 1665 | 1646 |
| A3 | 3304s | 3251br | 1686 | 1665 | 1647 |
| A4 | 3309sh | 3255br | 1689 | 1662 | 1660w |
| A5 | - | 3254br | 1688 | 1662 | - |
| Eutectic mixture (melt) | | (3309w+3278) | 1683 | 1659 | - |

If there were no interactions between lidocaine and prilocaine, the spectra obtained by simply adding lidocaine powder to prilocaine powder (A1 to A5) should be equal to the sum of the solid state spectra of lidocaine and prilocaine. As the two solids are added together, the eutectic mixture forms. Since the experiment was performed at room temperature, it is likely that the eutectic mixture was melted. Even so, it is clear that in spectra A1 to A5, NH stretching frequencies are found that are in between those of lidocaine and prilocaine on one hand and the eutectic mixture on the other.
It is difficult to draw conclusions from the two lower frequency carbonyl stretching frequencies, since their value lies in between those from lidocaine and prilocaine.
The higher carbonyl stretching frequency (~ 1686 $cm^{-1}$) in the 'mixtures' is higher than that in the eutectic mixture. Solubility of a lidocaine or prilocaine into their eutectic mixture is suspected. The values for the 'free' carbonyls (from solution infrared data) are 1690 $cm^{-1}$ and 1694 $cm^{-1}$ respectively.
The shifts in stretching frequencies of the NH and carbonyl groups are not linear with the amount added in this experiment, probably because on adding lidocaine to the prilocaine on the diamond crystal it was impossible to estimate to what extent any of the components were being probed.
To study the possibility of solubility of lidocaine and prilocaine in the eutectic mixture, similar experiments were performed by placing the eutectic mixture on the

diamond crystal and adding prilocaine or lidocaine in the crystalline form. Again, after each addition an ATR spectrum was recorded.

The spectra obtained after adding amounts of prilocaine to the eutectic mixture of lidocaine and prilocaine are shown in Figure 4.17.

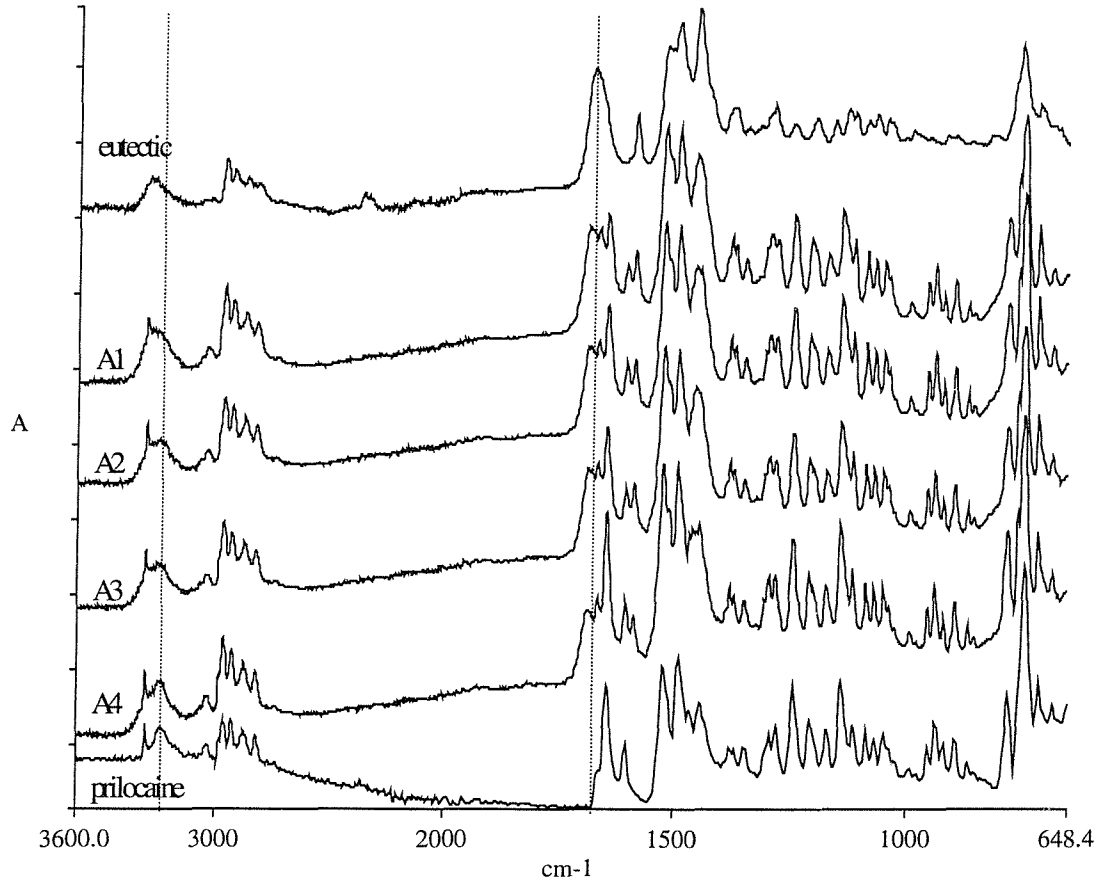


**Figure 4.17** ATR spectra of prilocaine, the eutectic mixture and 'other mixtures' A1 to A4. Moving downwards from spectra A1 to A4, more and more prilocaine powder was added to the eutectic mixture of lidocaine and prilocaine on the ATR crystal. The bands of particular interest are the NH (around 3300 $cm^{-1}$) and carbonyl stretching (around 1680 $cm^{-1}$).

The regions of interest, the NH and carbonyl stretching regions, were curve fitted and the shifts from the frequencies from the pure materials are displayed in Table 4.12.

**Table 4.12** Changes in NH and carbonyl stretching ATR frequencies as crystalline prilocaine is added to the eutectic mixture of lidocaine and prilocaine (spectra recorded are A1 to A4). The figures for pure prilocaine and the eutectic mixture are added as a reference. s: strong, br: broad

| Spectrum | NH stretching frequencies ($cm^{-1}$) | | Carbonyl stretching frequencies ($cm^{-1}$) | | |
|---|---|---|---|---|---|
| Eutectic mixture | - | (3293+3244w)br | 1684 | 1663 | - |
| A1 | 3303 | 3269br | 1686 | 1664 | 1646 |
| A2 | 3302 | 3254br | 1686 | 1665 | 1646 |
| A3 | 3303 | 3256br | 1686 | 1665 | 1646 |
| A4 | 3303 | 3246br | 1688 | 1665 | 1646 |
| Prilocaine | 3305s | 3235br | | 1666 | 1645 |

On adding the solid prilocaine to the eutectic mixture, we notice that a high frequency carbonyl stretching appears. This carbonyl group is not hydrogen bonded and has a frequency even higher than in its melt phase (which lies at 1684 $cm^{-1}$), which would suggest that the compound is in solution. In the NH stretching region, we find 1 sharp peak around 3303, which is only a little bit lower than in the solid material, but the second NH stretching frequency (around 3255 $cm^{-1}$), which is broad, has shifted towards higher values in comparison with the solid prilocaine. This frequency is lower than that of the eutectic mixture.

The shift in the highest carbonyl stretching frequency suggests that prilocaine has dissolved into the eutectic mixture. Unfortunately, it is unclear to whether the NH stretching frequency shift supports this idea.

Also it seems that the carbonyl stretching frequency remains fairly constant whereas the NH stretching frequency moves more up and down.

In a similar experiment crystalline lidocaine was added to the eutectic mixture and subsequently the ATR spectra were recorded. The spectra are shown in Figure 4.18.

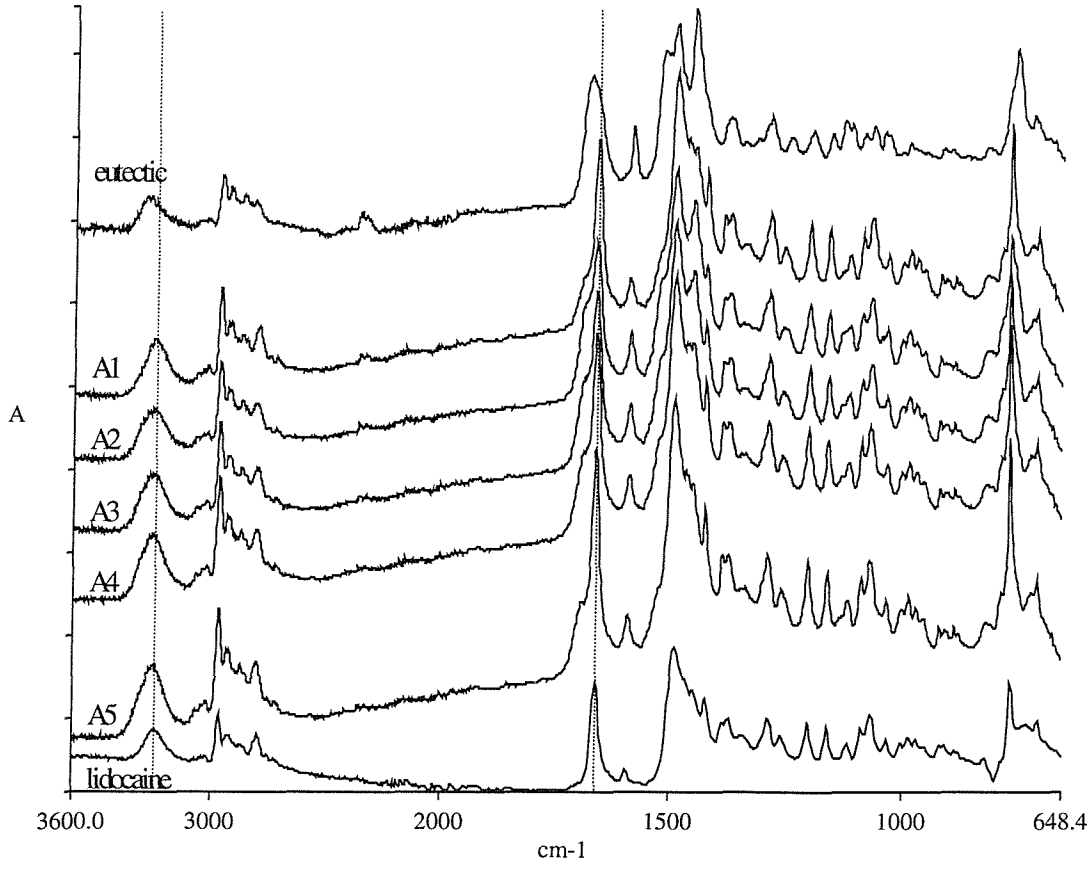


**Figure 4.18** ATR spectra of lidocaine, the eutectic mixture and 'other mixtures' A1 to A5. Moving downwards from spectra A1 to A5, more and more lidocaine powder was added to the eutectic mixture of lidocaine and prilocaine on the ATR crystal. The bands of particular interest are the NH (around 3300 $cm^{-1}$) and carbonyl stretching (around 1680 $cm^{-1}$).

The following shifts in NH and carbonyl stretching frequencies were observed. They are summarised in Table 4.13.

**Table 4.13** Changes in NH and carbonyl stretching ATR frequencies as crystalline lidocaine is added to the eutectic mixture of lidocaine and prilocaine (spectra recorded are A1 to A5). The figures for pure prilocaine and the eutectic mixture are added as a reference. br: broad

| Spectrum | NH stretching frequencies ($cm^{-1}$) | Carbonyl stretching frequencies ($cm^{-1}$) | |
|---|---|---|---|
| Eutectic mixture | 3293br, 3244br | 1684 | 1663 |
| A1 | 3250 | 1692 | 1662 |
| A2 | 3259 | 1689 | 1663 |
| A3 | 3259 | 1690 | 1662 |
| A4 | 3258 | 1691 | 1662 |
| A5 | 3257 | 1694 | 1662 |
| Lidocaine | 3242br | | 1662+1650 |

On adding lidocaine powder to the eutectic mixture of lidocaine and prilocaine, higher NH stretching frequencies are observed, in comparison with that of crystalline lidocaine. The frequencies are lower than those from the eutectic mixture.

The higher carbonyl frequency on the other hand shifts towards values that are higher then the infrared stretching frequency observed when lidocaine was dissolved in a non polar solvent. This is very odd. The lower carbonyl stretching frequency remains practically unchanged.

It seems that the NH and carbonyl stretching frequencies are not always coupled.

When comparing the highest carbonyl stretching frequencies from Tables 4.11 and 4.12, we notice that the values, obtained from adding lidocaine powder to prilocaine powder are similar to those of prilocaine in solution in the eutectic mixture. This is what we would expect

The fact that both the carbonyl and NH stretching frequencies in these 'solution' spectra are lower than those obtained from the solution infrared spectra recorded in a non polar solvent suggests that some sort of interactions between prilocaine and the eutectic mixture are taking place.

## 4.5 *Interactions between actives and excipients in the local anaesthetic system*

To study the possibility of interactions between the eutectic mixture of lidocaine and prilocaine and the aqueous solution of block copolymers Poloxamer F127 and F68, Raman spectra were recorded using a Raman microscope. As the only interactions to be expected are hydrogen bonding or weaker van der Waals interactions, vibrational spectroscopy provides a promising method for studying these interactions.

### Raman mapping of eutectic mixture-aqueous solution of block copolymers interface

Several mapping experiments using the Raman microscope were performed. The aim was to perform a mapping of the interface between the eutectic mixture and the aqueous solution of block copolymers. The microscope was in its confocal mode. A few droplets of aqueous solution of block copolymers were transferred into a special designed sample holder, after which a few droplets of the eutectic mixture of lidocaine and prilocaine were added. A very clear boundary between the two phases occurred, which made it possible to study the interface. A picture of the interface is shown in Figure 4.19.

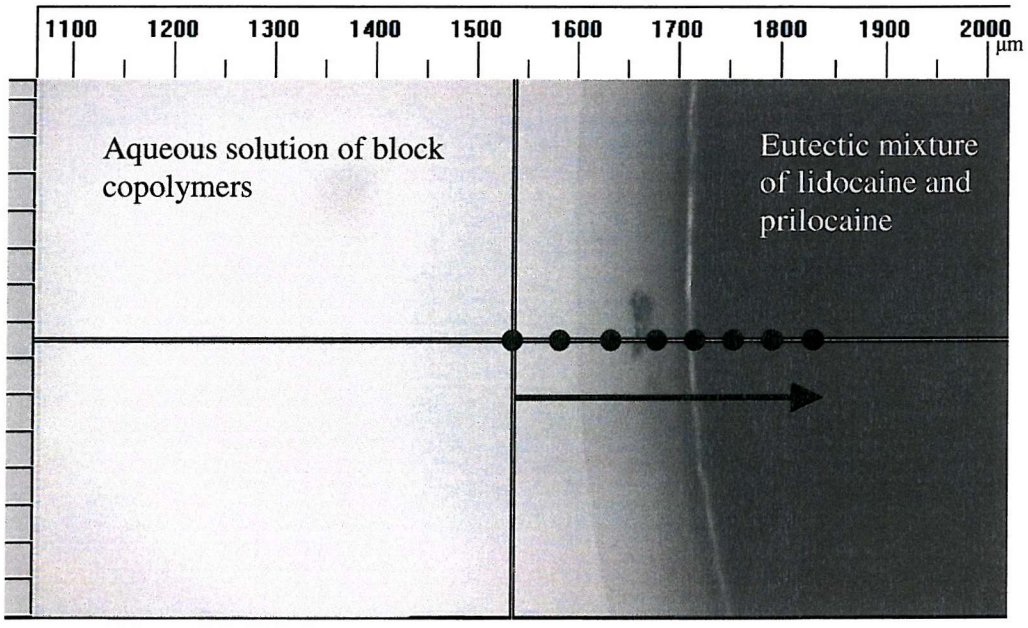


**Figure 4.19** Picture of the interface between the aqueous solution of block copolymers and the eutectic mixture of lidocaine and prilocaine. The line shows the direction of the mapping and the dots show the approximate positions where a Raman spectrum was recorded. The unit of the scale is in micrometers.

Since no variable temperature microscope stage was available to us, some improvisation was needed. A makeshift cold stage was made by using a Peltier element, which was cooled by attaching a metal block with flowing water to it. The temperature was controlled by using a thermistor coupled to a controller unit. To ensure good thermal contact, heat sink compound was used. The spectra were recorded at 16°C.

The mapping was performed so that every 70 μm a Raman spectrum was recorded over a distance of 500 μm. For every spectrum 10 scans were co-added, with each scan taking about 20 minutes collection time. With this experimental set-up, a typical mapping takes about 24 hours.

Unfortunately, the spectra are of poor quality due to the high water content and low laser power (20mW). Nevertheless it has been possible to discover some changes in the spectra.

In Figure 4.20, the different spectra are presented as the laser scans across the interface. For reference, the spectra of the eutectic mixture and that of the aqueous solution of block copolymers are included as well.

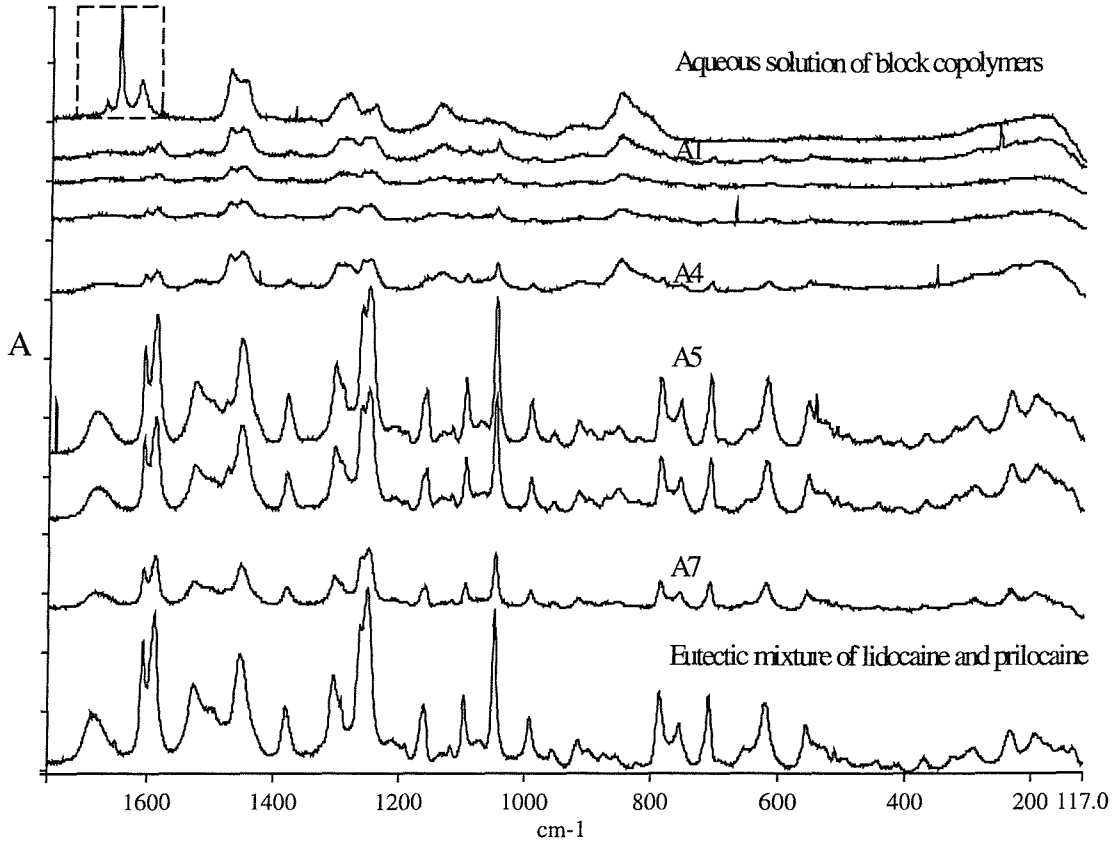


**Figure 4.20** Raman spectra of the aqueous solution of block copolymers (top spectrum), the eutectic mixture of lidocaine and prilocaine (bottom spectrum) and in between the Raman spectra obtained by mapping the boundary between the two. As one moves down in the spectra, a change of focal point from the aqueous solution towards the eutectic mixture is performed. As a sudden change in the spectra is observed between A4 and A5, the boundary between the two phases is expected to be found in between. The band of particular interest is the carbonyl stretching around 1680 $cm^{-1}$. The bands in the top spectrum that are boxed in should be neglected since they are spurious.

There are three regions in the spectra where we would expect changes in vibrational frequencies if there were any interactions between the two phases. The first region is that of the NH stretching frequencies from the eutectic mixture, but this region is overloaded by the water OH stretching bands. The second region of interest is that of the C-O stretching frequencies from the aqueous solution of block copolymers around 1140 $cm^{-1}$. Unfortunately, the spectra were too noisy in this region to perform any curvefittting. The last region of interest is that of the carbonyl stretching frequencies from the eutectic mixture around 1680 $cm^{-1}$. The peaks under this particular band were curvefitted. The frequencies are summarised in Table 4.14.

**Table 4.14** Changes observed in the Raman spectra when a mapping is performed going from the aqueous solution of block copolymers into the eutectic mixture. w:weak

| Spectrum | carbonyl stretching frequency ($cm^{-1}$) | |
|---|---|---|
| A1 | 1673w | |
| A4 | 1677w | |
| A5 | 1690 | 1672 |
| A7 | 1686 | 1664 |
| Eutectic mixture | 1690 | 1677 |

From the frequencies displayed in Table 4.14, some shifts in the carbonyl stretching frequencies have been observed. In spectrum A1, it seems that hydrogen bonding has increased, compared with the carbonyl frequency in the eutectic mixture. In the following spectra (A4-A7), it decreases again (shifts of the carbonyl frequency towards higher values). Why in spectrum A7 (now we are clearly probing the eutectic) the hydrogen bonding appears to be stronger again (lower frequencies) is unclear. Since it was impossible to comment on the C-O stretching frequency, these results with regards to the possibility of interactions between the eutectic mixture of lidocaine and prilocaine and the aqueous solution of block copolymers are inconclusive.

## *4.6 Influence of temperature on the vibrational spectra of the formulation and its components*

The aim of this subsection was to study the structural changes in the local anaesthetic block copolymer system induced by varying the temperature. Infrared and Raman spectroscopy are very good techniques to study structural changes hence spectra of the block copolymer system containing local anaesthetics and its components separately were recorded at different temperatures.

Raman spectroscopy is a good technique to study conformational changes in molecules. There are several regions in the spectrum that are particularly sensitive to conformational changes. A first region expands from 1200 $cm^{-1}$ to 1000 $cm^{-1}$ and contains the C-C and C-O stretching frequencies and the $CH_2$ wagging modes.

Another important region in this study is that of the CH stretching frequencies, between 3000 $cm^{-1}$ and 2800 $cm^{-1}$.

This study into conformation changes in the block copolymer system with variable temperature was focussed mainly on those two regions in the vibrational spectrum.

## Influence of temperature on the vibrational spectra of the block copolymers

When heated, these block copolymers in aqueous solution start to form micelles. In forming those micelles, some conformation changes have to take place. Therefore some variable temperature Raman spectra were recorded from both the poloxamer alone and the mixture of the two poloxamers F127 and F68 in aqueous solution. The variable FT-Raman spectra of poloxamer F127 are displayed in Figures 4.21 and 4.22. For clarification, the Raman spectra were split up in two regions, the CH stretching region and the fingerprint region.

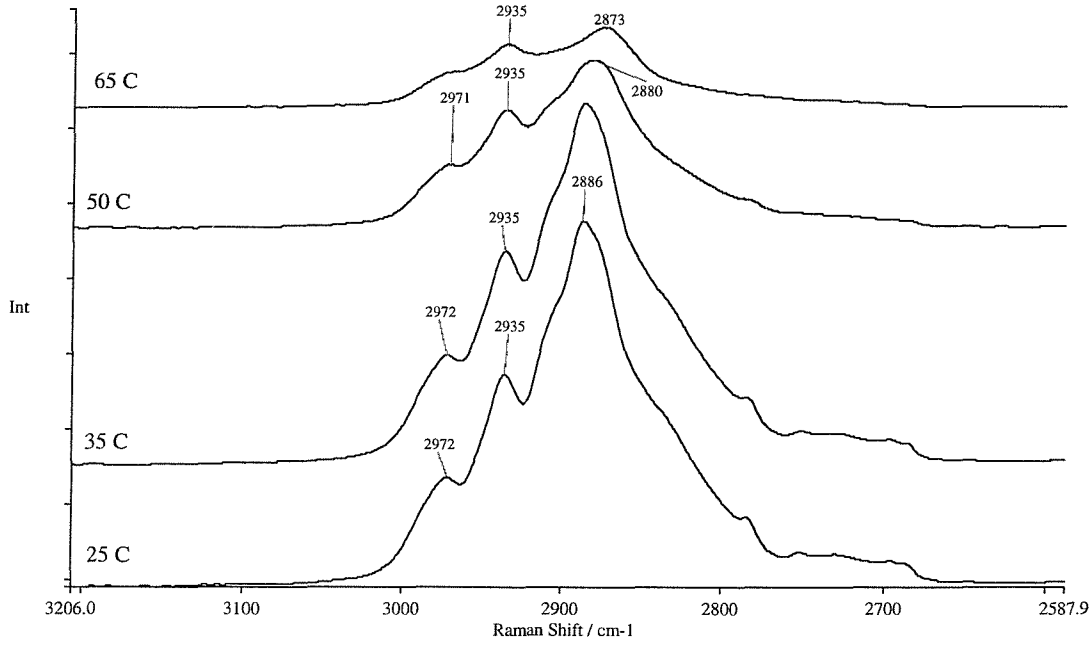


**Figure 4.21** Variable temperature FT-Raman spectra of poloxamer F127.

The melting point of poloxamer F127 lies above 50°C, but we see clear changes in the spectra already at the lower temperatures. The changes in the spectra with temperature are presented in Table 4.15.

**Table 4.15** Tentative assignment of the changes in vibrational frequencies in the variable temperature Raman spectra of poloxamer F127s: symmetric, as: asymmetric, ν: stretching

| Changes in the spectra on heating | | Tentative assignment |
|---|---|---|
| Shift towards lower frequencies | Relative Intensity decreases | |
| 2972 | | 2972 as $\nu CH_3$ |
| 2880 | 2880/2935 | 2935 s $\nu CH_3$ |
| | | 2880 as $\nu CH_2$ |
| 2850 | 2850/2935 | 2850 s $\nu CH_2$ |

The relative intensities of the following bands 2880 $cm^{-1}$ / 2935 $cm^{-1}$ and 2850 $cm^{-1}$ / 2935 $cm^{-1}$ are so-called order/disorder parameters. As the disorder increases these ratios of intensities will decrease. The effect is more pronounced for a poloxamer containing a higher polypropylene-oxide content. Guo et al. showed the effect of heating on the Raman spectra of a range of poloxamers [3]. For the poloxamers containing a high percentage of polypropylene-oxide, these ratios of intensities decreased by a large amount until the spectra appeared almost identical to that of polypropylene-oxide.

In addition to the CH stretching region many changes in conformation can be followed in the fingerprint region of our Raman spectra. The FT-Raman spectra of poloxamer F127 at varying temperatures is shown in Figure 4.22.

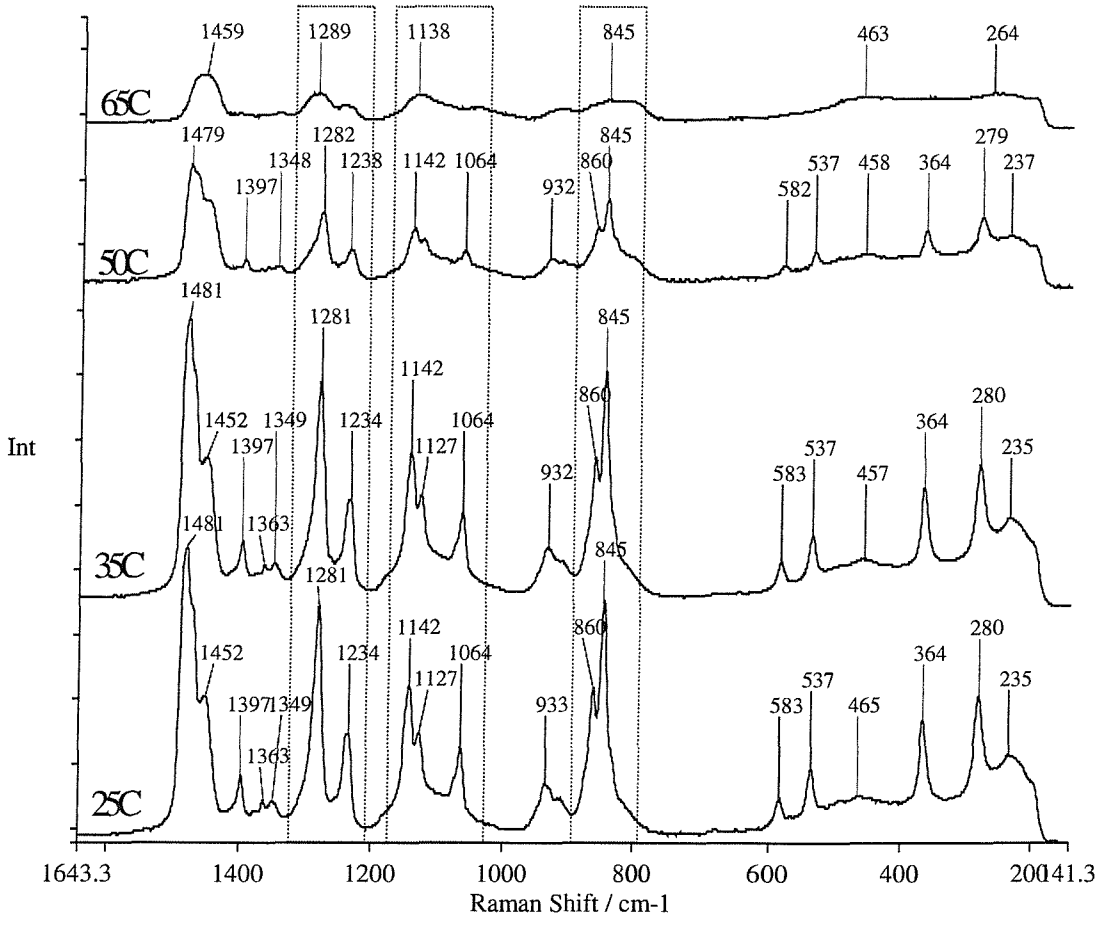


**Figure 4.22** Variable temperature FT-Raman spectra of poloxamer F127. The regions in the spectrum of particular interest are boxed in.

The vibrational frequencies of importance and their tentative assignments are displayed in Table 4.16.

**Table 4.16** Tentative assignment of the changes in vibrational frequencies in the variable temperature Raman spectra of poloxamer F127. s: symmetric, as: asymmetric, ν : stretching

| Wavenumber ($cm^{-1}$) | Relative intensity changes | Assignment |
|---|---|---|
| 860 | 845/860 > 1 | methyl rocking |
| 845 | | methylene rocking |
| 1142 | | νC-O |
| 1127 | | νC-C s trans |
| 1064 | | νC-C as trans |
| 1090 | | νC-C gauche |
| 1281, 1234, 1064, 845 | | Helical structure |

Within the polymer chains it is possible to assign different bands to either trans or gauche conformations. Bands typical for a trans conformation are the 1062 $cm^{-1}$ and 1127 $cm^{-1}$ C-C stretching frequencies. The 1090 $cm^{-1}$ band is typical for the gauche segments. In addition, the 1284 $cm^{-1}$ band has been assigned to the out-of-phase $CH_2$ bending motion of trans conformers, while 1350 $cm^{-1}$ and 1300 $cm^{-1}$ are typical for the bending motions of gauche conformers. At low temperatures, a shoulder at the high frequency side of the 1281 $cm^{-1}$ band is present. At higher temperatures the two bands 'melt' together, as the gauche conformation increases. This is in accordance with the literature from which it is known that on melting polyethyleneoxide, the ethyleneoxide configuration changes from a trans-gauche-trans sequence to a gauche-gauche-trans sequence [3].

The thermodynamically stable structure of polyethyleneoxide is a 7/2 helix structure. It takes a planar zigzag structure in the molten state or in aqueous solution.

## Influence of temperature on the vibrational spectra of the aqueous solution of block copolymers

The same principle on conformation changes for the crystalline block copolymers, applies to an aqueous solution of the poloxamers. The variable temperature FT-Raman spectra are presented in Figures 4.23 and 4.24.

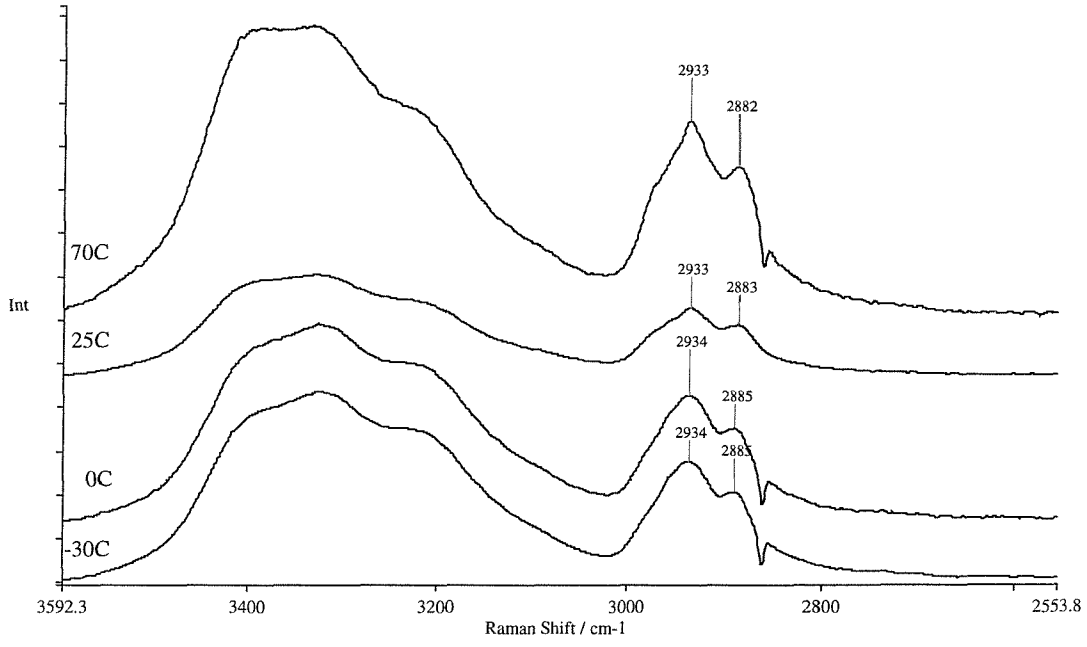


**Figure 4.23** Variable temperature FT-Raman spectra of a mixture of the two poloxamers F127 and F68 in aqueous solution.

A first thing that catches the eye is the broad bands at high frequency. This is due to the different states of water in this system [16]. Deconvolution of the bands under this broad area would allow us to assign the different vibrational frequencies to the different types of water. As the temperature increases, the structure of the water will change as micellization starts to set in.

Similarly to the temperature variations on the pure poloxamer, some changes in the CH stretching region can be assigned to conformational changes in the polymers. The changes are displayed in Table 4.17.

**Table 4.17** Tentative assignment of the changes in vibrational frequencies and intensities in the Raman spectra of the aqueous solution of block copolymers F127 and F68 with varying temperature. s: symmetric, as: asymmetric, ν : stretching

| Changes in the spectra with heating | | |
|---|---|---|
| Shift towards lower frequencies ($cm^{-1}$) | Relative Intensity increases | Tentative assignment |
| 2934 | | 2934 is $\nu CH_3$ s |
| 2885 | 2934/ 2880 | 2880 is $\nu CH_2$ as |
| 2850 | 2934/ 2850 | 2850 is $\nu CH_2$ s |

In aqueous solution the relative intensities of the bands 2934 $cm^{-1}$/ 2880 $cm^{-1}$ and 2934 $cm^{-1}$/ 2850 $cm^{-1}$ are already larger than 1 at room temperature. This indicates that there is more disorder in comparison with the pure poloxamer. Even at -30°C the structure is not a very ordered one.

When heating the aqueous solution, the methyl and methylene stretching frequencies shift towards lower values. When deconvoluting the bands, it is expected that the methyl group displays the largest shift in frequency. This is due to the dehydration of the more hydrophobic propyleneoxide groups as micellization takes place. Dehydration of the more hydrophilic ethyleneoxide group will occur to a lesser extend. The largest shift in stretching frequencies towards lower wavenumbers can be seen between 0°C and 25°C. In accordance with the literature [18], this is where the micellization temperature lies.

In Figure 4.24, the variable temperature Raman spectra of the poloxamer in aqueous solution in the fingerprint region are displayed.

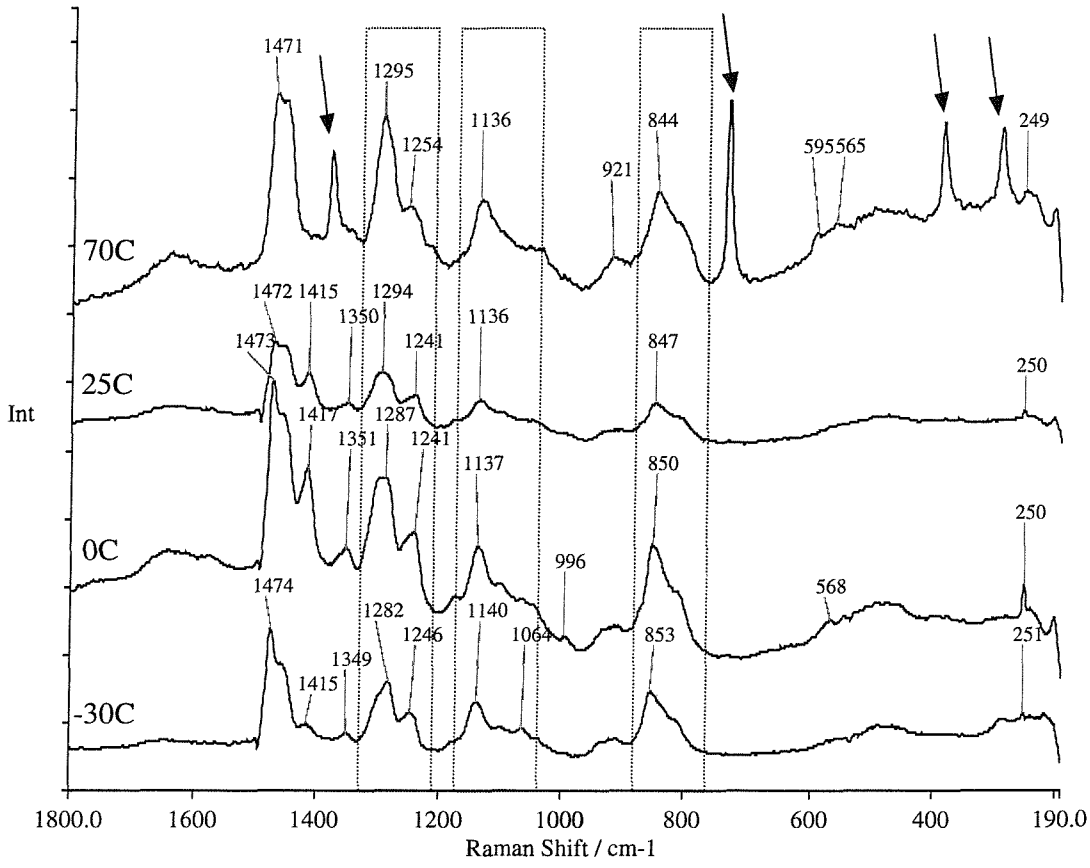


**Figure 4.24** Variable temperature FT-Raman spectra of poloxamers F127 and F68 in aqueous solution. The regions in the spectrum of particular interest are boxed in. The arrows indicate bands that are spurious.

As with the poloxamer, a similar tentative assignment was done on the vibrational frequencies of the mixture of poloxamers in aqueous solution. The results are shown in Table 4.18.

**Table 4.18** Tentative assignment of the changes in vibrational frequencies and intensities in the Raman spectra of the aqueous solution of block copolymers F127 and F68 with varying temperature. br: broad band. ν : stretching

| Wavenumber ($cm^{-1}$) | Relative intensity changes | Assignment |
|---|---|---|
| 853 br | | Methyl and methylene rocking |
| 1064 | | νC-C trans |
| 1096 | | νC-C gauche |
| 1140 | | νC-O |
| 1137 br | | νC-C and νC-O |
| 1250br, 1289br | 1295 / 1250 | $CH_2$ twist disorder parameter |

As expected, we were not able to assign as many bands as in the spectrum of the poloxamer alone, but when the two spectra are compared it is clear that the bands have shifted and broadened.

As was mentioned before, the bands that are typical for a trans conformation are the 1062 $cm^{-1}$ and 1127 $cm^{-1}$ C-C stretching frequencies. The 1090 $cm^{-1}$ band is typical for the gauche segments. In comparison with the variable temperature spectra of the pure poloxamers, the clear peaks at 1064 $cm^{-1}$ and 1127 $cm^{-1}$ have vanished.

The spectrum recorded at -30°C shows the 1064 $cm^{-1}$ band, typical of a trans conformation.

There is less of a structure in these spectra in aqueous solution, which is what we would expect.

## Influence of temperature on the vibrational spectra of the formulation containing local anaesthetics

As with the experiments with the aqueous solution of block copolymers, FT-Raman spectra were recorded at different temperatures, ranging from -90°C to 70°C.

*FT-Raman data*

On heating the formulation from -90°C to 70°C several changes in the FT-Raman spectra were observed. Unfortunately since the formulations are in aqueous solution, the most interesting bands with regards to hydrogen bonding are hidden under the water bands. So the observed changes can only be explained in terms of conformation

changes in the block copolymer chains. The FT-Raman spectra of the formulations at different temperatures are displayed in Figures 4.25 and 4.26.

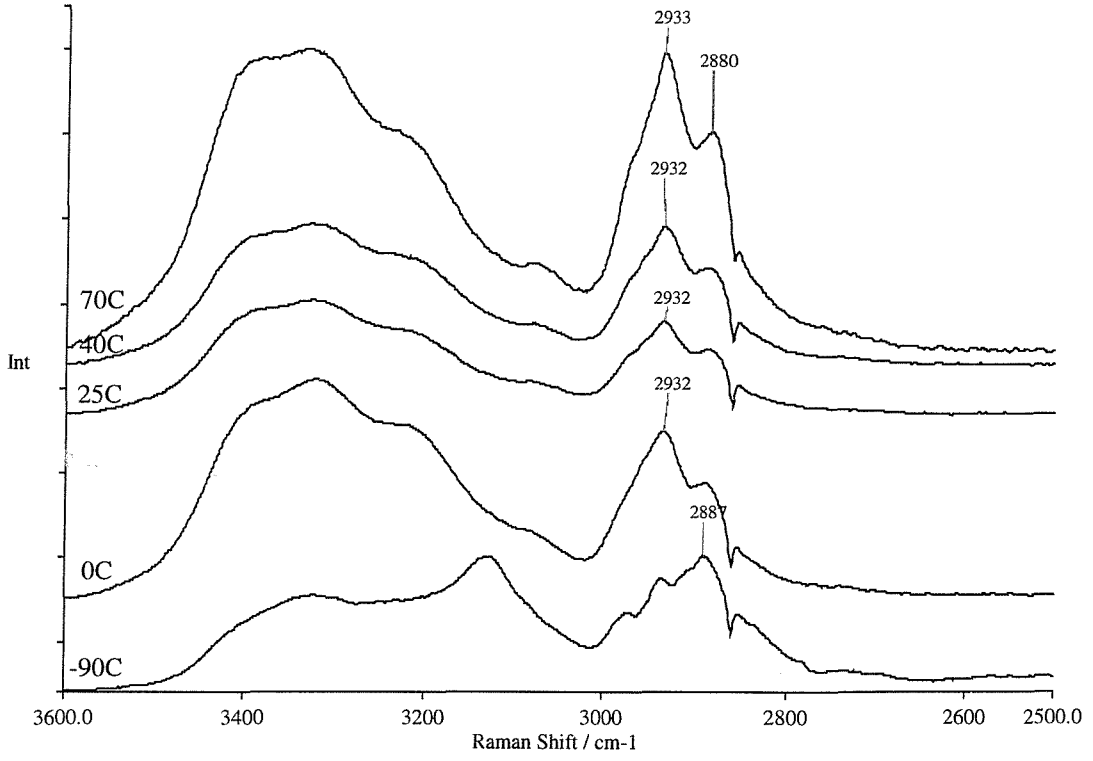


**Figure 4.25** Variable temperature FT-Raman spectra of the formulation containing local anaesthetics.

From these spectra it is clear that changes in the conformation of the block copolymer occur on heating. This is observed in the changes in relative intensities of the CH stretching bands (region below 3000 $cm^{-1}$). In addition, information on the different states of bound and 'free' water can be obtained from the underlying bands in the 3500 $cm^{-1}$ to 3150 $cm^{-1}$ region.

The changes observed in the spectra upon heating are summarised in Table 4.19.

**Table 4.19** Tentative assignment of the changes in vibrational frequencies and intensities in the Raman spectra of the formulation containing local anaesthetics with varying temperature. s: symmetric, as: asymmetric, ν : stretching

| Changes in the spectra on heating | | |
|---|---|---|
| Shift towards lower frequencies ($cm^{-1}$) | Relative Intensity decreases | Tentative assignment |
| 2972 | | 2972 is $\nu CH_3$ as |
| 2880 | 2880 / 2935 | 2935 is $\nu CH_3$ s |
| | | 2880 is $\nu CH_2$ as |
| 2850 | 2850 / 2935 | 2850 is $\nu CH_2$ s |

The variable temperature FT-Raman spectra of the formulation in the fingerprint region are shown in Figure 4.26.

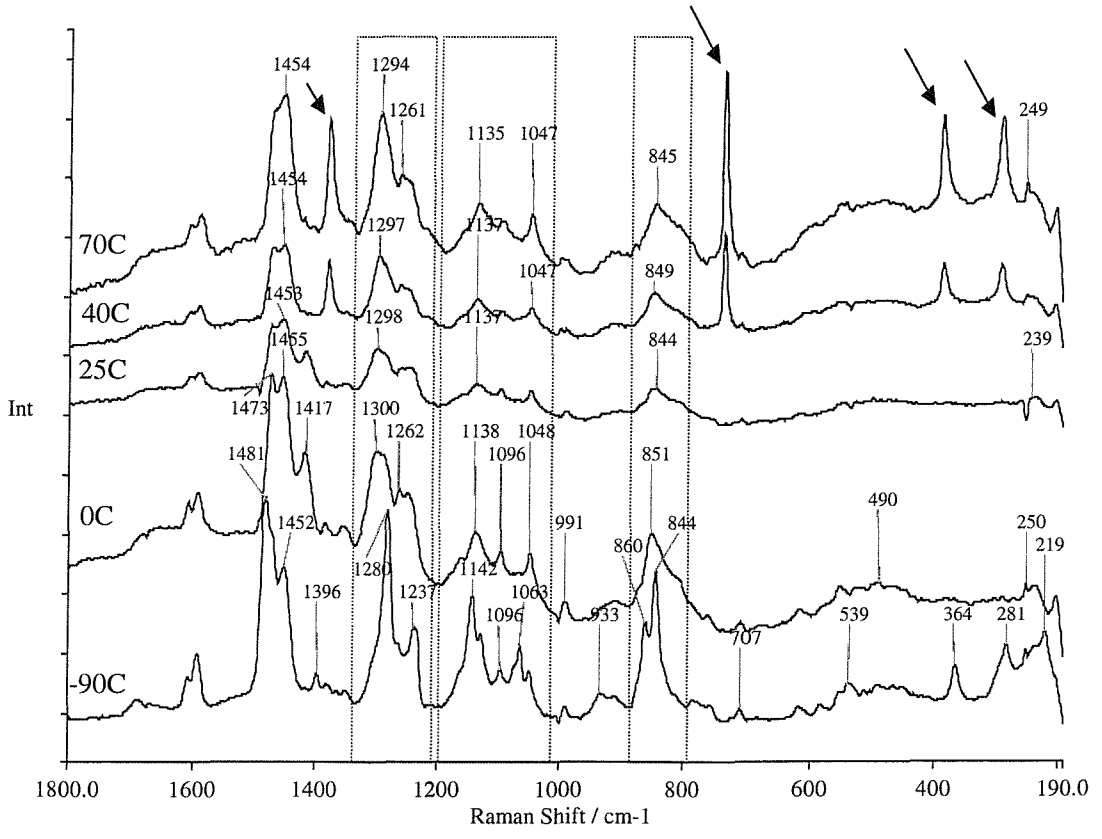


**Figure 4.26** Variable temperature FT-Raman spectra of the formulation containing local anaesthetics. The regions in the spectrum of particular interest are boxed in. The arrows indicate bands that are spurious.

The observed changes are similar to those observed from variable temperature Raman spectra of the aqueous solution of block copolymers, which is to be expected. Except for the spectrum at -90°C, which shows evidence of higher order in the polymer chains.

## 4.7 Conclusions

A comparison of the vibrational spectra of lidocaine and prilocaine with that of the eutectic mixture in the molten state provided inconclusive proof of interactions. The ATR spectra recorded when adding the two crystalline materials together in different stages, clearly shows that there are interactions between lidocaine and prilocaine on forming the eutectic mixture. The observed interactions involve the NH and carbonyl stretching frequencies, which suggests that on adding the two compounds in the crystalline state hydrogen bonding occurs. In addition, solid solubility of lidocaine and prilocaine in their eutectic mixture was observed.

The results on whether there are interactions between the eutectic mixture and the aqueous solution of block copolymers are not yet complete. Raman mapping of the boundary between the two phases showed an initial increase in hydrogen bonding, compared with the frequencies of the pure eutectic mixture. But since it was impossible to study the functional groups in the block copolymers sensitive to hydrogen bonding, it was difficult to judge the validity of these results. Repeating these Raman mapping experiments with increased scanning time would allow conclusive results to be obtained.

It is important to know what conformation changes happen in the aqueous solution of block copolymers as the temperature is varied. The Raman spectra recorded at different temperatures showed less variation compared with the variable temperature spectra of the poloxamers alone. The variable temperature FT-Raman spectra of the formulation containing local anaesthetics were similar to those without the active components. Except for the spectra recorded at -90°C where a very high order in the poloxamers was observed. The use of chemometric procedures could be advantageous in revealing many more changes with temperature.

## 4.8 References


[1] A. Brodin, A. Nyqvist-Mayer, T. Wadsten, B. Forslund, F. Broberg, J. Pharm. Sci, **73**, (1984), 481

[2] R.G. Snyder, S.L. Hsu, S. Krimm, Spectrochim. Acta, **34A**, (1978), 395

[3] C. Guo, H. Liu, J. Wang, J. Chen, J. Colloid Interface Sci., **209**, (1999), 368

[4] I.W. Levin & S.F. Bush, Biochim. Biophys. Acta, **640**, (1981), 760

[5] N. Yellin & I.W. Levin, Biochim. Biophys. Acta, **489**, (1977), 177

[6] A.T. Tu, *Raman Spectroscopy in Biology*, John Wiley & Sons, (1982), p.65

[7] K. Larsson & R.P. Rand, Biochim. Biophys. Acta, **326**, (1973), 245

[8] P. Alexandridis, T.A. Hatton, Colloids Surf. A, **96**, (1995), 1

[9] P. Linse, J. Phys. Chem., **97**, (1993), 13896

[10] J.H. Collett, E.A. Tobin, J. Pharm. Pharmacol., **31**, (1979), 174

[11] R. Nagarajan, M. Barry, E. Ruckenstein, Langmuir, **2**, (1986), 210

[12] A. Cabana, A. Ait-Kadi, J. Juhász, J. Colloid Interface Sci., **190**, (1997), 307

[13] C. Guo, J. Wang, H. Liu, J. Chen, Langmuir, **15**, (1999), 2703

[14] C. Guo, H. Liu, J. Chen, Colloid Polym. Sci., **277**, (1999), 376

[15] P. Chen-Chow & S.G. Frank, Int. J. Pharm., **8**, (1981), 89

[16] C. Guo, H. Liu, J. Chen, Colloids Surf. A, **175**, (2000), 193

[17] L.J. Bellamy and R.J. Pace, Spectrochim. Acta, 1972, 28A, 1869

[18] M. Scherlund, A. Brodin, M. Malmsten, Int. J. Pharm., **211**, (1-2), (2000), 37

# Chapter 5 Polymorphism

## 5.1 Introduction

Polymorphism in a material means that it can exist in different crystal forms. These crystal forms have the same molecular structure but differ in the way the molecules are packed within the crystal. The various forms also display different physical and thermodynamic properties such as their melting point, density, rate of dissolution, conductivity, heat capacity, etc. This is why the understanding of polymorphism is so very important to the pharmaceutical, food and specialty chemical industries where their specific products often involve structurally dependent properties.

In addition there is pseudo-polymorphism. The title is confusing because we speak about pseudo-polymorphism when the material can exist as different solvates. An example of pseudo polymorphism is Glucose. Glucose exists in the anhydrous form as well as in the monohydrate, but the two materials are quite different species with different molecular formulae.

The key question researchers have tried to answer is whether it is possible to predict the number and relative stability of a set of polymorphs of a chosen compound. The question is crucial because if the marketed polymorph is not the stable one, inevitably it will transform.

The techniques most used to study polymorphism are optical microscopy [1-3], X-ray diffraction [4-6], thermal analysis like DSC [7-9], solid-state NMR [10-12] and vibrational spectroscopy [13-16].

In this research, sulfathiazole and its polymorphic forms were studied with vibrational spectroscopy. For a long time it has been thought that sulfathiazole has four polymorphic forms [17,18], but recently papers have reported the existence of a fifth polymorph [19-21]. The different forms of sulfathiazole are distinguished by variations in the packing modes rather than in the molecular conformation. In addition, the least stable of the sulfathiazole polymorphs, form I, is thought to display unusual anisotropic lattice expansion on heating. This phenomenon was studied by infrared and FT-Raman spectroscopy.

## 5.2 Experimental

The FT-infrared spectra were recorded on a Perkin-Elmer Paragon 1000 system equipped with a KBr beamsplitter and LITA detector.

All FT-Raman spectra were acquired on a Perkin-Elmer System 2000 FT-Raman spectrometer that was equipped with a quartz beam splitter and an InGaAs detector, operating at room temperature. A Spectron continuous wave $Nd^{3+}$:YAG laser (1.064μm) provided the NIR excitation.

For the heated Infrared spectra, a Ventacon infrared hot cell was used. As window material KBr was used.

A Ventacon Raman hot cell was used to collect high temperature Raman spectra. For the low temperature work, a Ventacon cold cell was used.

For the rotated Raman spectra a Ventacon Rotator was used. This enables the user to rotate samples held in NMR tubes.

## 5.3 Sulfathiazole

Recently, a fifth polymorph of sulfathiazole has been reported [19-21]. The different forms of sulfathiazole are distinguished by the differences in the packing modes rather than their conformations in the unit cell. All five polymorphs of sulfathiazole have been assigned to monoclinic spacegroups with polymorphic forms IV and V having a single molecule in the asymmetric unit and the forms I, II and III with two molecules in the asymmetric unit. The molecular structure of sulfathiazole is shown in Figure 5.1.

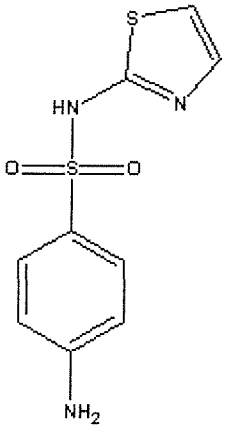


**Figure 5.1** Molecular structure of sulfathiazole.

## Hydrogen bonding in sulfathiazole

There are many different possibilities for hydrogen bonding in a sulfathiazole network. Our goal is to assign the vibrational frequencies to the different NH groups. This will in turn allow us to correlate the X-ray data on unusual large anisotropic lattice expansion of polymorph I with temperature, with our shifts in vibrational frequencies with temperature. The discussion about anisotropic lattice expansion follows in a later paragraph.

The packing arrangements of the different sulfathiazole polymorphs, as well as the clathrates have kindly been supplied to us by D. Hughes (a member of Prof. Hursthouse's X-Ray group at the Chemistry Department of the University of Southampton). They are displayed with the correct atom numbering in Figure 5.2

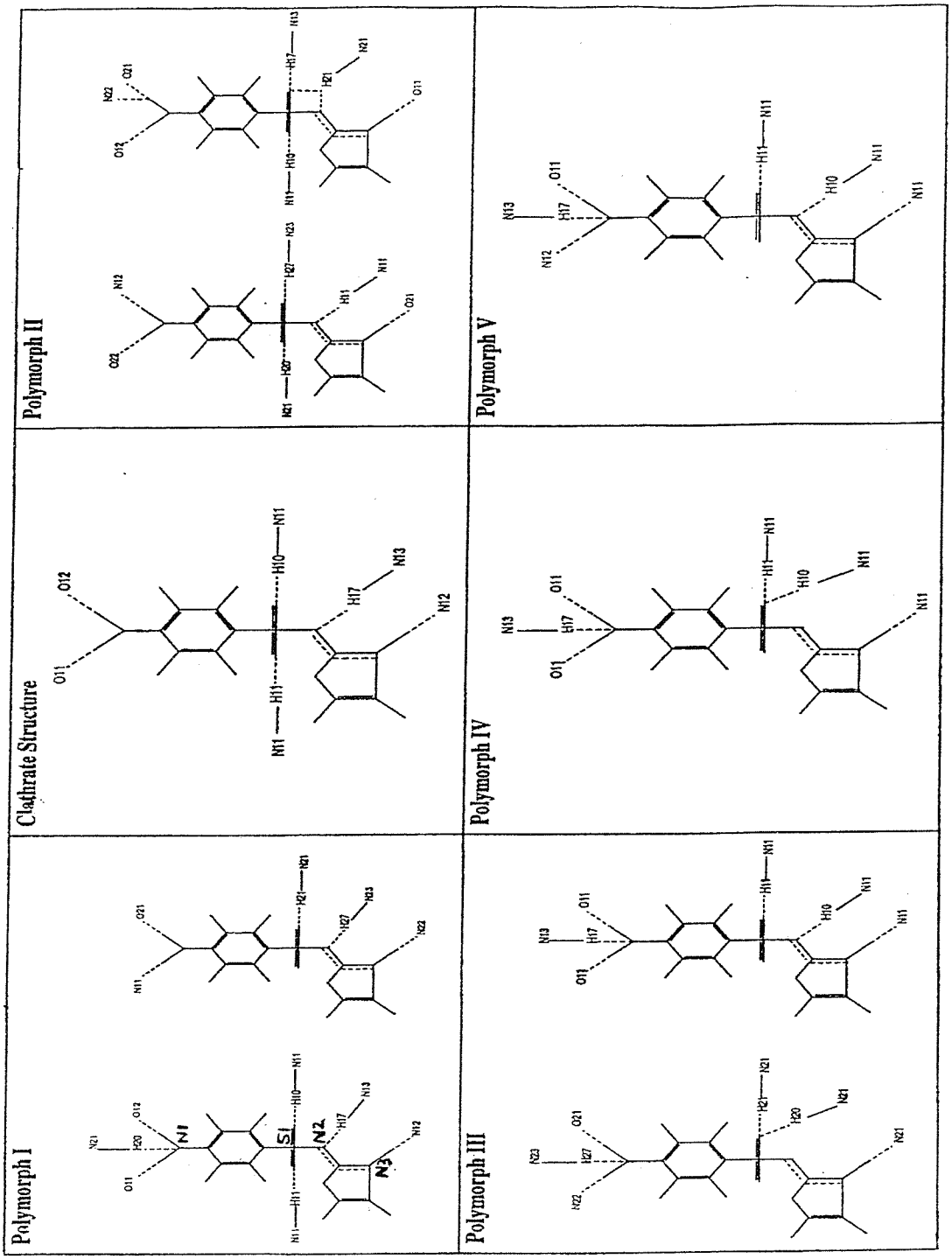


**Figure 5.2** Consistent atom numbering and connectivities of the different sulfathiazole polymorphs and clathrate. Where there are 2 molecules per unit cell, the first number corresponds to either of the molecules 1 or 2. The second number corresponds to the atom numbering within the molecule. The figures were supplied by D. Hughes.

As is clear from the recent obtained X-ray data 'translated' in Figure 5.2, there is a whole spectrum of hydrogen bonds in the different sulfathiazole polymorphs.

The most obvious hydrogen bonds are those between the amine N1H1 and the S=O group. The second 'obvious' hydrogen bond would be between the thiazole amine

N3H3 and the S=O group. In addition, Minceva-Sukarova et al. have discussed weak hydrogen bonding between ammonia hydrogen atoms and the $\pi$-electron cloud of benzene molecules in the clathrates they studied [22].

In Table 5.1 the moderate to strong hydrogen bonds within the different polymorphs are presented. The classification is based on that used by Jeffrey [23], in that strong hydrogen bonds have a distance between the hydrogen and the acceptor atom ranging from around 1.2 to 1.5 Å. In moderate hydrogen bonds this distance increases from around 1.5 to 2.2Å. As mentioned before, the X-ray data on hydrogen bond lengths was kindly supplied by D. Hughes.

**Table 5.1** Details of the different types of hydrogen bonds and their lengths in the different sulfathiazole polymorphs. A and B are used to differentiate between the twofferent molecules in the unit cell. The data was supplied to us by D. Hughes.

| Group | hydrogen bonds to | d(hydrogen...acceptor) (Å) | Polymorph |
|---|---|---|---|
| Amine in thiazole ring B | amine N22 B | 1.9867 | I |
| Primary amine A | S=O A | 2.0049 | |
| Amine in thiazole ring A | amine N12 A | 2.0409 | |
| Amine in thiazole ring B | S=O A | 1.938 | II |
| Amine in thiazole ring A | S=O B | 2.0365 | |
| Primary amine A | S=O B | 2.0871 | |
| Primary amine A | amine N12 A | 2.1378 | |
| Amine in thiazole ring B | Primary amine A | 1.9129 | III |
| Amine in thiazole ring A | Primary amine B | 2.0605 | |
| Primary amine A | S=O B | 2.0674 | |
| Primary amine B | S=O A | 2.1636 | |
| Primary amine B | S=O A | 2.1675 | |
| Amine in thiazole ring A | Primary amine A | 2.0099 | IV |
| Primary amine A | S=O A | 2.1897 | |
| Amine in thiazole ring A | Primary amine A | 2.0633 | V |
| Primary amine A | S=O A | 2.1437 | |

Within the sulfathiazole polymorphs, the amines are most capable of hydrogen bonding. Therefore it is important to know what happens to the amine vibrations when they hydrogen bond.

In aromatic amines the infrared frequencies of the NH stretching are usually higher, compared to their aliphatic counterparts. Compared to the hydroxyl group, hydrogen bonding has a less pronounced influence on the amino group. Generally, hydrogen

bonding leads to a decrease in the NH stretching frequency and an increase in the $NH_2$ bending frequencies, band broadening and an increase in intensity.
As the environment of the amine group varies, where the two NH bonds are affected in a similar way, the stretching frequencies will shift without affecting their separation. In fact, in several systems, the symmetric and asymmetric stretching ($\nu_s$ and $\nu_{as}$) frequencies are related according to the following formula first proposed by Bellamy and Williams [24].

$$\nu_s = 345.5 + 0.876\ \nu_{as}$$

This separation between the symmetric and asymmetric stretching frequencies is a measure of the difference in strength of the hydrogen bonds but also of the coupling between the two bonds [25]. Therefore, unlike with a secondary amine where the strength of the hydrogen bond can be assessed by measuring the frequency shift, it is more complicated for primary amines because of the overlying effect of coupling.
In another paper by Bellamy two solutions to eliminate the coupling of the bands are proposed [26]. A first solution is based on partially deuteration of the amine. As one hydrogen is replaced by a deuterium atom, the coupling of the two bands disappears and one sees the frequencies of the separate bonds.
A second solution is also based on partially deuteration, but simply looks at the mathematics behind it. It concludes that the sum of the shifts of the symmetric and asymmetric bands from a reference value (the vibrational frequencies from the 'free' molecule) provides a good measure for the strength of the hydrogen bond.

$$\Delta = \delta\nu_{as} + \delta\nu_s \qquad (5\text{-}1)$$

where $\Delta$ is the frequency shift due to hydrogen bonding of one of the NH bonds, $\delta$ is the shift from the frequency of the free $NH_2$ and $\nu_{as}$ and $\nu_s$ are the asymmetric and symmetric NH stretching frequencies. In our further calculations, this second solution is applied to the data.
As was mentioned before, polymorph I, II and III have two molecules in the asymmetric unit. In polymorph I, the two frameworks are connected by a weak hydrogen bond between the two primary amines in the two sulfathiazole molecules.

The two molecules per unit cell are not very different, hence we see only one pair of $NH_2$ stretching frequencies (symmetric and asymmetric). However, the appearance of a weak shoulder at the low frequency end of the two bands reveals a second pair of NH stretching frequencies.

The infrared NH-stretching frequency regions of the five different polymorphs are shown in Figure 5.3. The sulfathiazole polymorphs were kindly supplied to us by Dr. T. Threlfall from the Chemistry Department of the University of York.

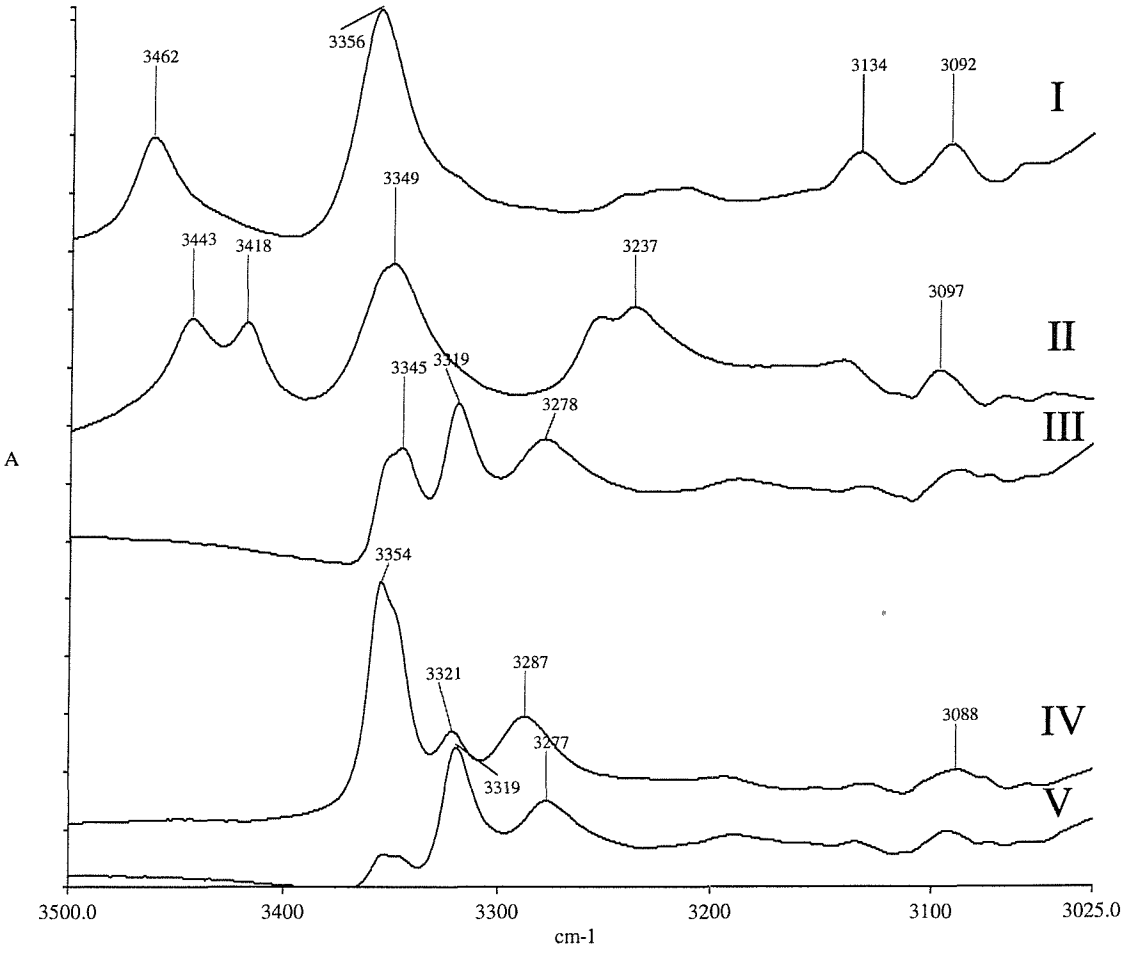


**Figure 5.3** Infrared spectra of the NH stretching region of the different polymorphs of sulfathiazole. 32 scans, 4 $cm^{-1}$ resolution

In polymorph II the two molecules are bonded differently in the unit cell, hence we see a doubling of the asymmetric NH stretching. The symmetric NH stretching is still a singlet but in theory it should be a doublet as well. Again, a weak shoulder at the lower frequency side reveals the existence of a second band.

Polymorph III is a combination of polymorph IV and V. X-ray data has shown that the structure of this polymorph is made up by alternating the structures of polymorphs IV and V, linked by hydrogen bonding.

When one of the NH bonds in the amine is weakened, then the lower frequency band will move downfield more than the higher frequency band resulting in an increase in the separation between the two. It appears that in polymorph V only one of the $NH_2$ hydrogens is bonded to the $SO_2$ group, which would create changes in the separation between the two frequencies when comparing to form IV where both $NH_2$ hydrogens are hydrogen bonded to a S=O group. In fact, in polymorph V the difference in frequency between the symmetric and asymmetric stretching has increased from 67 $cm^{-1}$ in polymorph IV to 76 $cm^{-1}$ in polymorph V. However, from the X-ray data, one hydrogen bond has strengthened and the other has weakened in polymorph V. The hydrogen bond lengths for the primary amine in Polymorphs III, IV and V are shown in Table 5.2.

**Table 5.2** Hydrogen bond lengths from the primary amines in sulfathiazole polymorphs III, IV and V.

| Sulfathiazole polymorph III | D(H...A) (Å) | Strength of the hydrogen bond |
|---|---|---|
| N11-H10...N22 | 2.4478 | weaker compared with form IV |
| N11-H11...O21 | 2.0674 | stronger compared with form IV |
| N21-H20...O11 | 2.1636 | |
| N21-H21...O11 | 2.1675 | |
| Sulfathiazole polymorph IV | | |
| N11-H10...O11 | 2.2041 | |
| N11-H11...O11 | 2.1897 | |
| Sulfathiazole polymorph V | | |
| N11-H10...N12 | 2.4347 | weaker compared with form IV |
| N11-H11...O11 | 2.1437 | stronger compared with form IV |

In polymorph III, the NH asymmetric stretching frequency has shifted even further downfield, suggesting even stronger hydrogen bonding to the primary amine. This strong hydrogen bond should accordingly give the shortest hydrogen-hydrogen acceptor distance, which is true for the hydrogen bond towards S=O (N11-H11...O21), but not for the other one (N11-H10...N22).

In these crude comparisons, it is assumed that the coupling between the two NH bonds in the primary amine remains the same in the three polymorphs.

Even when coupling between the two NH bonds was taken into account, a comparison of the hydrogen bond strength with the bond lengths from the X-ray data did not show any correlation.

A simpler relation to study is that between the (hydrogen) bond strength of the thiazole NH and the vibrational frequency shifts. But again no relation between the X-ray data and shifts in vibrational frequencies was observed.

From the X-Ray data, it has become clear that the hydrogen bonding network is more complicated and that it might be impossible to correlate the NH stretching frequencies to the specific hydrogen bonds between the functional groups in these polymorphs without vibrational spectra of partially deuterated primary amine compounds.

An attempt is made to assign the vibrational frequencies of the functional groups involved in hydrogen bonding. The assignments are presented in Table 5.3.

**Table 5.3** Tentative assignment of the most important infrared absorption frequencies in the different forms of sulfathiazole. w: weak

| Frequency region of infrared absorption ($cm^{-1}$) | Frequency assigned to : |
|---|---|
| Polymorph I/II | |
| 3462-3237 | $NH_2$ stretching |
| 3250 very broad | thiazole NH stretching - hydrogen bonded |
| 1629 (I) or 1644 (II) | $NH_2$ scissor |
| 1325 | Asymmetric $SO_2$ stretching |
| 1143 | Symmetric $SO_2$ stretching |
| Polymorph III/IV/V similar frequencies, except for : | |
| 3354-3277 | $NH_2$ stretching |
| Around 3280 | thiazole NH stretching - hydrogen bonded |
| 1628w | $NH_2$ scissor |
| 1322 or 1323 | Asymmetric $SO_2$ stretching |
| 1137 | Symmetric $SO_2$ stretching |

In Figure 5.4 and 5.5, the NH scissor frequency region in the infrared and Raman spectra of the different sulfathiazole polymorphs are shown.

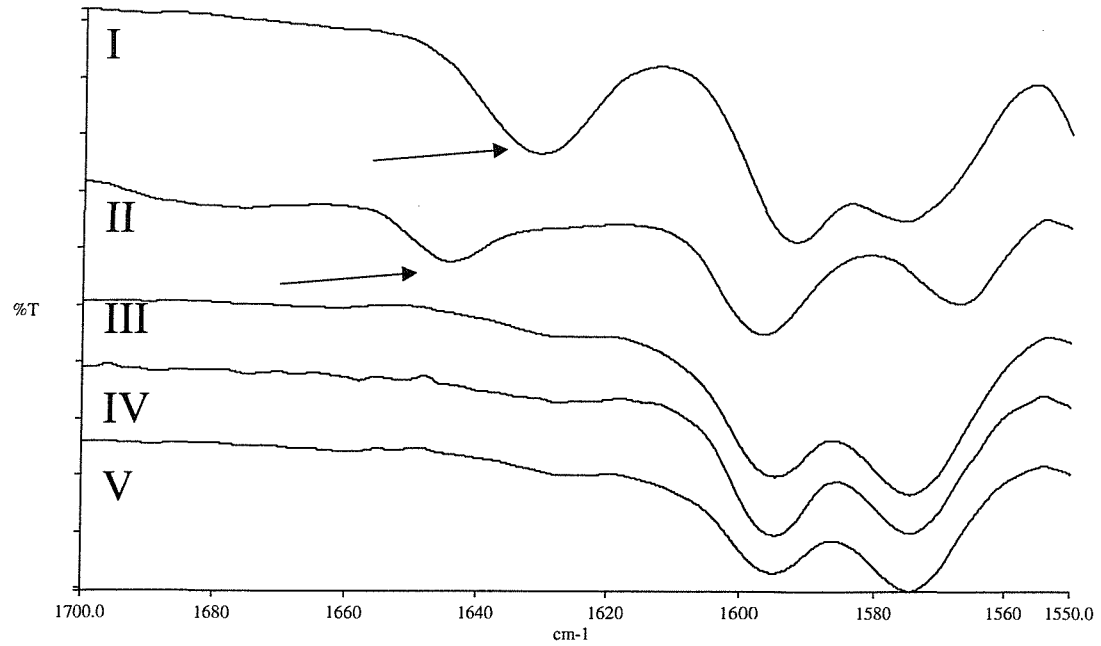


**Figure 5.4** Infrared spectra of the NH scissor frequency region in the different sulfathiazole polymorphs. 32 scans, 4 $cm^{-1}$ resolution.

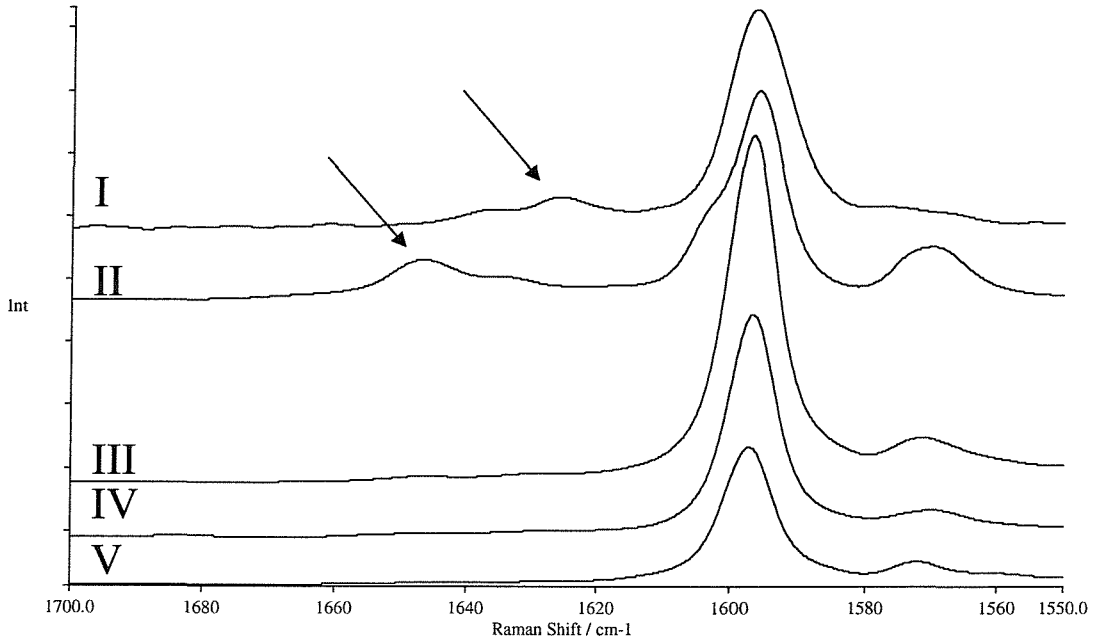


**Figure 5.5** FT-Raman spectra of the NH scissor region in the different sulfathiazole polymorphs. 500 scans, 4 $cm^{-1}$ resolution, 200mW laser power.

From the spectra, some clear differences between the different polymorphs are immediately apparent, e.g. the high frequency NH deformation is very weak in polymorphs III to V. It is not clear what the reason could be for this.

In polymorphs I, II and III, there are two different molecules per unit cell, hence we should see two different $NH_2$ scissor frequencies. A second scissor deformation

frequency is found in polymorphs I and II, but not in polymorph III. A tentative assignment of the vibrational frequencies is presented in Table 5.4.

**Table 5.4** Tentative assignment of the vibrational frequencies of the $NH_2$ scissor in the different sulfathiazole polymorphs. w: weak

| Polymorph No. | Infrared frequency ($cm^{-1}$) | Raman frequency ($cm^{-1}$) |
|---|---|---|
| I | 1634w,1629 | 1634w,1625 |
| II | 1644,1630w | 1646,1636w |
| III | 1629w | |
| IV | 1628w | |
| V | 1628w | |

There was no correlation found between the frequency shifts of the NH scissor deformation and (hydrogen) bond distance.

Another region in the vibrational spectra, susceptible to hydrogen bonds is the $SO_2$ stretching region. The asymmetric stretching appears to be more sensitive to hydrogen bonding, than the symmetric stretching. The asymmetric stretching frequency is found in the region 1380 $cm^{-1}$ to 1310 $cm^{-1}$, while the symmetric stretching frequency lies in the region 1180 $cm^{-1}$ to 1140 $cm^{-1}$. The approximate ratio of the wavenumbers of asymmetric stretching frequency over the symmetric stretching frequency is 1.16.

A tentative assignment of the S=O stretching frequencies is given in Table 5.5.

**Table 5.5** Tentative assignment of the vibrational frequencies of the $SO_2$ asymmetric and symmetric stretching frequencies in the different sulfathiazole polymorphs. ν: stretching, br: broad, asym: asymmetric, sym: symmetric.

| Polymorph No. | Infrared frequency ($cm^{-1}$) | | Raman frequency ($cm^{-1}$) | |
|---|---|---|---|---|
| | asym νS=O | sym νS=O | asym νS=O | sym νS=O |
| I | 1325 | 1143 | | 1129 |
| II | 1325 | 1143 | 1326 | 1129 |
| III | 1322 | 1138br | 1327 | 1133 |
| IV | 1323 | 1137br | 1327 | 1132 |
| V | 1322 | (1146,1135)br | 1326 | 1135 |

From the X-ray data it seems that the shortest hydrogen bond lengths are found in polymorphs I and II (see Table 5.1), but it is odd that the hydrogen bonds with these S=O groups seem weaker (higher frequencies). The reason for this could be due to difficulties in assigning the bands since they are not well-defined singlets. In addition, the symmetric $SO_2$ stretching could be buried under the C-N-C stretching.

## 5.4 Sulfathiazole solvates

There are two types of so-called guest molecule (here a solvent) which can reside in the structure of the sulfathiazole [27]. The first type is the clathrate where the guest molecules are enclosed within a cavity in the sulfathiazole network. There can be weak hydrogen bonding present. In the second type, the guest molecule forms hydrogen bonds with sulfathiazole and becomes a part of the primary network. In addition, in each class, structures where the guest is a base and abstracts a proton from sulfathiazole to form an ionic salt, have been found.

Before studying the anisotropic lattice expansion of sulfathiazole polymorph I, it was important to know whether a change in size of the unit cell produces considerable shifts in the Raman bands and more specifically, the NH stretching frequencies. Dr T. Threlfall of the Department of Chemistry, University of York kindly supplied us with seven iso-structural solvates of sulfathiazole:

- Sulfathiazole plus propylene carbonate (I)
- Sulfathiazole plus cyclopentanone (II)

- Sulfathiazole plus ß-butyrolactone (III)
- Sulfathiazole plus γ-valerolactone (IV)
- Sulfathiazole plus γ-butyrolactone (V)
- Sulfathiazole plus α-angelicalactone (VI)
- Sulfathiazole plus α-methyl-γ-butyrolactone (VII)

The chemical structures of the corresponding solvents are given below:

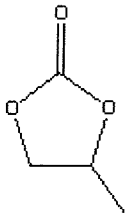

(I)

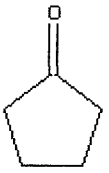

(II)

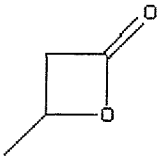

(III)

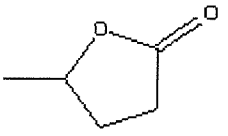

(IV)

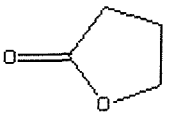

(V)

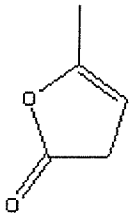

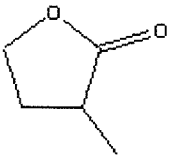

(VI) (VII)

As the term iso-structural already reveals, the structures of these solvates are very similar. It is known that these solvates all form clathrate type structures. From the data obtained from D. Hughes (Figure 5.2) it is clear that the sulfathiazole network in these clathrates contains one molecule per unit cell. These molecules form a 3-dimensional network similar to that of sulfathiazole polymorph I in that the molecules form a dimer structure where the guest molecule resides and only the primary amines hydrogen bond to the S=O groups.

Even though clathrates usually mean that the guest does not become part of the sulfathiazole network, there are still interactions like weak hydrogen bonding or van der Waals interactions between the guest and host. Since all the guest molecules possess a carbonyl group, weak hydrogen bonding to the amines in sulfathiazole is likely. Our aim is to compare the different solvates in terms of volume and draw

conclusions from the vibrational spectra, which in term will help in the study of anisotropic lattice expansion of sulfathiazole polymorph I.

D. Hughes kindly supplied X-ray data on the solvates from which we extracted the following data. All the solvates have P2(1)/n symmetry. In addition to the lattice parameters (a, b and c), the volume, lengths and angle of the hydrogen bonds were given for all the solvates. As for the sulfathiazole polymorphs, the moderate to strong hydrogen bonds are listed below:

- N11-H10...O11
- N11-H11...O12
- N13-H17...N12

The atom numbering is similar to that used in Figure 5.2.

The infrared and FT-Raman spectra were recorded and the bands in the spectra due to sulfathiazole were compared. The spectra are all similar in appearance as we would expect.

Although the solvates were prepared from commercial sulfathiazole (usually polymorph III, but likely to be a mixture) they all show evidence of sulfathiazole polymorph I, as was expected from the structure determinations. The spectra of one of the solvates and sulfathiazole polymorph I are shown in Figure 5.6.

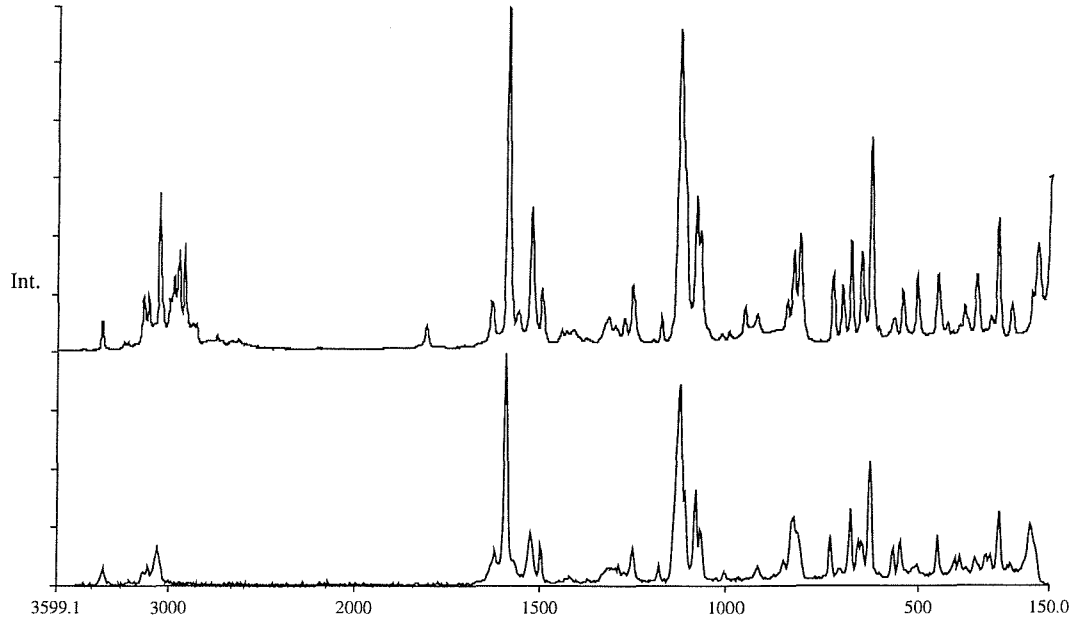


**Figure 5.6** FT-Raman spectra of the ß-butyrolactone sulfathiazole solvate (top) and sulfathiazole polymorph I (bottom).

When studying the NH-stretching region, it was noticed that the stretching frequency is shifted towards higher wavenumbers in the solvates. This would imply that the NH bond is getting more rigid, which means that hydrogen bonding is reduced. This is not surprising, since from the X-ray data on the solvates, it is clear that the volume of the unit cell has increased when the guest molecule was introduced.
Deviations of the NH-stretching frequency from those of sulfathiazole polymorph I are displayed in Table 5.6. Unfortunately, the asymmetric NH stretching was not visible in the Raman spectra.

**Table 5.6** The vibrational frequencies of the NH-stretching for the different sulfathiazole solvates are presented. For comparison, the NH-stretching frequency for sulfathiazole polymorph I is included in the data. When frequencies are printed in bold, it means that they are the lower intensity peak of the doublet.

| NH-stretching Frequency ($cm^{-1}$) | Raman | Infrared | |
|---|---|---|---|
| | Symmetric | Asymmetric | Symmetric |
| Sulfathiazole Polymorph I | 3350 broad | 3463 | 3356 |
| Sulfathiazole plus propylene carbonate | 3365 | 3462 | 3365 |
| Sulfathiazole plus cyclopentanone | 3378 | 3476 | 3377, **3357** |
| Sulfathiazole plus ß-butyrolactone | 3367 | 3464 | 3368 |
| Sulfathiazole plus γ-butyrolactone | 3376 | 3473 | 3376 |
| Sulfathiazole plus α-methyl-γ-butyrolactone | 3374 + shoulder **3363** | 3474, **3448** | **3375**, 3356 |
| Sulfathiazole plus γ-valerolactone | 3370 | 3465 | 3371 |
| Sulfathiazole plus α-angelicalactone | 3369 | - | 3368 |

Bellamy's rule [30] that predicts a linear relation between the asymmetric and symmetric NH stretching frequencies was applied to these solvates. But only for the

α-angelicalactone solvate, the rule gave a valid answer. This would suggest different strengths hydrogen bonds with the two NH bonds in the primary amine.

To discover whether there was a correlation between the NH stretching vibrational frequencies and the hydrogen bond strength or length in the different solvates, the following relationships were studied:

Possible correlation of the sum of NH asymmetric and symmetric frequency shifts from an arbitrary unit with:

- all hydrogen bond lengths and angles in the solvates
- all parameters of the unit cell

These are the calculations proposed by Bellamy [26] to eliminate the coupling between the two NH bands in order to study the strength of the hydrogen bond.

Of all these possible correlations (10 in total) none was valid.

## 5.5 Sulfathiazole polymorphs and anisotropic lattice expansion

The least stable of the sulfathiazole polymorphs, form I, is thought to display unusually large anisotropic lattice expansion on heating [21].

A. Bingham from Prof. M. Hursthouse's X-ray group supplied us with data on bond lengths and angles of sulfathiazole at the different temperatures studied. It would be interesting to see if it is possible to couple this data with changes in the vibrational spectra with temperature.

From the data kindly supplied to us by A. Bingham, there is evidence of unusual anisotropic lattice expansion in sulfathiazole polymorph I. The X-ray data were collected at four different temperatures, 150 K, 193 K, 295 K and 370 K. On increasing the temperature, the lattice parameters stay virtually constant, lattice parameter b increases by 2 %, lattice parameter a decreases by a lesser amount. The volume of the unit cell increases linearly with temperature. But the largest anisotropy is seen in the change of beta angle with temperature, from 107.77 at 150 K to 107.93 at 193K and 108.141 at 370 K.

The anisotropic lattice expansion was studied using infrared and FT-Raman spectroscopy.

## Infrared experiment

For the infrared experiment, the sulfathiazole powder was held in between two KBr flats. The windows were then transferred to an infrared hot-cell. The temperature was increased by 15°C increments and at each temperature a spectrum was recorded. The temperature was varied between room temperature (24°C) and 120°C. Spectra were also recorded as the sample cooled down again. To check reversibility of the anisotropic expansion, after cooling down the temperature was increased again as in the first phase of the experiment. Infrared spectra were recorded with 4 $cm^{-1}$ resolution, co-adding 32 scans.

As expected, the symmetric NH stretching showed the largest wavenumber shift towards higher wavenumbers. The infrared spectra in this region with varying temperature are shown in Figure 5.7.

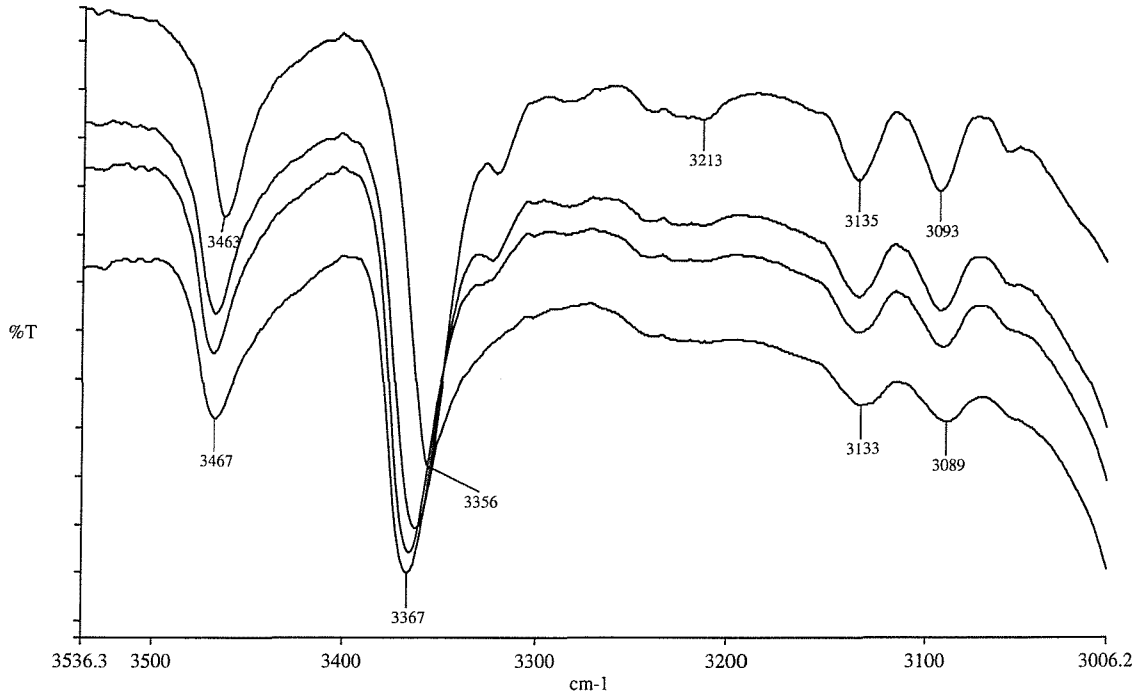


**Figure 5.7** FT-Infrared spectra of sulfathiazole polymorph I varying from 54°C (top spectrum) to 120°C (bottom spectrum). 32 scans, 4$cm^{-1}$ resolution. Nujol mull spectra

On heating sulfathiazole, most of the vibrational frequencies shift downward over 1 or 2 wavenumbers. Some exceptions are the frequencies around 1577 $cm^{-1}$, 1540 $cm^{-1}$ and 1419 $cm^{-1}$ that shift over 5 wavenumbers. In contrast to the other vibrational bands, the NH stretching frequencies shift towards higher frequencies on heating and the shift is considerably larger (up to 10 wavenumbers for the NH sym stretching).

The vibrations, showing the largest frequency shifts with temperature are summarised in Table 5.7.

**Table 5.7** On heating and cooling down of sulfathiazole polymorph I, shifts in the frequency of certain vibrations are observed. Wavenumbers obtained from infrared experiments. ν: stretching, as: asymmetric, s: symmetric

| Temperature (°C) | | | | | |
|---|---|---|---|---|---|
| heating | | cooling | heating | cooling | Assignment |
| 24 | 120 | 45 | 120 | 28 | |
| vibrational frequencies ($cm^{-1}$) | | | | | |
| 3458 | 3464 | 3463 | 3464 | 3459 | νNH as |
| 3354 | 3364 | 3359 | 3364 | 3355 | νNH s |
| 1577 | 1571 | 1571 | 1571 | 1576 | |
| 1540 | 1535 | 1534 | 1535 | 1540 | |
| 1143 | 1141 | 1143 | 1141 | 1143 | νS=O s |
| 1087 | 1086 | 1087 | 1086 | 1087 | |

On heating, one expects the lattice to expand and hence the X-H...B distance to increase i.e. the X-H frequency will move towards its isolated frequency.
To check whether the frequency shifts with changing temperature are reversible, several heating and cooling curves were applied to sulfathiazole polymorph I. The response of the symmetric NH stretching vibration with temperature is shown in Figure 5.8.

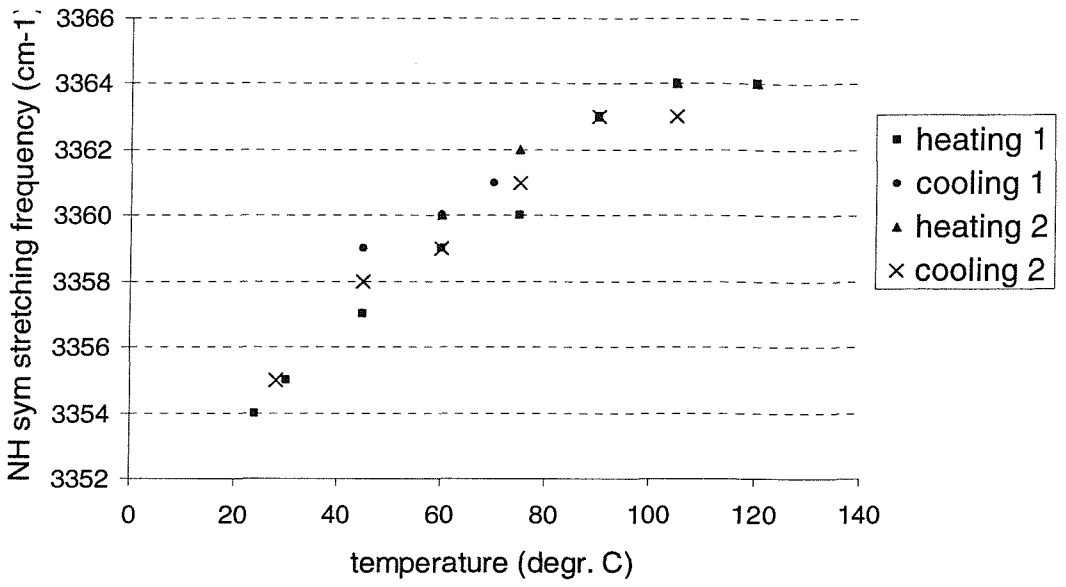


**Figure 5.8** Variation of the vibrational frequency of the symmetric N-H stretching with temperature. As the sample was heated, at several temperatures infrared spectra were recorded. Subsequently, the sample was cooled down, after which it was subjected to a second heating and cooling cycle.

From Figure 5.8 it is clear that the changes with temperature are more or less reversible.

In anisotropic lattice expansion, the lattice expands unevenly in different directions. It would be possible to link the shifts in NH stretching frequency to the anisotropic lattice expansion if it was possible to determine whether these hydrogen bonded NH bonds lie along a particular axis in the sulfathiazole network.

Figure 5.9 shows the sum of the NH stretching frequency shifts (asymmetric and symmetric) versus temperature. Because of the lack of data on the symmetric and asymmetric NH stretching frequencies of the isolated sulfathiazole, to which the shifts with temperature are compared, these frequency values were chosen arbitrarily. In fact rearranging Bellamy's rule (5-1) eliminates the frequencies of the free molecule, hence these frequency values are not needed when comparing hydrogen bond strengths of compounds with a similar gas phase spectrum.

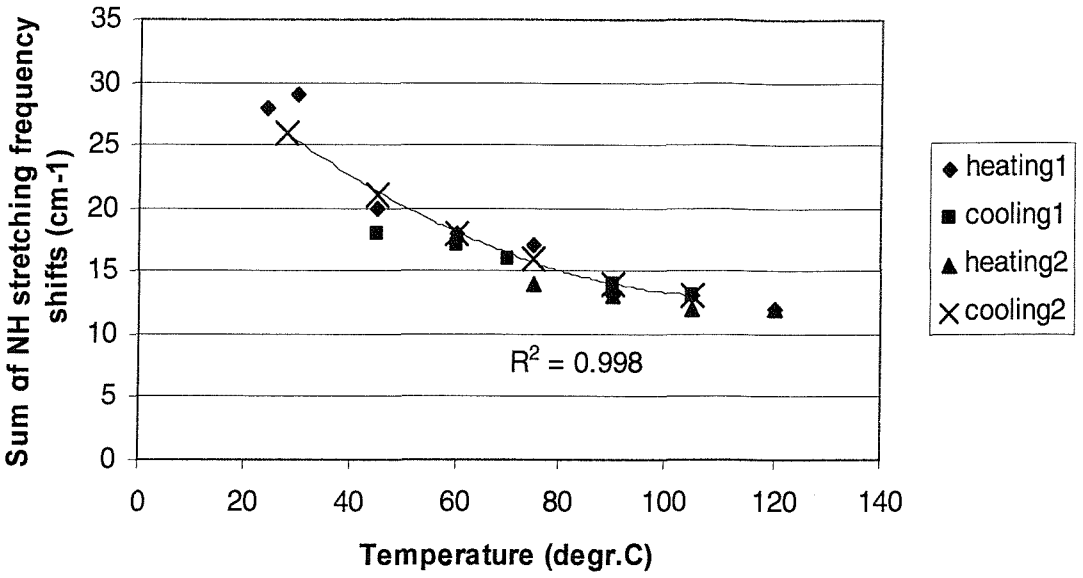


**Figure 5.9** Plot of the sum of the infrared symmetric and asymmetric NH stretching frequency shifts against temperature for sulfathiazole polymorph I. A second order trendline is fitted to the data and the correlation coefficient ($R^2$) is shown in the graph. The different data points for each temperature indicate that several spectra were recorded at that temperature, depending on whether the sample was being heated or subsequently cooled down again.

The plot in Figure 5.9 is not a linear one, indicating that the strength of the hydrogen bond is not linearly related to the change in temperature. The graph suggests that at higher temperature the frequencies will only produce a small shift compared with the lower temperature differences. This result is to be expected since the hydrogen bond will become weaker and weaker on heating.

Molecular modelling performed by Prof. M. Hursthouse's group suggests that the hydrogen bonds lie along all 3 axes throughout the sulfathiazole network. Therefore we expect that some of the NH stretching frequencies are buried underneath the other bands or they are too weak to be observed. These results suggest that it is difficult to link these shifts in vibrational frequency with an anisotropic lattice expansion.

## Raman experiment

FT-Raman spectra of sulfathiazole polymorph I with varying temperatures were recorded. The temperature was varied between –75°C and 90°C. All spectra were recorded with 200mW laser power and the co-addition of 50 scans.

Figure 5.10 and 5.11 show two Raman spectra of sulfathiazole polymorph I, recorded at room temperature and at a lower temperature.

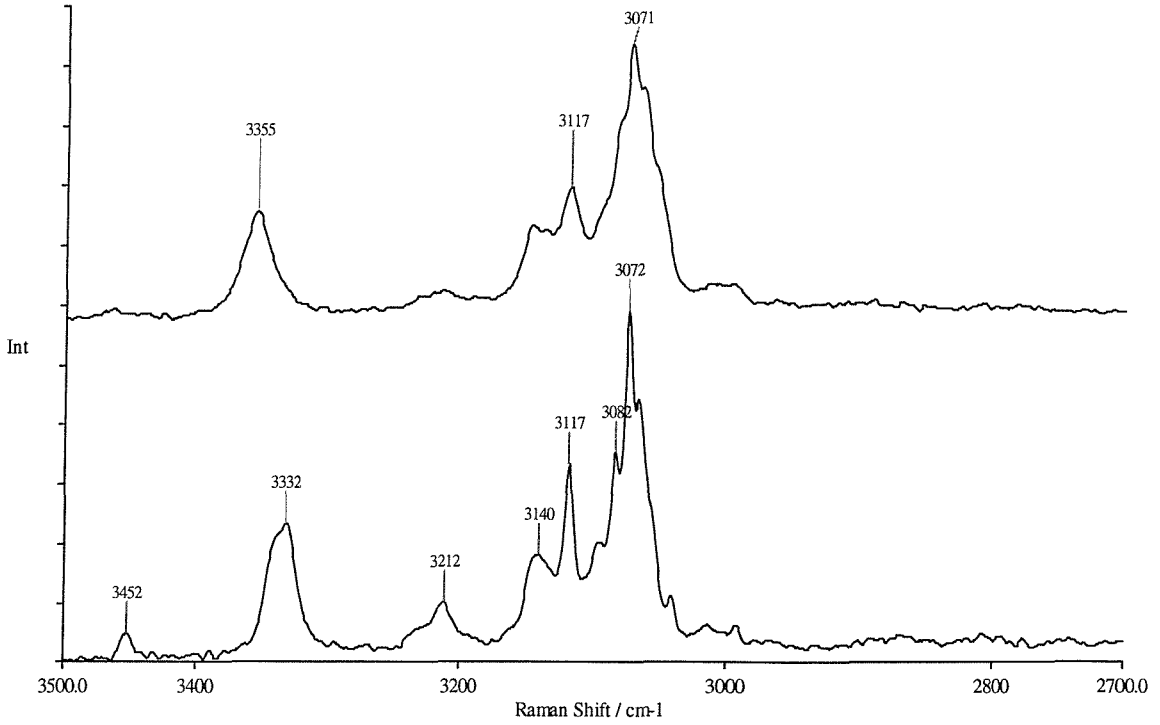


**Figure 5.10** FT-Raman spectra of sulfathiazole polymorph I at two different temperatures. The top spectrum was recorded at room temperature (20°C). The bottom spectrum was recorded at -75°C. 200mW laser power, 50 scans, resolution: 4 $cm^{-1}$.

From Figure 5.10, it is clear that the NH stretching frequency shows a very large shift with varying temperature. Unfortunately, the asymmetric stretching frequency is only visible in the low temperature Raman spectrum.

For comparison, in Figure 5.11 the fingerprint region of the spectrum of sulfathiazole polymorph I is shown. Again the two spectra were recorded at two different temperatures.

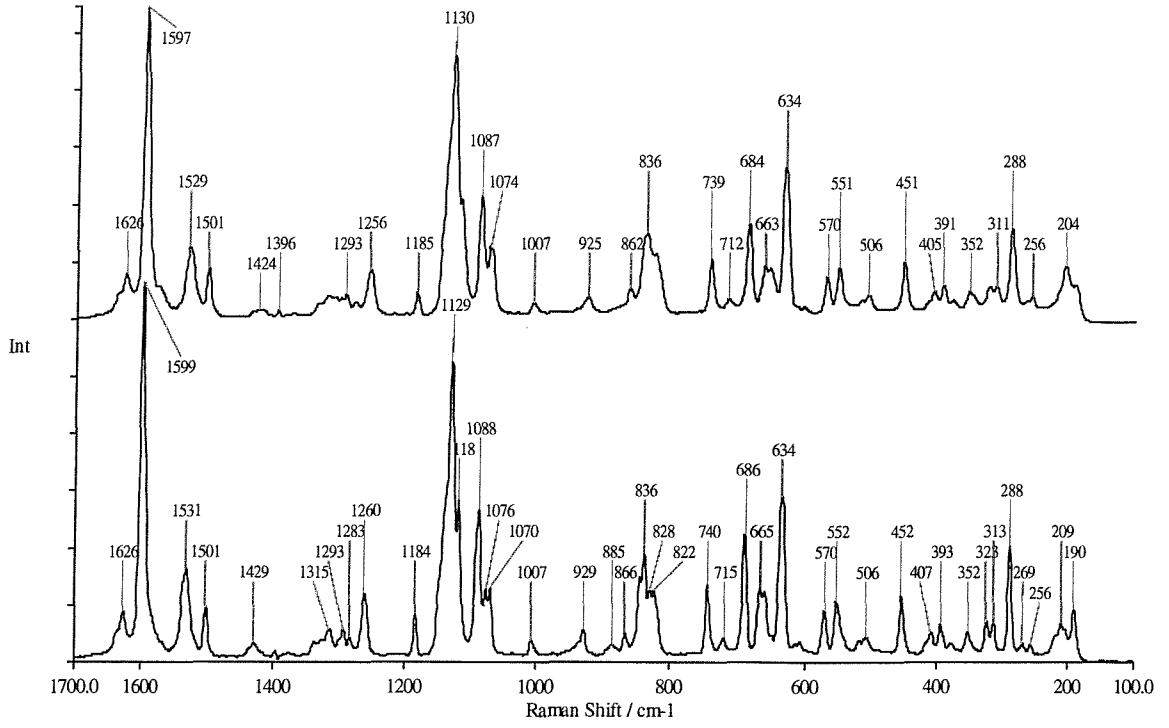


**Figure 5.11** FT-Raman spectra of sulfathiazole polymorph I at two different temperatures. The top spectrum was recorded at room temperature (20°C). The bottom spectrum was recorded at -75°C.

As with the infrared spectra, most vibrational frequencies shift to higher values on cooling the sample. Over the temperature range from -75°C to 90°C, most bands show shifts less than 4 wavenumbers. However, the symmetric NH stretching band shows the largest shifts upon changes in temperature, 35 wavenumbers. The bands that showed the largest wavenumber shift with temperature are displayed in Table 5.8.

**Table 5.8** On heating and cooling down of sulfathiazole polymorph I, shifts in the frequency of certain vibrations are observed. Wavenumbers obtained from Raman experiments. v: stretching, as: asymmetric, s: symmetric

| Temperature (°C) | | | | | Tentative assignment |
|---|---|---|---|---|---|
| | cooling | heating | | heating | |
| 20 | -75 | 20 | 30 | 90 | |
| vibrational frequencies ($cm^{-1}$) | | | | | |
| 3458 | 3452 | 3462 | - | - | vNH as |
| 3355 | 3332 | 3355 | 3358 | 3367 | vNH s |
| 1424 | 1429 | 1424 | - | - | |
| 1278 | 1283 | 1279 | 1278 | 1275 | |
| 1256 | 1260 | 1256 | 1256 | 1253 | |

To check whether these shifts are reversible, the shift of the vibrational frequency of the symmetric N-H stretching as a function of temperature is shown in the following graph, Figure 5.12.

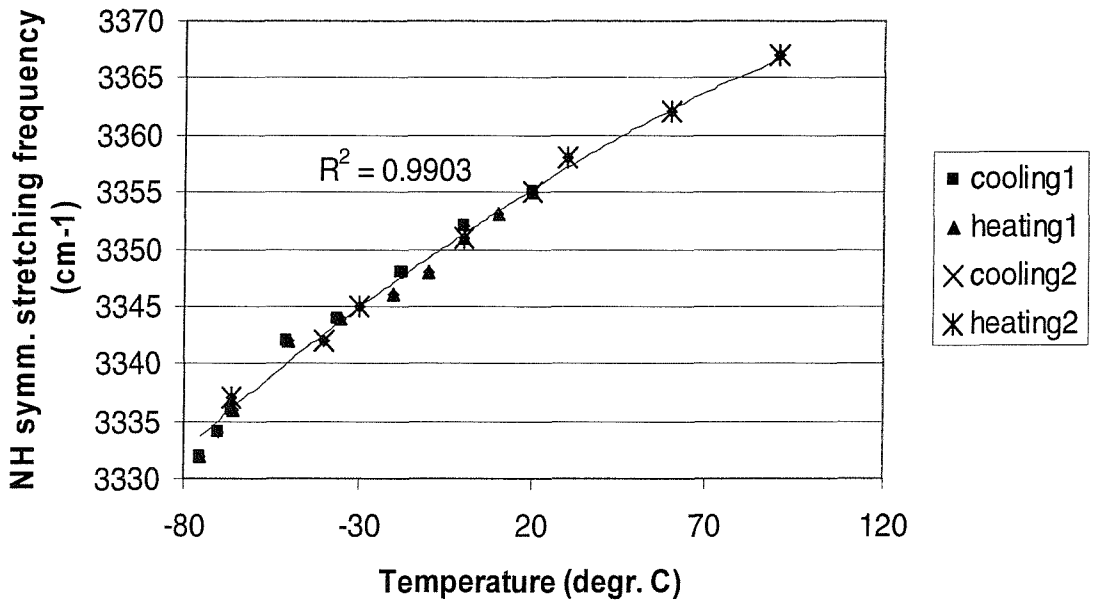


**Figure 5.12** Variation of the vibrational frequency of the symmetric N-H stretching of sulfathiazole polymorph I with temperature. As the sample was heated, at several temperatures Raman spectra were recorded. A second order trendline was fitted to the data. The correlation coefficient ($R^2$) is presented.

It seems that the frequency shift with variable temperature is reversible. Other shifts in frequencies with heating or cooling sulfathiazole polymorph I were also reversible. As for the infrared data, the sum of the symmetric and asymmetric NH stretching frequency shifts, as an indication of hydrogen bond strength, was plotted against the temperature. The result is shown in Figure 5.13.

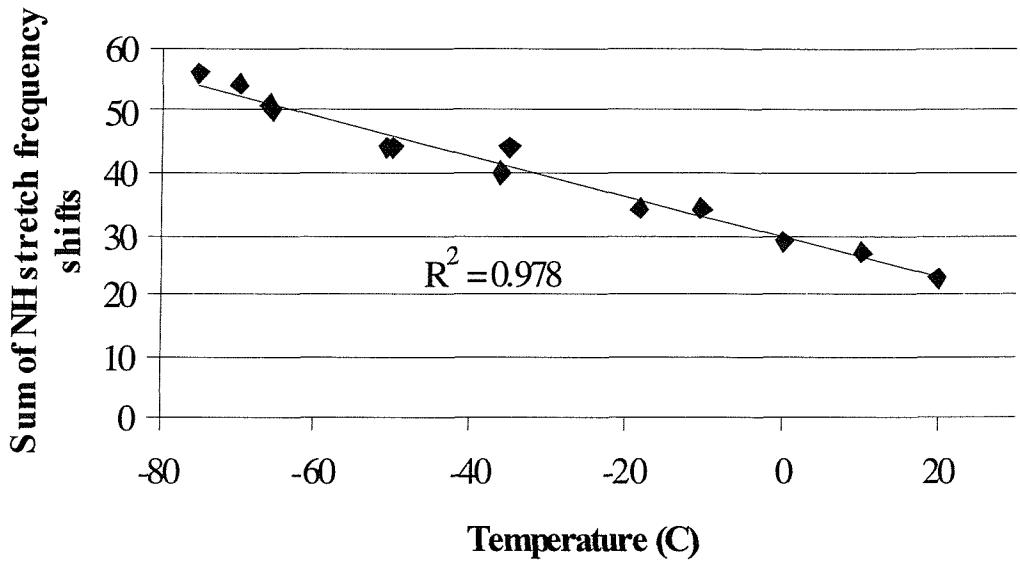


**Figure 5.13** Plot of the sum of the Raman symmetric and asymmetric NH stretching frequency shifts against temperature for sulfathiazole polymorph I. A first order trendline is fitted to the data and the correlation coefficient ($R^2$) is shown in the graph.

When this figure is compared with the same plot of the infrared frequencies, one can't but notice the non linearity of the infrared data in Figure 5.9 and the linearity of the Raman data. An explanation would be that they are showing different temperature ranges. The change in hydrogen bond strength is expected to be linear at low temperatures and then asymptotes off at higher temperatures as the hydrogen bond becomes very weak. The Raman spectra at higher temperature are available but the asymmetric NH stretching is too weak to be distinguished.

In Figure 5.14, both the infrared and Raman data are plotted against the temperature. A straight line was inserted as trendline connecting the Raman data. However, some curvature is observed and for fitting both the Raman and infrared data, a second order trendline was preferred.

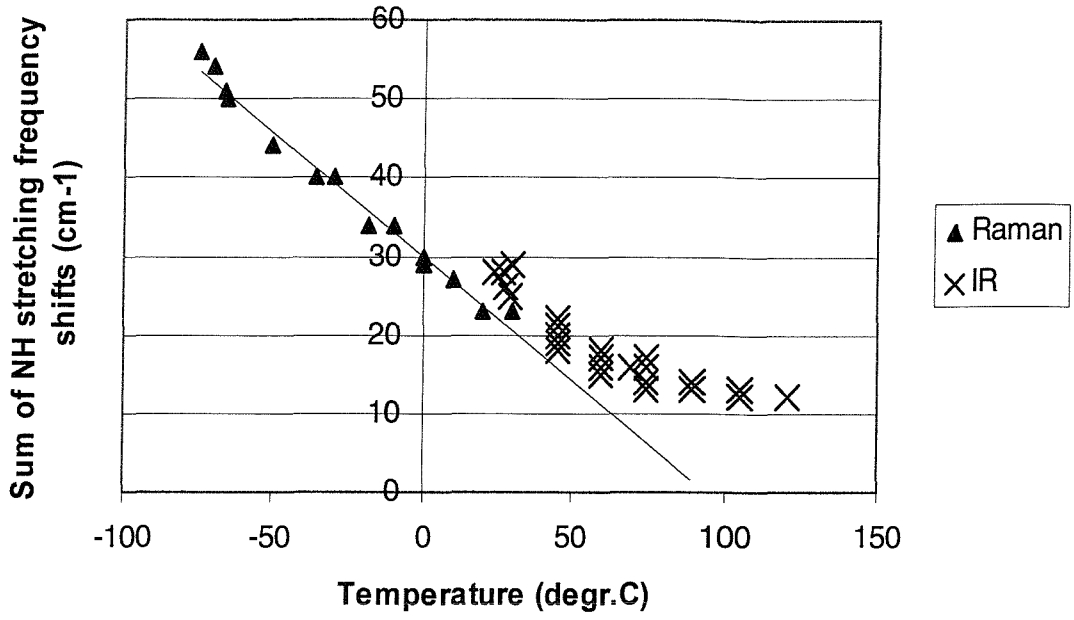


**Figure 5.14** Plot of the sum of the symmetric and asymmetric NH stretching frequency shifts against temperature for sulfathiazole polymorph I. A first order trendline is fitted to the Raman data.

It is unclear why the Infrared data shows such large deviation from the Raman data at room temperature. In order to correlate this data with the variable temperature X-ray data, a second order trendline, correlating both the infrared and Raman data with the temperature, was fitted to the data. From this equation the 'sum of the NH stretching shifts' for the temperatures at which the X-ray data were recorded were calculated. This will give us an estimation of the hydrogen bond strength for those particular temperatures based on NH stretching frequency shifts. Correlating these calculated hydrogen bond strengths with the X-ray data on hydrogen bond lengths gave no matches for any of the hydrogen bond lengths. The correlation with the shortest hydrogen bond gave a correlation coefficient of 0.95.

One key question, we need to ask ourselves is what do these shifts with temperature mean? As one compares the vibrational spectra of a molecule in the different states, undoubtedly many bands will shift, hence a shift in band frequencies would be expected on heating a sample over almost 150°C. But when do we speak about a very large anisotropic expansion ?

For comparison, the ß-butyrolactone sulfathiazole solvate was heated from -60°C to 20°C and FT-Raman spectra were recorded at regular intervals. Shifts in vibrational frequencies on heating the solvate are presented in Table 5.9.

**Table 5.9** On heating and cooling down of the ß-butyrolactone sulfathiazole solvate, shifts in the frequency of certain vibrations are observed. The frequencies were obtained from the Raman experiments. v: stretching, as: asymmetric, s: symmetric

| Temperature (°C) | | Assignment |
|---|---|---|
| -60 | 20 | |
| vibrational frequencies ($cm^{-1}$) | | |
| 3467 | 3464 | νNH as |
| 3369 | 3370 | νNH s |
| 1817 | 1818 | |
| 1423 | 1421 | |
| 1287 | 1287 | |
| 1265 | 1262 | |

On heating the solvate, most bands shift only over 1 or 2 wavenumbers towards higher frequency. Even the symmetric NH stretching only shifts downwards over 1 wavenumber.

In the same experiment performed on sulfathiazole polymorph I, most bands produced a 4 or 5 wavenumbers shift towards higher frequencies, with exception of the NH stretching frequency which produced shifts over 20 wavenumbers. The effect of heating on the NH stretching frequencies of the ß-butyrolactone sulfathiazole solvate is shown in Figure 5.15. For comparison, the carbonyl stretching region is also included in the spectrum.

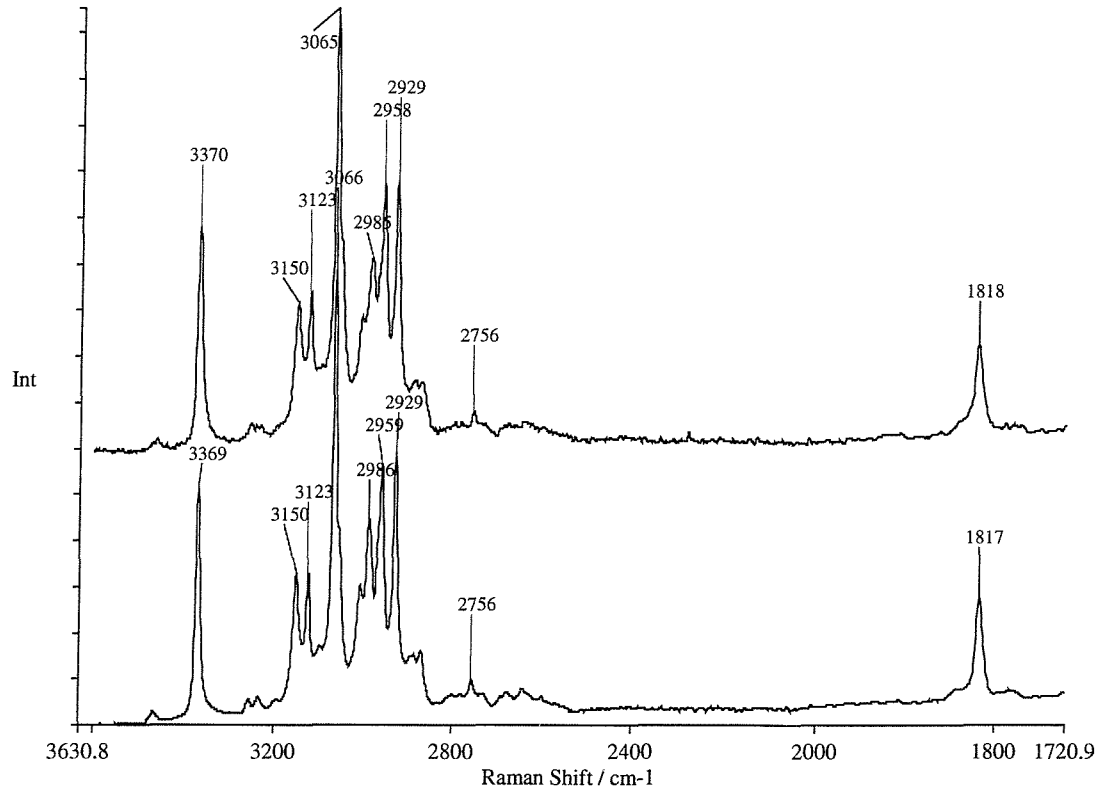


**Figure 5.15** FT-Raman spectra of the ß-butyrolactone sulfathiazole solvate at two different temperatures. The top spectrum was recorded at room temperature (20°C). The bottom spectrum was recorded at -60°C. 1 W laser power, 100 scans, resolution: 4 $cm^{-1}$

Unfortunately the symmetric NH stretching frequencies were not observable at each temperature. Therefore it was not possible to compare the plot of the sum of the NH symmetric and asymmetric shifts with variable temperature with that obtained from the variable temperature experiments on sulfathiazole polymorph I.

## 5.6 Conclusions

The results from our study into the sulfathiazole solvates are disappointing. There seems to be no correlation between the observed shifts in our vibrational spectra and the hydrogen bond lengths for the different sulfathiazole polymorphs.

An unusual large shift in the vibrational frequencies with varying temperatures for sulfathiazole polymorph I were observed. The largest shifts are noticed in the NH stretching region. Other conclusions that can be drawn from the variable temperature data is that the hydrogen bond strength is linearly related to temperature variations at low temperatures. At higher temperatures the linearity vanishes.

## 5.7 References


[1] J.K. Halebian and W.C. McCrone, J. Pharm. Sci, 1969, **58**, 911

[2] M. Kuhnert-Brandstätter, Thermomicroscopy in the Analysis of Pharmaceuticals, Pergamon Press, Oxford, 1974

[3] J. Krc, Microscope, 1977, **28**, 25

[4] H. Takahashi, T. Takenishi and N. Nagashima, Bull. Chem. Soc. Japan, 1962, **35**, 925

[5] K. Ashizawa, J. Pharm. Sci., 1989, **78**, 256

[6] A. Forni, I. Moretti, G. Torre, S. Brueckner, L. Malpezzi and G. DiSilvestro, J. Chem. Soc., Perkin Trans. **2**, 1984, 791

[7] D. Giron and C. Goldbronn, J. Therm. Anal., 1997, **49**, 907

[8] M. Sacchetti, J. Therm. Anal. Calorim., 2000, **63**, 2, 345

[9] T.M. Wu and C.S. Liao, Macromol. Chem. Physic., 2000, **201**, 18, 2820

[10] S.P. Srivastara, J. Handoo, K.M. Agrawal and G.C. Joshi, J. Phys. Chem. Solids, 1993, **54**, 639

[11] D.P. Ip, G.S. Brenner, J.M. Stevenson, S. Lindenbaum, A.W. Douglas, S.D. Klein and J.A. McCauley, Int. J. Pharm., 1986, **28**, 183

[12] R.A. Fletton, R.W. Lancaster, R.H. Harris, A.M. Kenwright, K.J. Parker, D.N. Waters and A.J. Yeadon, J. Chem. Soc., Perkin Trans. 2, 1986, 1705

[13] C.M. Deeley, R.A. Spragg and T.L. Threlfall, Spectrochim. Acta **47A**, 1991, 1217

[14] W.P. Findlay and D.E. Bugay, J. Pharm. Biomed. Anal., **16**, 1998, 921

[15] S.O. Paul, C.J.H. Schutte and P.J. Hendra, Spectrochim. Acta **46A**, 1990, 323

[16] L.S. Taylor and F.W Langkilde, J. Pharm. Sci, 2000, **89**, 10, 1342

[17] G.J. Kruger and G. Gafner, Acta Cryst., 1971, B**27**, 326

[18] N. Blagden, R.J. Davey, H.F. Lieberman, L. Williams, R. Payne, R. Roberts, R. Rowe and R. Docherty, J. Chem. Soc., Faraday Trans., 1998, **94**(8), 1035

[19] D. Hughes, M.B. Hursthouse, R.W. Lancaster, S. Tavener, T.L. Threlfall and P. Turner, J. Pharm. Pharmacol., 1997, **49**, S4, 20

[20] D.S. Hughes, M.B. Hursthouse, T. Threlfall, S. Tavener, Acta Cryst., 1999, C**55**, 1831

[21] D.C. Apperley, R.A. Fletton, R.K. Harris, R.W. Lancaster, S. Tavener and T.L. Threlfall, J. Pharm. Sci.,1999, **88**, 12, 1275

[22] B. Minceva-Sukarova, L. Andreeva, L. Pejov et al., J. Serb. Chem. Soc., 2000, **65**, (5-6), 417

[23] G.A. Jeffrey, An Introduction to Hydrogen Bonding, Oxford University Press, 1997, p12

[24] L.J. Bellamy and R.L. Williams, Spectrochim. Acta, 1957, 9, 341

[25] L.J. Bellamy and R.J. Pace, Spectrochim. Acta, 1972, 28A, 1869

[26] L.J. Bellamy, Appl. Sp., 1979, 33, 5, 439

[27] A.L. Bingham, D.S. Hughes, M.B. Hursthouse, R.W. Lancaster, S. Tavener and T.L. Threlfall, Chem. Commun., 2001, 603

# Chapter 6 Conclusions and Future Work

The Southampton Raman group under supervision by Prof. Patrick Hendra, has been involved with the development of FT-Raman spectroscopy right from the beginning. Therefore many new applications in a wide range of areas have been investigated over the years. The work I have done continues from the basis laid out over all those years.

In **Chapter 2**, Raman sampling by means of rotation was studied. The advantages of rotating a sample are twofold. Firstly, by rotating a sample heating of the sample by the laser is reduced. This is particularly important in heat sensitive samples like polymorphs. The concept was shown by comparing two FT-Raman spectra of prilocaine. In the stationary spectrum, the sample had clearly started to melt, whereas in the spectrum while rotating, a crystalline spectrum was obtained.
The second advantage of rotating samples is the avoidance of sub-sampling. Especially when analysing multi ingredient tablets with uneven surfaces (due to logos being imprinted) the possibility of subsampling when recording stationary spectra is of real concern. A comparison was made between two random spectra of a two component tablet, both recorded while the tablet was stationary. A third spectrum was recorded while the tablet was rotating. It was shown that the spectrum of the rotating tablet gave a more realistic estimate of the tablet's composition.
However, rotation of samples in FT-instruments can lead to problems. When a sample is rotated too rapidly, spurious lines can start to appear in the lower frequency range of the spectrum. When rotating faster and faster, these spurious lines move towards higher wavenumbers in the spectrum. The reason for these spurious lines appearing in the spectra stems from modulation and double modulation and the Fourier Transform process. Other parameters that influence the position of these spurious lines is particle size of the sample probed and the laser spot size.
It is demonstrated that when rotational speeds are kept reasonably low (below 1500 rpm), that the increase in noise is not too problematic and that the induced spurious bands stay well away from the actual spectrum.

For future work, it would be interesting to use chemometric procedures to try to reduce the movement induced noise. Development of such a 'correction' algorithm would be advantageous for quantitative Raman analyses as well.

**Chapter 3** dealt with the feasibility of using FT-Raman spectroscopy as a quantitative technique.

The reproducibility of FT-Raman spectra in terms of band height and area for both liquids and solids was assessed. For reasonably good scatterers, spectra recorded and averaged as we described are reproducible within 98% provided the laser and measurement equipment are stable. This in turn leads us to conclude that formulations with reasonable high concentrations of most actives can be monitored reliably and rapidly even if the tablets are inhomogeneous.

Turning to our experiments in more detail, it is clear that although internal calibration would be ideal, the use of an external intensity standard is feasible. Using external standardisation is not always favourable for reproducibility values. When the instrument is stable (Relative Standard Deviation $\leq 1.5\%$), external standardisation is not necessary. When the reproducibility from tablet to tablet is around 98%, our external reference enhances the reproducibility. But when the tablet reproducibility falls below 97.5%, ratioing against an external reference only makes the results worse.

For the liquid formulations, correlation coefficients from our regression lines display values of over 0.99 in all 4 sets of calibration samples.

Calibration curves were generated for tablets made from $Na_2SO_4$ or $K_2SO_4$ and maleic acid. These were compared with others fabricated from sodium sulphate and potassium chromate. It was found that the organic/inorganic mixtures produced better results suggesting that the softness of the organic is advantageous.

For the tablet calibration sets, correlation coefficients over 0.995 are possible when internal standardisation is used. External referencing reduces the linearity and correlation. The correlation coefficients are still better than 0.99 for the $K_2SO_4$/maleic acid mixtures. Since I had to gravimetrically prepare the calibration sets myself, the biggest problem arose from de-mixing as the powders were transferred into the KBr press. Hence, for some tablets intensity variations up to 30% from one side of the tablet to another were observed. Therefore, it was decided to leave clear outliers out of the calibration set.

There seems to be no correlation over the entire concentration range (0 to 100%) for the tablet mixtures made up from two hard crystalline materials, $K_2CrO_4$ and $Na_2SO_4$. But for a restricted region (up to 70% w/w%) correlation coefficients better than 0.99 have been obtained.

There was a influence on the Raman intensities as the packing density was varied. It appears that the Raman intensity decreases around 5% for tablets compressed with 9 tons of weight, compared with tablets compressed with 3 tons of weight. The relative standard deviation was rather large, 2% on the average intensities at the different pressures.

There is one problem left unsolved though. That is the fact that different slopes for the correlation graphs are obtained for similar sets of tablets. One explanation could be day to day variation of the instrument response. Unfortunately, our external reference as it stands is not able yet to correct for this. But in the recommendations for future work, some suggestions are lied out.

Finally, we compared the use of peak heights and peak areas. To our surprise, height measurements were more satisfactory. We suspect that the explanation lies in the noise. Noise in the background makes it very hard to define the background line for integration. This, of course, is disastrous because the background line affects the root of the band and hence its position has a disproportional large effect on the area. Peak height, on the other hand is also affected by the noise in the background but the effect is less apparent when broader bands are studied. Thus, our conclusion that the use of band height is more satisfactory than band areas in quantitative Raman spectroscopy.

Recommendations for future work are to:

- cut the tablets in half and analyse these by HPLC to confirm our suspicion of sample inhomogeneity being the major cause of the flaws in the analysis
- prepare a new set of 'thinner' calibration standards, so that the whole tablet is probed and de-mixing does not cause such a big problem anymore
- find a new external reference that is a stronger Raman scatterer which will improve its reproducibility
- modify the tablet analyser so that the tablet stays perfectly in focus

- use chemometrics to reduce the influence of noise on the calibration curves and to study the possibilities for correcting the differences in slopes for the calibration curves

In **Chapter 4** a local anaesthetic system was studied. The two active ingredients lidocaine and prilocaine form a eutectic mixture. In addition, two block copolymers in aqueous solution are present in the formulation.

Interactions between the two active components were studied. Some evidence of hydrogen bonding was evident from the infrared spectra, but this was not observed in the Raman spectra. In addition solubility of the components in their eutectic mixture was observed.

The possibility of interactions between the eutectic mixture and an aqueous solution of block copolymers was investigated. Again a change in hydrogen bonding in the eutectic mixture was observed, as the boundary between the eutectic mixture and the aqueous solution was probed. Unfortunately, due to overlapping water bands and overall low signal to noise, the other regions in the spectrum significant for hydrogen bonding could not be studied. Therefore the results on the possibility of interactions between the actives and excipients in the formulation are inconclusive. The aims for future work should be to improve the experimental set-up so that a vibrational spectrum of the eutectic mixture in the solid state can be recorded. This way, the spectra of the eutectic mixture and its components can be compared in the solid state where hydrogen bonding is stronger.

To study the possible interactions between the eutectic mixture of lidocaine and prilocaine and the aqueous solutions of block copolymers, new Raman mapping experiments are needed. It took considerable time to get the experiment to work, but now it is at the stage where, given enough time, conclusive results can be obtained.

From the variable temperature experiments performed on the formulation containing local anaesthetics, a lot of data on conformation changes in the polymer system can be extracted. Especially the use of chemometrics would give a considerable advantage over simply curvefitting. As a result, more conclusions will be drawn with regards to thermal stability.

In the last chapter, **Chapter 5**, sulfathiazole and its polymorphs were studied. In the literature, it was shown that sulfathiazole polymorph I displays a rather large

anisotropic lattice expansion on heating. It is also known that the change in hydrogen bond lengths can be related to shifts in the vibrational frequencies.

Both infrared and Raman spectra of a series of iso-structural solvates of sulfathiazole were recorded. The changes in the different bond lengths and unit cell parameters were related to the shifts in vibrational frequencies of specific groups, but no correlation could be found.

Variable temperature vibrational spectra of sulfathiazole polymorph I were recorded and an attempt was made to relate the observed shifts in the NH stretching frequencies with the changes in hydrogen bonds and unit cell parameters. But again, no correlation was found.

Recommendations for future work would be to include a wider range of solvates with clear differences in hydrogen bonding capacities into the study.

Deconvolution and curve fitting procedures to reveal underlying bands would be beneficiary to be able to correlate the shifts in frequencies with the X-ray data on bond lengths.

# Publications

1) 'Rotating samples in FT-RAMAN spectrometers', De Paepe ATG, Dyke JM, Hendra PJ, Langkilde FW, Spectrochim. Acta, **A53,** (1997), 2261

2) 'The use of reference materials in quantitative analyses based on FT-Raman spectroscopy', De Paepe ATG, Dyke JM, Hendra PJ, Langkilde FW, Spectrochim. Acta, **A53,** (1997), 2267

3) ' Rotation of samples in FT-Raman Spectroscopy : Control of sample heating and averaging in inhomogeneous specimens', De Paepe ATG, Hendra PJ, Langkilde FW, Taylor LS, Arbin AV, Eriksson UE, Russell AE, Appl. Spectr. - submitted for publication.

4) 'Reproducibility of FT-Raman Intensities' - paper in preparation

5) 'Quantitative Analysis on tablets using FT-Raman Spectroscopy' - paper in preparation